COMPRESSIVE MECHANICAL MODELS OF HIGH STRENGTH MORTAR AND CONCRETE UNDER SEVERE ENVIRONMENTAL ACTON

過酷環境下における高強度コンクリートおよびモルタルの圧縮応力場における力学モデルの構築

By
Muhammad Aboubakar FAROOQ

Division of Engineering and Policy for Sustainable Environment
Graduate School of Engineering
Hokkaido University
Sapporo, Japan

September 2019

COMPRESSIVE MECHANICAL MODELS OF HIGH STRENGTH MORTAR AND CONCRETE UNDER SEVERE ENVIRONMENTAL ACTON

過酷環境下における高強度コンクリートおよびモルタルの圧縮応力場における力学モデルの構築

By
Muhammad Aboubakar FAROOQ

A dissertation submitted to Hokkaido University
in partial fulfilment of the requirements for the Degree of
Doctor of Philosophy in Engineering

Division of Engineering and Policy for Sustainable Environment
Graduate School of Engineering
Hokkaido University
Sapporo, Japan

September 2019

ACKNOWLEDGEMENT

I would like to express my sincere gratitude to my supervisor Professor Hiroshi YOKOTA, for his inclusive guidance, invaluable suggestions, caring attitude and endless support throughout this research work. I also wish to extend my warm gratitude to my co-supervisor Professor Yasuhiko SATO of Waseda University for giving me opportunity to continue PhD program from Master program and supervising my research work despite of long distance and busy schedule. Without their guidance and support, this piece of work could not have been accomplished. Moreover, I am grateful to them for providing me opportunity to learn from their expertise and working under their supervision has been a great experience.

My gratitude is also extended to the examination committee members Prof. Takafumi SUGIYAMA and Prof. Takashi MATSUMOTO for their comments during the evaluation, spending time reading this dissertation, which led to improving the quality of this research work.

Taking this opportunity, I also would like to acknowledge Ministry of Education, Science and Culture, Government of Japan for awarding me generous MEXT Scholarship to make my study and stay possible in Japan during Mater and Doctoral program. I am also thankful to English Engineering Education (e3) program administration for their kind cooperation throughout the whole period.

I also would like to thank to Dr. Takeru KANAZAWA of Hokkai Gakuen University, who was always there to lend me a hand whenever I needed help. My gratefulness and thanks are also extended to all other members of Lifetime Engineering Laboratory and Laboratory of Engineering for Maintenance System for their kind assistance and support throughout my stay here.

I would like to take the opportunity to thank technical staff Mr. Kimura T. (late), Mr. Ookuma T. and Mr. Yamakami T. for their cooperation and assisting me during the experimentation. In addition, I am also obliged to my undergraduate advisor, Dr. Muhammad Aun Bashir, for encouraging and supporting me to pursue higher studies at Hokkaido University.

Last but not least, I would like to extend my sincere and heartiest gratitude to my parents and siblings for their permanent unconditional support, endless love and prayers during all times.

ABSTRACT

In recent years, it has been reported that the durability-related properties of mortar and concrete can be greatly improved with the incorporation of blast furnace slag (BFS) as the full amount of fine aggregates. Nevertheless, the mechanical properties of such mortar and concrete were not clarified yet. In the previous study, the author found slightly improved monotonic behavior of high strength mortar with BFS fine aggregates compared to the ordinary mortar of high strength with crushed river sand (CS) in air and water. However, the mechanical behavior of high strength concrete with BFS fine aggregates subjected to the combined action of freezing and thawing and mechanical loading is not evaluated yet. Moreover, the constitutive laws for the analysis of RC structures built and repaired with such high strength mortar and concrete are not available. Therefore, this study aims to clarify the fatigue behavior and propose a simplified fatigue model of high strength mortar with BFS sand as fine aggregates in compression in air and water. The monotonic behavior of air-entrained (AE) and non-AE high strength concrete with BFS fine aggregates subjected to freezing and thawing cycles (FTC) is investigated and the stress-strain models of such concrete are formulated. Thereafter, the fatigue behavior of intact and frost-damaged AE high strength concrete with BFS fine aggregates is investigated and the S_{max}-N_f relationships for such concrete are proposed.

The fatigue compression tests were carried out on cylindrical BFS mortar specimens in air and water and the results are compared with those of ordinary CS mortar. The load was applied in the form of sine signal with constant amplitude and the frequency was kept as 5 Hz. The stress level was varied from 60%, 70% and 80% of uniaxial compressive strength (f'_c). The damage progress is discussed based on the strain developments measured by using high-speed measuring system. Fatigue life (N_f) of both BFS mortar and CS mortar was also examined in air and in water. The experimental results reveal that BFS mortar exhibits longer N_f compared to CS mortar in air. Nevertheless, both types of mortar exhibit similar N_f in water and the N_f each mortar is reduced in water compared to air. This is because the adsorbed layers of moisture in the mortar during saturated state reduce the surface energy of the particles and consequently fracture energy of hydrated product is reduced, resulting in a reduction in compressive strength of mortar in water. The other possible reasons for the reduction of N_f of both mortars in water are because of pumping action and wedge effect of pore water pressure during the cyclic loading, and due to leaching of $Ca(OH)_2$ while testing in water. Thereafter, the static stress-strain relationships for each mortar proposed by author in the previous study are extended to formulate the simplified fatigue model for the assessment of change in mechanical properties and for prediction of failure under cyclic loading. It is observed that the change in fracture parameter of each mortar under fatigue in air is almost similar as that of static loading. However, the fracture parameter for mortar subjected to cyclic loading in water reduces sharply compared to that in air and that of static loading. Therefore, the N_f of mortar in water is shorter compared to air. Moreover, at each stress level, the plastic strain development in CS mortar is higher in air and water compared to BFS mortar, resulting is rapid degradation and shorter fatigue life of CS mortar. The experimental results are compared those of

obtained using proposed model, which shows satisfactory agreement.

In order to study the monotonic behavior of AE and non-AE high strength concrete with BFS fine aggregates concrete for different frost damage levels, the cylindrical and cuboidal specimens were used for carrying out freeze-thaw cycle (FTC) test according to ASTM C-666 type-A in 3% NaCl solution and the results are compared with AE normal concrete of normal strength and high strength concrete. The plastic strain measured during FTC test was used to explain the damage process. After certain number of FTC, the specimens were taken out from FTC chamber and were stored in controlled temperature room until the start of static compression tests. The experimental results show that overall rate of FTC equivalent plastic strain development in non-AE high strength concrete with BFS sand is slightly higher than that of AE high strength concrete with BFS and CS sand. However, it is slightly less than that of AE normal concrete. Higher the compressive strength of concrete, lower is the rate of plastic strain development for both AE and non-AE concrete. Moreover, the compressive strength and Young's modulus of AE concrete of both normal and high strength degrade at slower rate with the increase in FTC compared to non-AE concrete with BFS fine aggregates, because of less plastic strain development due to FTC in AE concrete. However, the mechanical properties of non-AE BFS concrete deteriorate at slower rate compared to non-AE normal concrete from the past study owing to high strength of non-AE BFS concrete. Nevertheless, the mechanical properties of each concrete change at almost same rate with the increase in FTC equivalent plastic strain. It is observed that Young's modulus of frost-damaged concrete reduces sharply compared to the compressive strength. In addition, the stress-strain model for frost-damaged high strength concrete are proposed based on the concept of elasto-plastic and fracture theory. It is observed that the rate of mechanical plastic strain in high strength concrete is slower compared to that of normal concrete and consequently the fracture parameter of high strength concrete reduces slowly. The rate of mechanical plastic strain development increases with the increase in frost-damage, nevertheless, the change is fracture parameter is almost same for all frost damage levels. The relationships for fracture parameter and plastic strain for high strength concrete are formulated. The comparison between experimental and calculated results using proposed model show good agreement validating the model.

Lastly, the compressive fatigue tests were performed on intact and frost-damaged AE high strength concrete using BFS and CS fine aggregates. The sinusoidal wave of constant amplitude with frequency of 3.5 Hz was used for fatigue loading. The maximum stress levels (S_{max}) of 70% and 80% of f'_c were adopted. The S_{max}-N_f relationships for AE high strength concrete with BFS and fine aggregates are formulated. The fatigue life of AE BFS concrete is longer than that of AE high strength normal concrete at all stress levels and for all frost damage level. No significant effect of FTC is found on the fatigue life of AE high strength concrete because of very less frost damage caused by FTC. Moreover, overall the fatigue life of AE high strength concrete is more than that of non-AE high strength plain concrete from the literature. This difference is pronounced as the maximum stress level decreases.

TABLE OF CONTENTS

LIST OF TABLES

LIST OF FIGURES

LIST OF SYMBOLS

f_c'	Ultimate static compressive strength,
ε'_{co}, ε'_{peak}	Peak strain corresponding to ultimate static compressive strength,
ε'_p	Plastic strain,
$\varepsilon'_{\max}$	Maximum compressive strain,
v	Poisson's ratio,
σ'_c	Compressive stress,
σ_{min}	Minimum applied stress,
σ_{max}	Maximum applied stress
f	Frequency of applied cycles,
k	Experimental constant depending upon moisture content and type of mortar,
$\varepsilon'_{p,exp}$	Plastic strain measured during experiment,
$\varepsilon'_{p,cal}$	Calculated plastic strain by proposed equation,
$f'_{c,exp}$	Experimental compressive strength,
$f'_{c,cal}$	Calculated compressive strength by proposed model,
$\varepsilon'_{p,Ni}$	Plastic strain corresponding to Number of cycle N_i under fatigue load,
$\varepsilon'_{max,Ni}$	Maximum strain corresponding to Number of cycle N_i under fatigue load,
α	Effective parameter,
β	FTC fracture parameter,
E_0	Initial Young's modulus of elasticity,
E	Equivalent strain as a function of axial and lateral strains,
E_{pftc}	FTC induced Equivalent strain
K	Mechanical facture parameter,
S	Stress level or Equivalent Stress
S_{max}	Normalized maximum stress level,
S_{min}	Normalized minimum stress level,
N, N_i	Number of applied loading cycles,
N_f	Number of loading cycles up to failure,
K_{exp}	Fracture parameter measured during experiment,
K_{cal}	Calculated fracture parameter by proposed equation,
K_{static}	Fracture parameter under monotonic or static loading,
K_{Ni}	Fracture parameter at Number of cycle N_i during cyclic loading,
$K_{water,Ni}$	Fracture parameter for mortar under fatigue in water for cycle N_i after 1st cycle.

Chapter 1

INTRODUCTION

1.1 BACKGROUND AND MOTIVATION

Cementitious materials, mainly in the form of concrete are the most widely used construction material in the world because of easy availability of its constituent materials and unique properties; every year more than 1 m^3 of concrete is produced per person worldwide **[1,2]**. However, the sustainability and durability of reinforced concrete (RC) structures are still the main issues because of their exposure to a variety of loading including environmental and mechanical actions during the service life. Freeze-thaw action, which is among such environmental actions in sub-zero temperature climate regions, poses detrimental effects on the structural performance of RC structures due to deterioration in the mechanical properties of concrete **[3-5]** because of surface scaling and internal micro-cracking of concrete **[5,6]**. In real RC structures mainly bridges, the frost action is always coupled with mechanical loading i.e. repetitive cyclic loading from vehicles, also known as fatigue, leading to severe and rapid degradation of structural performance of bridge decks. Therefore, the development of durable material, which can resist the mechanical and environmental actions efficiently, is need of the time.

Numerous research work has been conducted to enhance the durability of concrete by incorporating mineral admixtures, steel fibers and industrial wastes e.g. silica fume, fly ash and blast furnace slag etc. Utilization of industrial wastes into concrete helps to protect the environment by minimizing the environmental loads, energy consumption and also to conserve the natural resources **[7]**. Moreover, the usage of industrial wastes in concrete is a viable option considering the economy compared to steel fibers and admixtures. Blast furnace slag (BFS) is among such industrial wastes; generated during the production of iron and steel. This slag is a by-product obtained by quenching molten iron slag from blast furnace in water or steam to produce glassy and granular product that is then dried and ground into fine powder or sand particulates. In Japan, over 20 million tons of slag is produced annually and 90% of it is consumed in cement and concrete production **[8]**. Concrete containing granulated blast furnace slag (GBFS) is well known for improving its properties due to pozzolanic activity of GBFS resulting in dense matrix, high strength at long-term age and better durability properties like water tightness, chemical resistance and chloride ion permeation **[8,9]**. In the previous studies, the ground granulated BFS (GGBFS) has been used as percentage of cementitious materials with the maximum percentage replacement of binder with GGBFS as 50% in concrete because the higher proportion of GGBFS can impair the 28 days compressive strength of concrete **[10]**. Valcuende et al. (2015) studied the properties of

concrete with GBFS sand as percentage of fine aggregates and found that early age compressive strength of concrete with GBFS sand is almost similar to the concrete with river sand, but the compressive strength improves at longer age with increased replacement of fine aggregates by slag **[11]**. On contrary, it is pointed out that high quantity of non-ground GBFS as fine aggregates results in high porosity and less compressive strength of concrete **[12,13]**. However, in the recent years, it has been found that the durability related properties of mortar and concrete can be improved by using GGBFS as percentage of binder and BFS sand as total amount of fine aggregates **[9,14,15]**. Murata et al. (1983) investigated the freeze-thaw resistance of non-air entrained (non-AE) concrete using GBFS as sand and found the presence of large volume of pores of same radii as that of AE voids resulting in improved durability of such concrete **[14]**. Jariyathitipong (2014) and Ayano and Fujii (2014) reported that the mortar and concrete containing BFS fine aggregates show significant resistance against various severe environmental actions like frost damage and corrosion **[9,15]**. In addition, significant improvement in resistance was observed when mortar and concrete with BFS were exposed to sulfuric acid compared to ordinary one **[9]**. However, the mechanical characteristics of BFS mortar and concrete are not clarified yet. Farooq et al. (2017) investigated and found slightly improved monotonic behavior of mortar with BFS fine aggregates compared to ordinary mortar **[16]**. Moreover, many researches have been carried out to study the change in mechanical properties of normal concrete subjected to frost action **[3,17-26]**. Nevertheless, very few studies have focused on the mechanical properties change of frost-damaged concrete with BFS fine aggregates. Yuksel et al. (2007) evaluated the 90-days compressive strength of concrete containing different GBFS sand replacement ratios up to 50% with and without freeze-thaw cycles and reported that the loss in compressive strength was less than that of concrete without GBFS sand with the lowest loss for 20-30% replacement ratio **[27]**. However, the freeze-thaw cycles (FTC) induced plastic strain and mechanical properties of high strength concrete with BFS fine aggregates subjected to freeze-thaw cycles are not clarified yet compared to ordinary concrete and no stress-strain model is available to predict the response of intact and frost-damaged high strength concrete with BFS fine aggregates is available under monotonic loading. In addition, although much progress has been made in the development of high strength and durable concrete in the recent years. However, understanding the fatigue behavior of high strength concrete is still a main concern due to its brittle nature compared to normal concrete and owing to conflicting information on fatigue performance of high strength concrete presented in the literature **[28-31]**.

To utilize such material in reinforced concrete (RC) structures subjected to combined environmental and mechanical loading, it is essential to have relevant understanding of the various conditions that ensures durable concrete performance so that the design method for structures with such concrete can be developed. Therefore, it is necessary to evaluate the mechanical performance of such high strength mortar and concrete with BFS fine aggregates combined with environmental actions mainly freezing and thawing for cold regions. In this study, firstly, the compressive fatigue

performance of high strength mortar with BFS fine aggregates is investigated and a simplified fatigue model for the assessment of change in mechanical properties and for prediction of failure is proposed. Thereafter, the monotonic behavior of high strength concrete containing BFS fine aggregates with and without air-entrainment (AE) subjected to frost action is studied and the static stress-strain relationships for high strength frost-damaged concrete are developed. Lastly, the fatigue performance of AE high strength concrete is evaluated for intact and frost-damaged specimens.

1.2 OBJECTIVES OF THE STUDY

Owing to improved durability properties of mortar and concrete with BFS fine aggregates against environmental actions, this study aims to elucidate the mechanical behavior of high strength mortar and concrete with BFS sand for different frost damage levels and to formulate the respective constitutive laws, so that such mortar and concrete can be applied in the construction works. The main objectives of this research work are:

- To clarify of compressive fatigue behavior including fatigue life, S-N relationships, stiffness change and strain development of BFS mortar at different stress levels in different environmental conditions i.e. in air and in water along with crushed sand mortar, and to propose the simplified fatigue model for the assessment of change in mechanical properties at different interval of loading cycles along with the prediction of fatigue life.

- To investigate the behavior of AE and non-AE high strength concrete with BFS fine aggregates under static loading for different degrees of frost damage and to formulate the stress-strain relationships for intact and frost-damaged high strength concrete based on elasto-plastic and fracture model.

- To study the compressive fatigue behavior of AE high strength concrete with BFS fine aggregates compared with companion concrete with crushed river sand and to propose the S_{max}-N_f relationships.

1.3 OUTLINE OF THE DISSERATION

The dissertation comprises of five chapters. The organization of this dissertation is given as follows:

Chapter 1 summaries the background of the research work carried out related to durability properties of mortar and concrete with BFS fine aggregates. Moreover, the past research work carried out related to mechanical behavior of intact and frost-damaged concrete of normal strength and high strength under monotonic and cyclic loading is reviewed. The problems and the objectives of this research work are presented, and outline of the dissertation is given.

Chapter 2 presents the experimental and numerical investigation of high strength mortar under fatigue loading in air and water. The S_{max}-N_f relationships for BFS mortar and CS mortar are developed. Moreover, the compressive stress-strain relationships for BFS mortar and CS mortar developed in the previous study are extended to formulate the simplified fatigue model of high strength mortar for the assessment of change in mechanical properties i.e. fracture parameter, plastic and total strain development and for the prediction of fatigue life of each mortar.

In **Chapter 3**, the experimental investigation for monotonic behavior of AE and non-AE high strength concrete with BFS fine aggregates in comparison with AE normal concrete of normal and high strength for different frost-damage levels is presented. Moreover, the compressive stress-strain model for intact and frost-damaged high strength concrete are also formulated.

Chapter 4 presents the experimental study to elucidate the compressive fatigue behavior of AE high strength concrete with BFS fine aggregates and crushed river sand. The S_{max}-N_f relationships for AE high strength concrete are formulated in comparison with non-AE high strength concrete from the literature. The damage progress is discussed based on the plastic strain development.

In the end, **Chapter 5** leads to the summary and conclusions drawn from the research work carried out in this study. Moreover, the recommendations for future work are also suggested.

REFERENCES:

[1] Neville A. M., (2004). "Properties of concrete." 4th and final edition. Harlow: Pearson Prentice Hall.

[2] Scrivener K. L., Kirkpatrick R. J. (2008). "Innovation in use and research on cementitious material." Cement and Concrete Research, Vol. 38, pp. 128-136.

[3] Shi, S., (1997). "Effect of Freezing-Thawing Cycles on Mechanical Properties of Concrete." China Civil Engineering Journal, Vol. 30, No. 4, pp. 36-42, DOI: 10.15951/j.tmgcxb.1997.04.005

[4] Pigeon M., Pleau R., (1995). "Durability of concrete in cold climates." Taylor & Francis, London.

[5] Fagerlund G., Somerville G., Jeppson J. (2001). "Manual for Assessing Concrete Structures Affected by Frost, Division of Building Materials," Lund Institute of Technology, Lund, Sweden.

[6] Valenza, J. J. and Scherer, G. W. (2007). "A review of salt scaling: II. Mechanisms." Journal of Cement and Concrete Research, Vol. 37, No. 7, pp. 1022-1034.

[7] Mun J.S., Yang K.H., Kim S.J. (2016). "Tests on compressive fatigue performance of various concretes." ASCE Journal of Materials in Civil Engineering, Vol. 28, No. 10, DOI:

10.1061/(ASCE)MT.1943-5533.0001612

[8] Nippon Slag Association, (2011). “Statistical annual report of iron and steel slag.” pp. 2-3.

[9] Jariyathitipong P. (2014). “Improving the durability of concrete through the use of ground granulated blast furnace slag and blast furnace slag sand.” PhD Dissertation, Okayama University, Japan.

[10] Guo L., Sun W., Zheng K., Chen H., Liu B. (2007). “Study on the flexural fatigue performance and fractal mechanism of concrete with high proportions of ground granulated blast furnace slag.” Cement and Concrete Research, Vol. 37, pp. 242-250.

[11] Valcuende M., Benito F., Parra C., Miñano I. (2015). “Shrinkage of self-compacting concrete made with blast furnace slag as fine aggregate.” Construction and Building Materials, Vol. 76, pp. 1-9.

[12] Yüksel I., Özkan Ö., Bilir T. (2006). “Use of granulated blast-furnace slag in concrete as fine aggregate.” ACI Material Journal, Vol. 103, No. 3, pp. 203-208.

[13] Yüksel I., Genç A. (2007). “Properties of concrete containing non-ground ash and slag as fine aggregate.” ACI Material Journal, Vol. 104 No. 4, pp. 397-403.

[14] Murata J., Kawasaki M., Sakai T., and Kawai T. (1983). “Resistance to Freezing and Thawing of Concrete Using Ground Blast-Furnace Slag.” ACI Materials Journal, Vol. 79, pp. 999-1012.

[15] Ayano T. and Fujii T. (2014). “Resistance to Freezing and Thawing Attack of Concrete with Blast Furnace Slag Fine Aggregates.” Journal of Japan Society of Civil Engineers, Ser. E2 (Materials and Concrete Structures), 70(4), pp. 417-427.

[16] Farooq M.A. (2016). “Static and fatigue behavior of mortar with blast furnace slag as fine aggregates in air and water.” Masters’ Dissertation, Hokkaido University, Japan.

[17] Hasan M., Nagai K., Sato Y., and Ueda T. (2002). “Stress-strain behavior in Tension and Compression of Concrete damaged by Freezing and Thawing Cycles.” M. J. Setzer, R. Auberg and H. J. Keck, Eds. Proceedings of 2nd International RILEM Workshop on Frost Resistant of Concrete, Essen 8-19. Cachan Cedex: RILEM Publications S.A.R.L., 197-204.

[18] Hasan M., Okuyama H., Sato Y., and Ueda T. (2004). “Stress-Strain Model of Concrete Damaged by Freezing and Thawing Cycles.” Journal of Advanced Concrete Technology Vol. 2, No. 1, pp. 89-99.

[19] Shang H., and Song Y. (2006). “Experimental study of strength and deformation of plain concrete under biaxial compression after freezing and thawing cycles.” Cement and Concrete Research, Vol. 36, pp. 1857–1864.

[20] JI X. (2007). “The Experimental Study and Theoretical Analysis on the Mechanical Performance of Concrete and Bond Behavior between Concrete and Steel Bar after

Freezing and Thawing." Doctoral Dissertation, Dalian University of Technology, China.

[21] Zou C., Zhao J., Liang F. (2008). "Stress-strain relationship of concrete in freeze-thaw environment." Frontier Architecture Civil Engineering, China, Vol. 2, No. 2, pp. 184–188, DOI: 10.1007/s11709-008-0029-3.

[22] Wardeh G., Mohamed A., Ghorbel E. (2010). "Analysis of concrete internal deterioration due to frost action." Journal of Building Physics, Vol. 35, No. 1, pp. 54-82, DOI: 10.1177/1744259110370854.

[23] Duan A., Jin W., Qian J. (2011). "Effect of freeze–thaw cycles on the stress–strain curves of unconfined and confined concrete." Materials and Structures, Vol. 44, pp. 1309–1324.

[24] Hanjari K.Z., Utgenannt P., Lundgren K. (2011). "Experimental study of the material and bond properties of frost-damaged concrete." Cement and Concrete Research, Vol. 41, pp. 244–254.

[25] Liu M. and Wang Y. (2012). "Damage Constitutive Model of Fly Ash Concrete under Freeze-Thaw Cycles." ASCE Journal of Materials in Civil Engineering, Vol. 24, No. 9, pp. 1165-1174.

[26] Liu K., Yan J., Zou C., Wu H. (2018). "Cyclic Stress-Strain Model for Air-Entrained Recycled Aggregate Concrete after Freezing-and-Thawing Cycles." ACI Structural Journal, Vol. 115, No. 3, pp. 711-722, Title No. 115-S54.

[27] Yuksel I., Bilir T., Ozkan O. (2007). "Durability of concrete incorporating non-ground blast furnace slag and bottom ash as fine aggregate." Building and Environment, Vol. 42, No. 7, pp. 2651-2659.

[28] Petkovic G., Lenschow R., Stemland H., Rosseland S. (1990). "Fatigue of High-Strength Concrete." ACI SP-121: High-strength Concrete, pp. 505-525.

[29] Do M-T, Chaallal O., Aitin P-C (1993). "Fatigue behavior of High-Performance Concrete." ASCE Journal of Materials in Civil Engineering, Vol. 5(1), pp. 96-111.

[30] Hordijk D.A., Wolsink G.M., Vries J. de (1995). "Fracture and Fatigue Behavior of a High Strength Limestone Concrete as Compared to Gravel Concrete" HERON Vol. 40, No. 2, pp. 125-146.

[31] Kim J-K., Kim Y-Y. (1996). "Experimental Study of Fatigue Behavior of High Strength Concrete." Journal of Cement and Concrete Research, Vol. 26, No. 10, pp. 1513-1523.

Chapter 2

FATIGUE OF HIGH STRENGTH MORTAR – EXPERIMETNAL AND MODELING

2.1 GENERAL

Although, the mortar and concrete with blast furnace slag (BFS) as fine aggregates have improved durability related properties against environmental actions, but the mechanical properties of such mortar and concrete were not evaluated yet. In the previous study, the author found the improved monotonic behavior of BFS mortar compared to ordinary one. In this chapter, to elucidate the fatigue behavior of mortar with BFS sand, the compressive fatigue tests were carried out on cylindrical specimens in air and water and the experimental results are compared with those of ordinary mortar using crushed sand (CS). The S-N relationships for both types of mortar are developed based on experimental results in both environmental conditions. The deformation is discussed based on strain development under the fatigue loading. It is found that BFS mortar has overall slightly better fatigue behavior in air compared to CS mortar, however, it is same in water. Furthermore, the static stress-strain relationships developed in the previous study are extended to propose the simplified fatigue model for the assessment of change in mechanical properties and for the prediction of the failure under cycle loading.

2.2 EXPERIMENTAL OUTLINE

2.2.1 Materials

Two series of mortar specimens were casted, blast furnace slag (BFS) mortar and crushed sand (CS) mortar. Ordinary Portland cement (OPC) was used as binder in both types of mortar. The density of ordinary Portland cement is 3.15 g/cm^3, while the Blaine fineness is 3300 cm^2/g.

In the preparation of BFS mortar specimens, BFS sand is used as full amount of fine aggregates which is cooled rapidly by pressurized water jets after it is ejected from blast furnace at 1500 ^{o}C, then it is granulized into required size. Granulated blast furnace slag has an amorphous structure containing a large amount of silica and alumina and it shows pozzolanic properties when it is ground to very fine size. For CS mortar specimens, crushed river sand is used as fine aggregates. Fine aggregates with particle size of 0.3 to 5 mm are used in this study. The physical properties of fine aggregates are given in Table 2.1.

Table 2.1: Physical properties of fine aggregates

Property	Crushed sand	Blast furnace slag sand
Saturated density (g/cm^3)	2.65	2.72
Fineness modulus	2.96	2.23
Water absorption (%)	1.97	1.12

Table 2.2: Mix-proportion of blast furnace slag mortar and crushed sand mortar

Mortar Type	W/C (%)	Unit Content (kg/m^3)				HRWRA (kg/m^3)	AFA (kg/m^3)
		W	OPC	BFS	CS		
BFS Mortar	35	268.45	767	1533	0	3.835	2.301
C.S. Mortar		271.6	776	0	1552		

BFS: Blast furnace slag, CS: Crushed sand, W: Water content, OPC: Ordinary Portland cement, HRWRA: High range water reducing admixture, AFA: Antifoaming Agent.

2.2.2 Mix Proportions and Specimens Preparation

Table 2.2 presents the mix proportion of BFS mortar and CS mortar. The cement to sand ratio is kept as 1:2 with water to cement ratio of 35% for both types of mortar. The polycarboxylate type of high range water reducing admixture is used as an additional admixture. Various researches show that with the use of high range water reducing admixture, excessive air bubbles are formed inside the mortar decreasing the surface tension during liquid phase **[1]**. Therefore, the antifoaming agent is used to control the air content inside the mortar. One batch for each BFS mortar and CS mortar was prepared. The cylindrical specimens were casted with diameter of 50 mm and height of 100 mm in steel molds for each type of mortar. After demoulding, the specimens were cured in normal water for seven days. The top casted surface of the cylindrical specimens was ground to make it smooth and parallel to the hinge surface placed between loading platen and specimen. For strain measurement, two vertical and two horizontal strain gauges of 30 mm gauge length were attached to the surface of cylindrical specimens. The vertical and horizontal strain gauges were attached parallel and perpendicular to the axial loading direction respectively using epoxy resin.

2.2.3 Compressive Fatigue Test Method

Prior to the compressive fatigue tests, the uniaxial static compression tests were carried out on three cylindrical specimens of each BFS mortar and CS mortar in air at the age of 1-year accordance with JIS A1108:2006 **[2]** using displacement control at a rate of 0.01 mm/sec.

The fatigue test in compression was performed using servo hydraulic dynamic testing machine with a loading capacity of 750 kN immediately after monotonic uniaxial tests in compression. At the beginning of test, the specimen was loaded to mean value of maximum and minimum stress level at a standard rate and after which the load was applied in form of sine signal

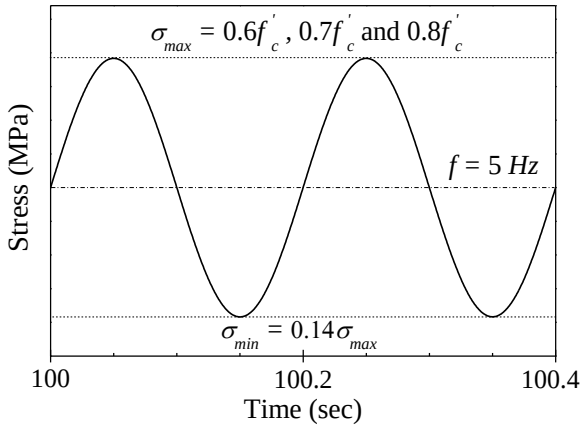

Figure 2.1: Sinusoidal wave of loading cycle

with a constant amplitude as shown in Fig. 2.1. The influence of the frequency of loading has been investigated by several researchers. It has been reported that variation of loading frequency within the range of 1-15 Hz has minor effect on the fatigue strength of concrete when the maximum stress level is less than 75% of compressive strength **[3]**. However, for higher stress levels, the fatigue life of plain concrete decreases with the decrease in frequency due to creep effects **[4,5]**. In this study, the frequency was kept as 5 Hz, because there was possibility that higher frequency could result in instability of loading arrangement. The maximum stress level was kept as 60%, 70% and 80% of static compressive strength of mortar specimens. The load ratio between minimum and maximum stress level was maintained as 0.14 for each fatigue test. Loading cycles were applied until the failure of specimens except for 60% stress level in air, where test was stopped at 1 million cycles. The maximum stress ratio S_{max} and minimum stress ratio S_{min} are given by Eq. (2.1) and Eq. (2.2) respectively.

$$S_{max} = \sigma_{max} / f_c' \tag{2.1}$$

$$S_{min} = \sigma_{min} / f_c' \tag{2.2}$$

Where σ_{max} is the maximum stress, σ_{min} is the minimum stress and f'_c is the uniaxial compressive strength of each mortar. Three cylinders of each mortar were tested at each stress level in air as well as in water. To avoid the eccentricity of applied cyclic loading, steel hinge was placed between the specimen and loading head of the machine. Four strain gauges of 30 mm gauge length were mounted on cylindrical specimens using epoxy resin and pressure of approximately 30-50 kPa was applied on strain gauges for 24 hours for their proper adhesion throughout the test. To record the strain values, high speed measuring system is used with the sampling frequency of 100 Hz. Prior to testing in water, the strain gauges were protected with water proof adhesive tape to prevent the moisture effect on strain measurement and specimens were submerged in water for 48 hours prior

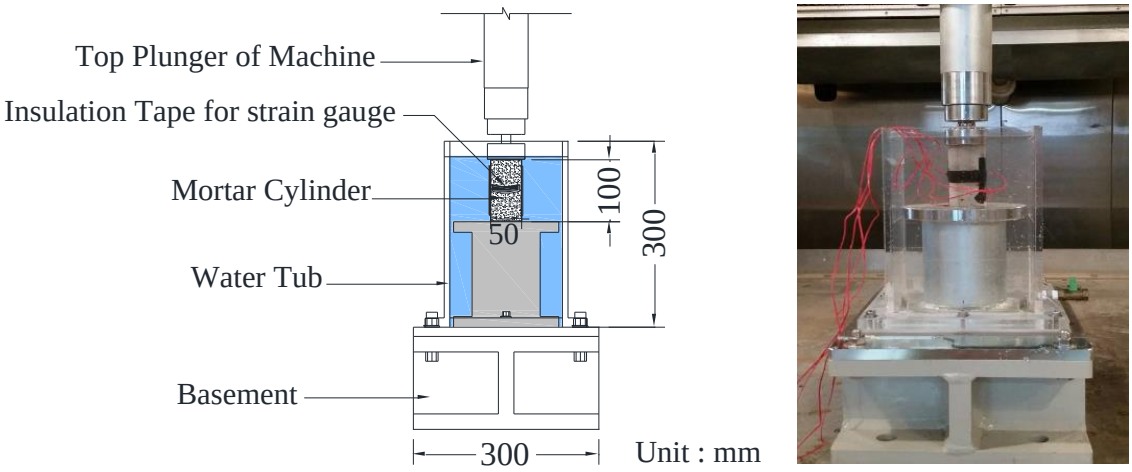

Figure 2.2: Loading Arrangement

to testing for uniform saturation inside the specimen. The schematic diagram of loading arrangement is shown in Fig. 2.2.

2.3 RESULTS AND DISCUSSION

The average static compressive strength, Young's modulus, Poisson's ratio and strain at ultimate strength of each mortar in air and in water are summarized in Table 2.3. BFS mortar showed more compressive strength than CS mortar both in air as well as water. The compressive strength of both types of mortar was decreased in water because the adsorbed water layers due to saturation reduce the surface energy of hydration product significantly because of surface tension of water. This leads to remarkable reduction of fracture energy and strength of mortar **[6]**. Especially, CS mortar has pronounced tendency of reducing compressive strength in water because CS mortar specimens have more voids and higher water absorption capacity (2.26%) compared to that of BFS mortar (0.58%). The water absorption capacity of each mortar was determined by submerging the specimens in water for 48 hours. The higher water absorption capacity of CS mortar reduced the surface energy by large amount resulting in more reduction of compressive strength of CS mortar compared to BFS mortar. It is reported that higher the voids and liquid content of cement

Table 2.3: Mechanical properties of blast furnace slag mortar and crushed sand mortar

Environmental condition	Mortar type	f'_c (MPa)	E_0 (GPa)	v	ε'_{co} (micron)
Air	BFS	109	40.6	0.28	3492
	CS	104	34.9	0.26	4270
Water	BFS	101	39.6	0.30	3117
	CS	87	33.8	0.25	3490

BFS: Blast furnace slag, CS: Crushed sand, f'_c: Compressive strength, E_0: Young's modulus, v: Poisson's ratio, ε'_{co}: Strain at ultimate compressive strength

-based material lead to large reduction in surface energy **[7]**. The Young's modulus is calculated by determining the slope of stress-strain curve between longitudinal strain of 50 microns and point corresponding to one third of ultimate compressive strength. BFS mortar showed more Young's modulus compared to CS mortar both in air and water.

2.3.1 Fatigue Stress-Strain Curves

The stress-strain curves were recorded by high speed measuring system during the whole fatigue test. Figure 2.3 represents the typical stress-strain loops at certain loading cycles for each mortar under 70% and 80% stress level in air as well as in water along with stress-strain curves under static loading. The numbers in the figure denote the number of respective loading cycle for which stress-strain loops are drawn and N_f represents the average fatigue life. The stress and ultimate strain under fatigue test are normalized by the compressive strength (f'_c) and strain at peak stress during static compression test respectively. During fatigue test, the loading part of stress-strain curve for the first cycle is similar to that of obtained from the static test, but after that the plastic strain started to increase with the increase in loading cycles, shifting the stress-strain loops to the right. The ultimate strain of each mortar is not in close agreement for static and fatigue test.

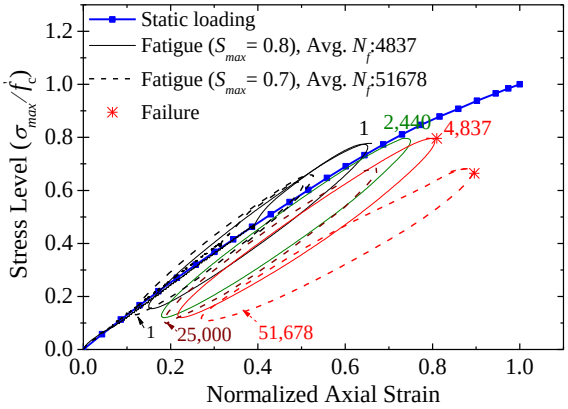

(a) BFS mortar in air

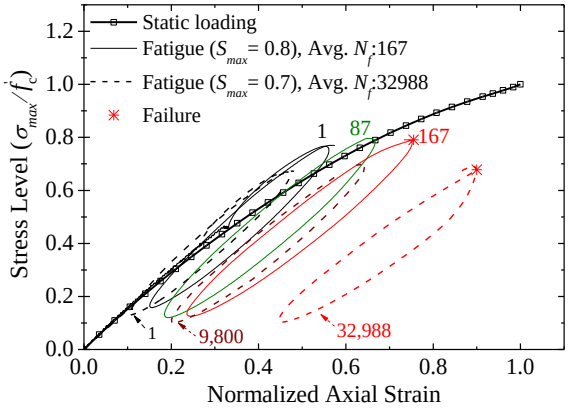

(b) CS mortar in air

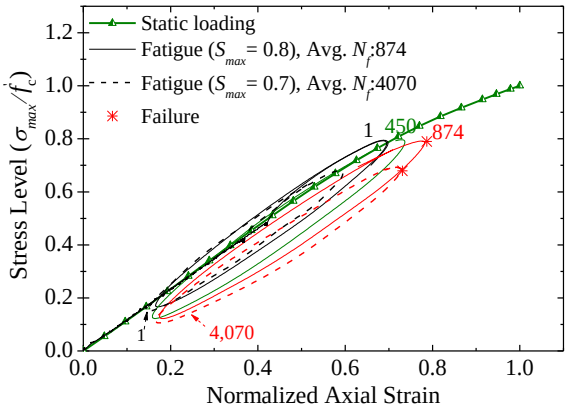

(c) BFS mortar in water

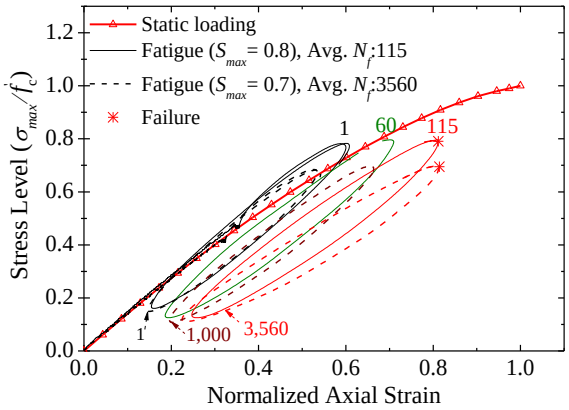

(d) CS mortar in water

Figure 2.3: Stress-strain loops for BFS mortar and CS mortar under cyclic loading

The difference in ultimate strain for static and fatigue test is found at each stress level both in air and water. The specimens under fatigue test failed at less ultimate strain compared to static test. This may be because the failure occurred earlier due to localization inside the mortar specimen under cyclic loading.

2.3.2 Wöhler Curves

The S_{max}-N_f curves for BFS mortar and CS mortar in air and water are shown in Fig. 2.4 depicting the fatigue life of each mortar at different stress levels. The solid line shows the regression line of experimental data for BFS mortar while dash line represents the regression line for CS mortar in both figures (Fig. 2.4(a) and (b)). Regardless of mortar type and environmental condition, a negative linear relationship between stress level and fatigue life is observed, showing increase in fatigue life (N_f) with the decrease in stress level (S_{max}). However, under the same stress level, the fatigue life of CS mortar is shorter compared to BFS mortar both in air and water. This may be attributed to the weaker interfacial transition bond for CS mortar resulting in rapid growth of cracks leading to shorter fatigue life than that of BFS mortar.

Moreover, the fatigue life of mortar in water becomes very short than that in air. This is because of reason that microcracks propagate quickly due to reduction of surface energy released on new microcracks due to surface tension of water. Matsushita and Tokumitsu (1979) and Matsushita (2006) evaluated the fatigue life of concrete immersed in different liquids and found the considerable reduction of fatigue life in water compared to that in air **[7,8]**. The other reasons for the reduction of fatigue life in water are wedge effect of pore water pressure at crack tip due to pumping action of water under cyclic loading and possible leaching of $Ca(OH)_2$ from the interface of aggregates and matrix. The leaching of $Ca(OH)_2$ from the interface of aggregate and matrix increases the porosity inside the cement based material resulting in weakened matrix and change in internal pore water pressure which in turn reduces the compressive strength **[9]**. Due to reduced

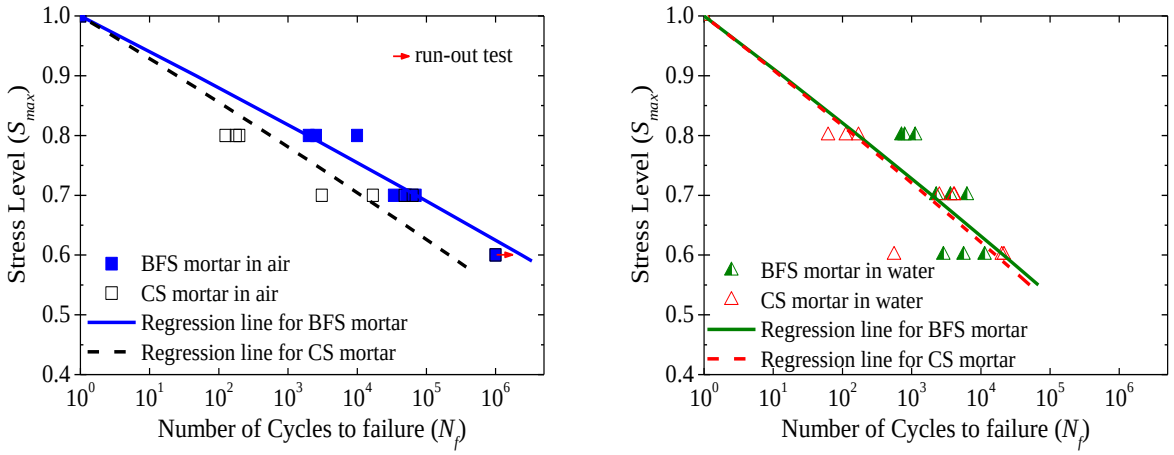

(a) In air (b) In water

Figure 2.4: *S-N* relationships for BFS mortar and CS mortar

compressive strength, the fatigue life of mortar in water is shortened. The leaching phenomenon of $Ca(OH)_2$ is supported by the evidence that surrounding water inside the water tub became turbid during fatigue test. The same phenomenon was observed by Sugata N. and Ozaki S. (1998) **[10]**. It can be seen that the overall fatigue life of BFS mortar is slightly longer than that of CS mortar in air while no difference between CS mortar and BFS mortar in water is observed. The increase in fatigue strength of BFS mortar in air is because of improvement in the interfacial bond between matrix and aggregates and dense matrix due to formation of additional C-S-H gel in BFS mortar. Guo L.P. et al. (2010) and Zhang H. and Tian K. (2011) reported that with the incorporation of ground granulated blast furnace slag (GGBS), the amount of C-S-H gel in matrix and matrix-aggregate interfacial transition zone (ITZ) is increased due to pozzolanic reaction of GGBS grains. This additional C-S-H gel improves the ITZ between matrix and aggregate resulting in better crack resistance and fatigue performance of concrete with slag compared to normal concrete **[11,12]**.

2.3.3 S_{max}-N_f Relationships based on Minimum Stress Ratio

The relationship between the stress ratios and fatigue life is given by Eq. (2.3).

$$log\, N = k\frac{1-S_{max}}{1-S_{min}} \tag{2.3}$$

Where S_{max}, S_{min} are maximum and minimum stress ratios, and k is an experimental constant depending upon moisture content and type of mortar or concrete **[7]**. The regression lines between fatigue life $log\ N$ and $(1 - S_{max})/(1 - S_{min})$ for both types of mortar in air and water are shown in Fig. 2.5. It can be seen that for a constant maximum stress ratio, the fatigue life increases with the increase in minimum stress ratio. The S_{max}-N_f equations for BFS mortar and CS mortar considering minimum stress ratios are developed based on Eq. (2.3) and values of constant (k) for each mortar in air and water are shown in Table 2.4. The value of constant (k) is the slope of regression lines

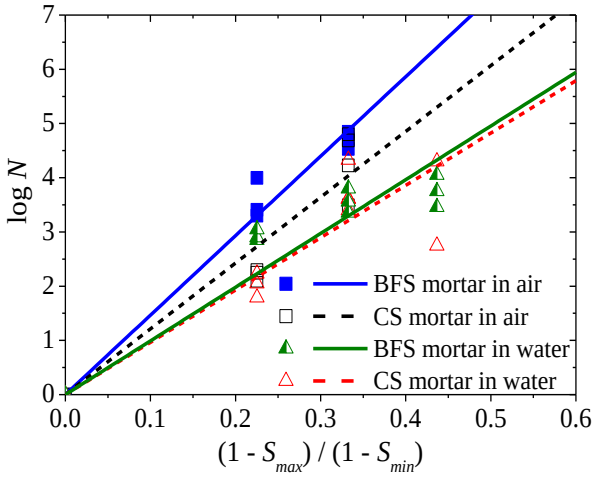

Figure 2.5: Relationship between fatigue life and stress ratios

Table 2.4: Value of experimental constant (k) for BFS mortar and CS mortar

Environmental condition	Mortar type	k	Correlation coefficient (R^2)
Air	BFS	14.66	0.99
	CS	12.14	0.97
Water	BFS	9.91	0.97
	CS	9.65	0.95

which is highest for BFS mortar in air followed by CS mortar in air, while it is almost same for both mortar in water.

2.3.4 Cycle-Strain Curve

The cycle-strain curves represent the development of strain with the increase in number of loading cycle. The cycle ratio, defined as the ratio between cycle number (N) to number of loading cycles until failure (N_f), is used for analysis of fatigue deformation characteristics. The specimens of BFS mortar and CS mortar were not failed at 1 million cycles at 60% stress level in

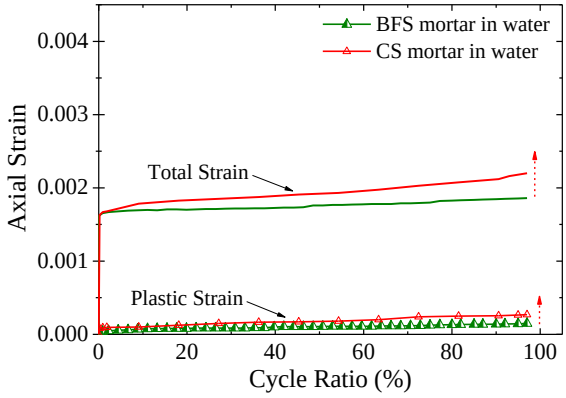

(a) 60% stress level

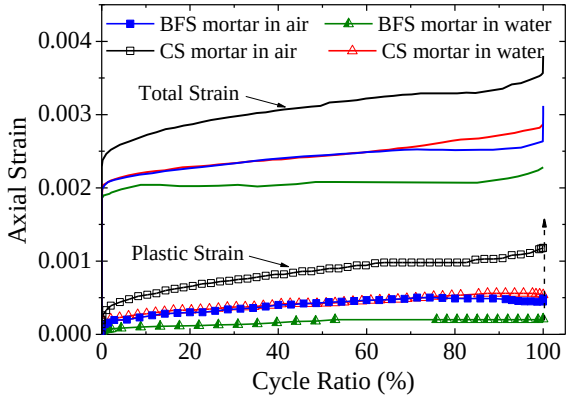

(b) 70% stress level

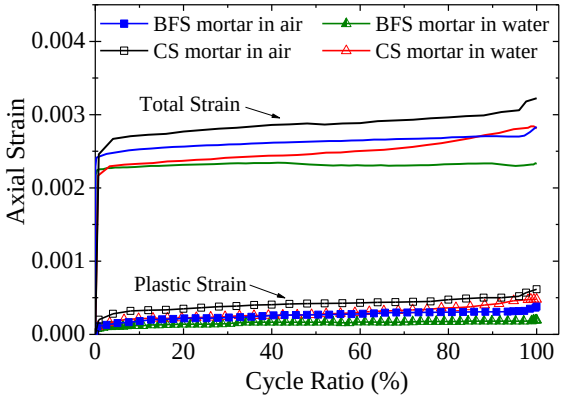

(c) 80% stress level

Figure 2.6: Cycle-strain curves for BFS mortar and CS mortar in air and water

air, for which the strain data are not used for comparison. The total strain and plastic strain are calculated by using the recorded stress-strain loops at different number of loading cycles. The total strain is the axial strain at maximum stress level after certain number of loading cycle, while the plastic strain is determined at zero stress level by extending the line joining points of total strain at maximum stress level and strain at minimum stress level. The strain variation of each mortar under cyclic loading followed the three phases as shown in Fig. 2.6. In Phase-I, the total and plastic strain increased rapidly during the first 5% of total fatigue life due to initiation of microcracks at the location of voids and already existing discontinuities. In Phase-II, there is gradual increase in strain between 5% and 95% of fatigue life, which is due to growth and formation of new microcracks and cyclic creep followed by the joining of microcracks to form macro cracks resulting in rapid increase in strain in Phase-III during last 5% of fatigue life **[13,14]**. It can be seen that Phase-I and Phase-III are mild and shorter for BFS mortar in water as compared to CS mortar. Moreover, the rate of strain development for CS mortar is higher compared to BFS mortar at each stress level both in air as well as in water leading to earlier failure and hence shorter fatigue life. During fatigue test in water, the axial strain very near to failure could not be recorded, which may be because of penetration and disturbance of water and appearance of microcracks due to cyclic loading at location of strain gauges.

2.4 SIMPLIFIED FATIGUE MODEL

2.4.1 Previous Static Stress-Strain Model

In the previous study, Farooq (2016) proposed the static stress-strain relationships of BFS mortar and CS mortar **[15]** based on the concept of elasto-plastic and fracture (EPF) model for concrete developed by Maekawa and Okamura (1983) **[16]**. In EPF model, the stress-strain relationship is given as shown in Fig. 2.7 and Eq. (2.4).

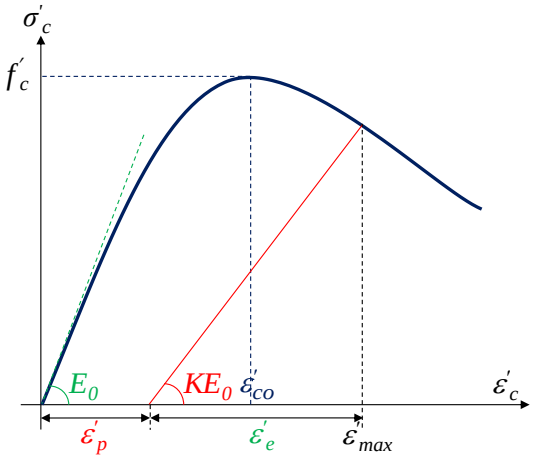

Figure 2.7: Stress-strain relationship

$$\sigma_c^{'} = KE_0\left(\varepsilon_{max}^{'} - \varepsilon_p^{'}\right) \tag{2.4}$$

Where $\sigma_c^{'}$ is compressive stress, $\varepsilon_{max}^{'}$ is maximum compressive strain which is the sum of elastic strain and plastic strain and $\varepsilon_p^{'}$ is plastic strain. K is the fracture parameter and E_0 is the Young's modulus of concrete. Fracture parameter (K) and plastic strain ($\varepsilon_p^{'}$) are the function of maximum compressive strain ($\varepsilon_{max}^{'}$) and strain corresponding to ultimate strength ($\varepsilon_{co}^{'}$). The relationships for fracture parameter (K) and plastic strain ($\varepsilon_p^{'}$) for concrete given in EPF model are shown in Eq. (2.5) and Eq. (2.6) respectively **[16]**.

$$K = \exp\left\{-0.73\frac{\varepsilon_{\max}^{'}}{\varepsilon_{peak}^{'}}\left(1-\exp\left(-1.25\frac{\varepsilon_{\max}^{'}}{\varepsilon_{peak}^{'}}\right)\right)\right\} \tag{2.5}$$

$$\varepsilon_p^{'} = \varepsilon_{\max}^{'} - \frac{20}{7}\varepsilon_{peak}^{'}\left(1-\exp\left(-0.35\frac{\varepsilon_{\max}^{'}}{\varepsilon_{peak}^{'}}\right)\right) \tag{2.6}$$

The mechanical properties of the mortar such as strength, stiffness and deformation characteristics are affected differently compared to that of concrete under the application of load, because of absence of coarse aggregates in mortar. Therefore, the equations for fracture parameter (K) and plastic strain ($\varepsilon_p^{'}$) developed for concrete in EPF model **[16]** as shown in Eq. (2.5) and Eq. (2.6) are not applicable for mortar. To formulate the stress-strain relationships of high strength mortar, Farooq (2016) proposed the relationships for fracture parameter and plastic strain of mortar **[15]** as given in Eq. (2.7) and Eq. (2.8).

$$K = exp\left\{-0.43\left(\frac{\varepsilon_{max}^{'}}{\varepsilon_{peak}^{'}}\right)^{exp\left(0.95\frac{\varepsilon_{max}^{'}}{\varepsilon_{peak}^{'}}\right)}.\left(1-exp\left(-0.74\frac{\varepsilon_{max}^{'}}{\varepsilon_{peak}^{'}}\right)\right)\right\} \tag{2.7}$$

$$\varepsilon_p^{'} = \varepsilon_{peak}^{'}.exp\left(-a+b\,ln\left(\frac{\varepsilon_{max}^{'}}{\varepsilon_{peak}^{'}}\right)\right) = 0 \text{ at } \varepsilon_{max}^{'} = 0 \tag{2.8}$$

Where a and b are the constants and the respective values are shown in Table 2.5 for both types of mortar in air and water. The input for the plastic strain equation are the value of strain corresponding to the ultimate strength of respective mortar as given in Table 2.3 and maximum strain along with the values of constant a and b.

Table 2.5: The value of constant *a* and *b* for BFS and CS Mortar in air and water

Test condition	Mortar type	Constant *a*	Constant *b*
Air	BFS	2.96	1.66
	CS	2.07	1.99
Water	BFS	3.54	1.62
	CS	2.39	2.15

2.4.2 Basic Concept and Formulation of Fatigue Model

In the past studies, the fatigue life models for concrete with respect to time and deformational paths have been developed based on similar concept of elasto-plastic and fracture model to consider the non-linearity of concrete under cyclic compression **[17]** and for the assessment of fatigue life of damaged RC structures **[18]**. In this study, the static model for mortar developed by Farooq (2016) in the previous study **[15]** is extended to propose the simplified fatigue model, which can not only assess the total strain, plastic strain and change in fracture parameter of each mortar at respective number of loading cycle but also predict the fatigue life at different stress level. The model is based on the relationship between the ratio of $\varepsilon'_{p,Ni}/\varepsilon'_{max,Ni}$ and number of loading cycle (N_i) developed for each mortar in air and water at different stress levels using the experimental data. The illustration for prediction of failure of mortar under fatigue is shown in Fig. 2.8. To predict the failure of mortar under cyclic loading, the residual strength of mortar is determined which is equal to the peak stress in the proposed stress-strain relationship under monotonic load. If residual strength of mortar reduces below the maximum applied stress, it implies the failure of the mortar specimen.

The flowchart showing the procedure for determination of change in fracture parameter and prediction of failure is shown in Fig. 2.9. Firstly, the stress strain curve is drawn using the proposed static σ-ε model **[15]** up to maximum stress level, which represents the loading part of first cycle and the maximum strain for the first cycle ($\varepsilon'_{max,1}$) is noted. Thereafter, the maximum

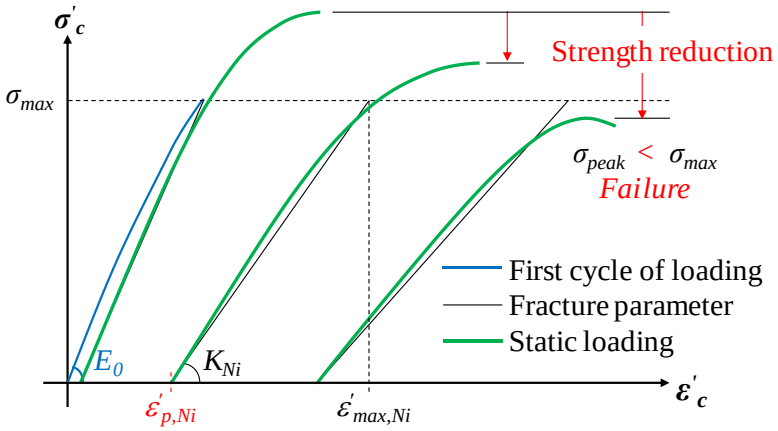

Figure 2.8: Illustration for method of prediction for failure under fatigue loading

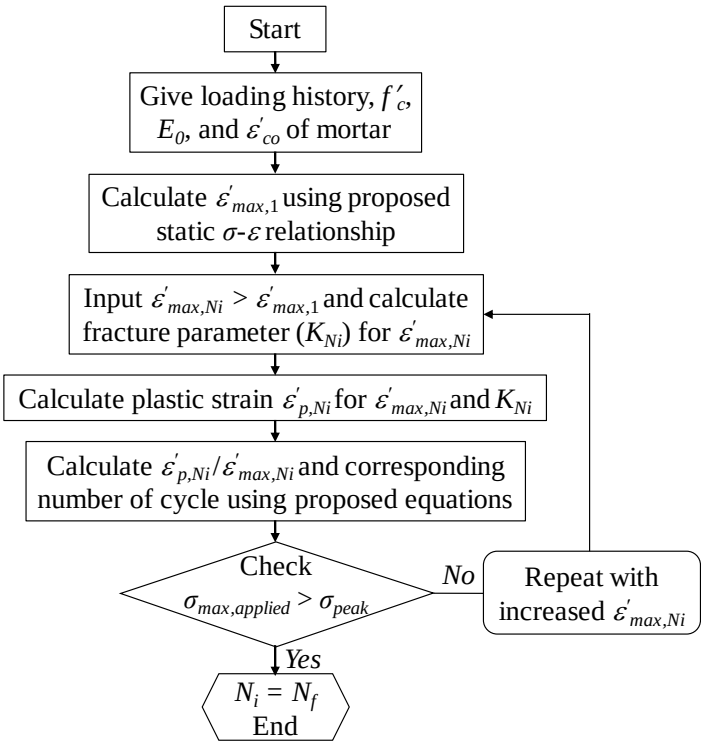

Figure 2.9: Procedure for the calculation of fracture parameter and prediction of fatigue life using proposed fatigue model

strain ($\varepsilon'_{max,Ni}$) greater than that of first cycle is given and corresponding fracture parameter of mortar is calculated. The rate of change of fracture parameter of each mortar under cyclic loading in air is similar to that of calculated by proposed Eq. (2.7) for static stress-strain model, therefore, the equation for fracture parameter under fatigue in air remains same. However, the fracture parameter of mortar under cyclic loading in water decreases rapidly, therefore the Eq. (2.9) and Eq. (2.10) developed for the determination of fracture parameter of BFS mortar and CS mortar under fatigue loading in water will be used. After that, the plastic strain ($\varepsilon'_{p,Ni}$) is determined corresponding to given maximum strain ($\varepsilon'_{max,Ni}$) and calculated fracture parameter (K_{Ni}) using the static stress-strain relationship and the ratio $\varepsilon'_{p,Ni}/\varepsilon'_{max,Ni}$ is calculated. The number of cycle (N_i) corresponding to $\varepsilon'_{p,Ni}/\varepsilon'_{max,Ni}$ is determined using the relationship developed for BFS mortar and CS mortar in air and water as given in *Sec. 2.4.4*. The whole procedure is repeated until the residual strength of mortar becomes less than maximum applied stress showing the failure of mortar specimen. The number of cycle (N_i) will be the end of fatigue life (N_f) of mortar at which the residual strength becomes less than maximum applied stress level.

2.4.3 Fracture Parameter and Plastic Strain Development under Fatigue Loading

The relationship between fracture parameter (K) and normalized axial strain of BFS mortar and CS mortar under fatigue test in air and water along with calculated fracture parameter of mortar and normal concrete is shown in Fig. 2.10. Here the fracture parameter (K) is defined as the ratio

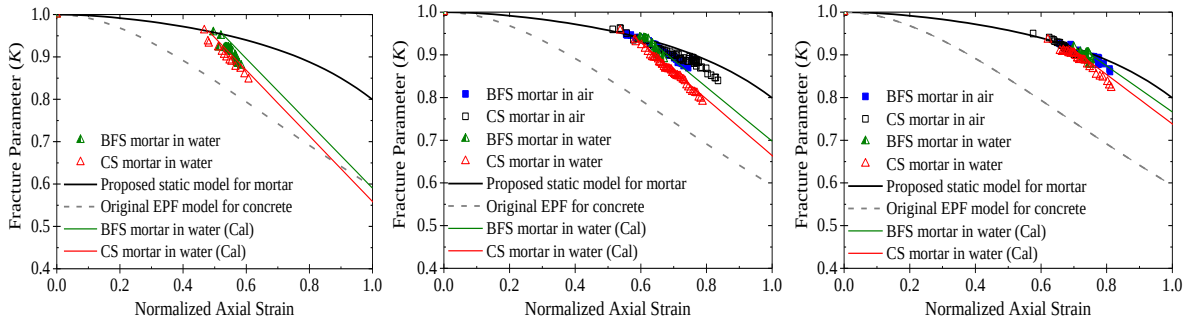

(a) 60% Stress level (b) 70% Stress level (c) 80% Stress level

Figure 2.10: Relationship between fracture parameter (K) and normalized axial strain for BFS and CS mortar in air and water

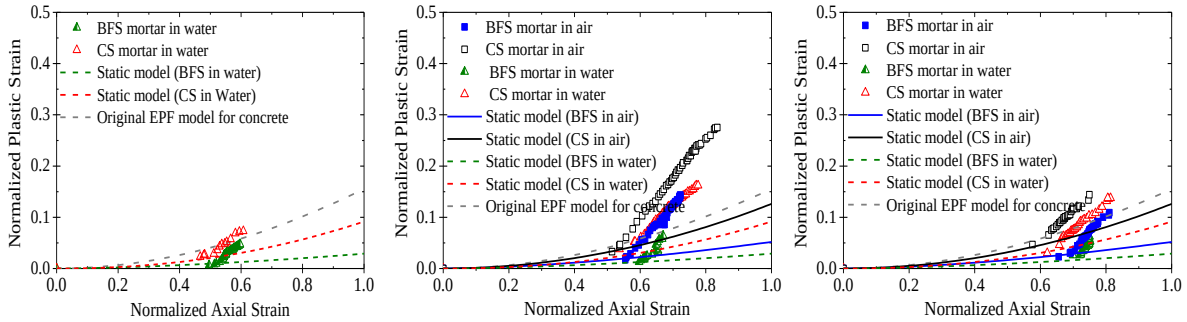

(a) 60% Stress level (b) 70% Stress level (c) 80% Stress level

Figure 2.11: Plastic strain development for BFS mortar and CS mortar under fatigue test in air and water along with calculated by static model

between chord modulus of stress-strain loop at certain loading cycle and initial Young's modulus (E_0) of mortar representing the degree of internal damage of mortar, whereas normalized axial strain is defined as axial strain during each cycle under fatigue loading divided by strain at ultimate compressive strength under static compression test. It is found that the elastic stiffness of concrete reduces rapidly with the increase in axial strain compared to that of mortar in air and water. This is because of the reason that there are more, and large voids present inside the concrete and upon the application of load, the voids are collapsed, and more slip takes place between mortar and coarse aggregates leading to more plastic strain development and resulting in rapid decrease in stiffness of concrete. However, the stiffness of mortar changes at slow rate due to less plastic strain development and failure takes place due to localization inside the mortar.

The stiffness change of each mortar under cyclic loading in air is almost similar to the proposed fracture parameter Eq. (2.7) for monotonic load, however, it is observed that the fracture parameter of both mortars decreases rapidly under cyclic loading at each stress level in water. This may be attributed to the fact that in addition to reduced surface energy of saturated specimens, pumping action of surrounding water is pronounced during unloading and reloading of cyclic loading resulting in rapid degradation. The other possible reason is the leaching of $Ca(OH)_2$ from ITZ of mortar, which is supposed to take place more in CS mortar because most of $Ca(OH)_2$ in

BFS mortar is consumed in producing more C-S-H gel. Keeping in view the rapid deterioration of stiffness of mortar in water, the relationships for fracture parameter of BFS mortar and CS mortar under fatigue test in water are formulated as given in Eq. (2.9) and Eq. (2.10) respectively.

$$K_{water,Ni} = K_{s,1} - \left\{ \frac{0.41}{S_{max}^{1.22}} \left(\frac{\varepsilon'_{max,Ni} - \varepsilon'_{max,1}}{\varepsilon'_{peak}} \right) \right\} \quad (2.9)$$

$$K_{water,Ni} = K_{s,1} - \left\{ \frac{0.46}{S_{max}^{1.02}} \left(\frac{\varepsilon'_{max,Ni} - \varepsilon'_{max,1}}{\varepsilon'_{peak}} \right) \right\} \quad (2.10)$$

Where $\varepsilon'_{max,Ni}$ is the maximum strain corresponding to N_i cycle and $K_{s,1}$ is the fracture parameter for first loading cycle corresponding to $\varepsilon'_{max,1}$ as determined by the Eq. (2.7). The fracture parameter calculated by proposed Eq. (2.9) and Eq. (2.10) is close to the obtained during fatigue test in water.

For each stress level, the axial strain of BFS mortar is less than that of CS mortar both in air and water. Figure 2.11 represents the plastic strain development of both BFS mortar and CS mortar under fatigue loading in air and water along with equivalent plastic strain of each mortar calculated by the proposed static model and equivalent plastic strain for normal concrete calculated by original EPF Model. It has been found that plastic strain development for each mortar under cyclic loading is not in close agreement with the equivalent plastic strain of mortar and normal concrete calculated by the model under static loading. This is because of the reason that during fatigue test, two types of plastic strains are involved i.e. time independent strain calculated by the plastic strain equation of static model and time dependent strain due to creep during cyclic loading **[19]**. Moreover, the increased creep is resulted due to changes caused by the additional energy imparted during cyclic loading **[20]**. It is observed that higher plastic strain is developed in CS mortar due to weak bond between crushed sand and matrix compared to BFS mortar both is air as well as in water, therefore fatigue life of CS mortar might be shortened. Moreover, the amount of plastic strain developed in air for both types of mortars is higher than in water.

2.4.4 Relationship between $\varepsilon'_{p,Ni}/\varepsilon'_{max,Ni}$ and $logN_i$

The relationship between the ratio of plastic strain to maximum strain ($\varepsilon'_{p,Ni}/\varepsilon'_{max,Ni}$) and respective number of loading cycle ($\log N_i$) is formulated based on experimental data of fatigue test of BFS mortar and CS mortar in air and water at different stress levels as shown in Fig. 2.12. It is important to note that for same number of cycle, the ratio $\varepsilon'_{p,Ni}/\varepsilon'_{max,Ni}$ is higher for higher stress level for both mortar in air and water. For same stress level, higher ratio $\varepsilon'_{p,Ni}/\varepsilon'_{max,Ni}$ is observed in CS mortar compared to BFS mortar because of more plastic strain occurred in CS mortar. The relationships between $\varepsilon'_{p,Ni}/\varepsilon'_{max,Ni}$ and $\log N_i$ for BFS mortar and CS mortar can be realized by exponential approach as given in Eq. (2.11) and values of parameter A, B and C can be calculated

using the relationships shown in Table 2.6. Here, parameter A, B and C are the function of normalized maximum stress level (S_{max}), which consider the slope of $\varepsilon'_{p,Ni}/\varepsilon'_{max,Ni}$ with the increase in number of loading cycles (N_i). It can be seen that the experimental values are close to that the calculated curves.

$$\log N_i = A\left(1-\exp\left(-B\frac{\varepsilon'_{p,Ni}}{\varepsilon'_{max,Ni}}\right)\right)-C \qquad (2.11)$$

Table 2.6: Summary of Parameter A, B and C for Eq. (2.11)

Test condition	Mortar type	Parameter		
		A	B	C
Air	BFS	$11.71/(0.7S_{max})^{0.15}$	$11.5(12.5S_{max})^{0.63S_{max}}$	$(20S_{max})^{0.8}$
	CS	$10.46/(1.7S_{max})^{0.45}$	$4(4.65S_{max})^{1.2S_{max}}$	$(5.22S_{max})^{1.25}$
Water	BFS	$6.85/(0.21S_{max})^{0.24S_{max}}$	$50(1.25S_{max})^{0.2S_{max}}$	$(15.1S_{max})^{0.75}$
	CS	$6.86/(0.1S_{max})^{0.3S_{max}}$	$26(3S_{max})^{0.1S_{max}}$	$(7.5S_{max})^{1.3}$

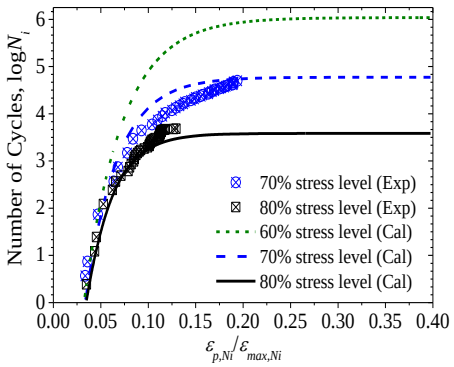

(a) BFS mortar in air

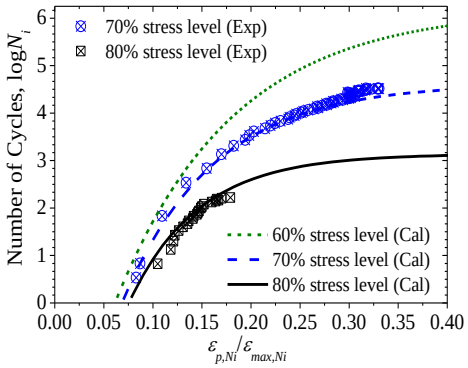

(b) CS mortar in air

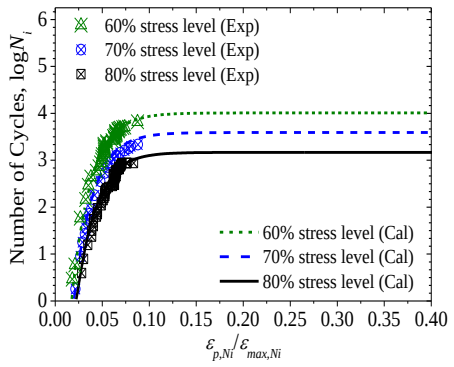

(c) BFS mortar in water

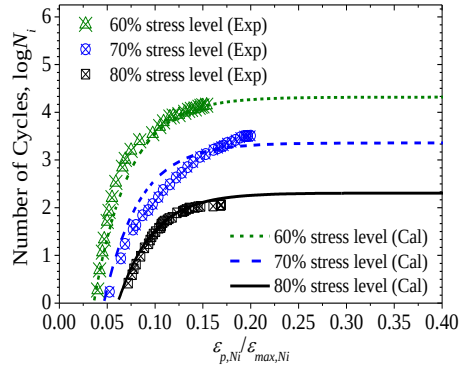

(d) CS mortar in water

Figure 2.12: Relationship between $\varepsilon'_{p,Ni}/\varepsilon'_{max,Ni}$ and logN_i for BFS and CS mortar in air and water

2.4.5 Comparison of Proposed Model and Experiment

The fatigue life of each mortar is calculated at different stress levels using the proposed simplified fatigue model in air and water as shown in Fig. 2.13. It can be seen that the calculated fatigue life at different stress levels is within the range of experimentally measured fatigue life showing the satisfactory agreement between the two. The difference in the slope of *S*-*N* curve obtained from regression of experimental data and calculated one is because of the reason that the regression lines of experimental data are bound at maximum stress level equal to one. Moreover, the fracture parameter change for BFS mortar and CS mortar at particular number of loading cycle is calculated using the presented simplified fatigue model at different stress levels in air and water. The calculated results are compared with those of obtained from experiments as shown in Fig. 2.14. The numbers in the figure represent the loading cycle number for which experimentally measured stress-strain loops and calculated fracture parameter are drawn. Moreover, the fatigue life of each mortar at failure is also predicted in air and water using the proposed model. It can be seen that overall, there is good agreement between the calculated and experimental results. However, the calculated maximum strain for first loading cycle is more compared to obtained during the experiment because the maximum stress level could not be achieved during first few cycles of experiment. The strain near to failure for each mortar during fatigue test at 60% stress level in water could not be recorded accurately, this may be because of penetration of water and appearance of cracks at the location of strain gauges. Therefore, the last measured loading cycle is compared with the calculated fracture parameter at 60% stress level in water.

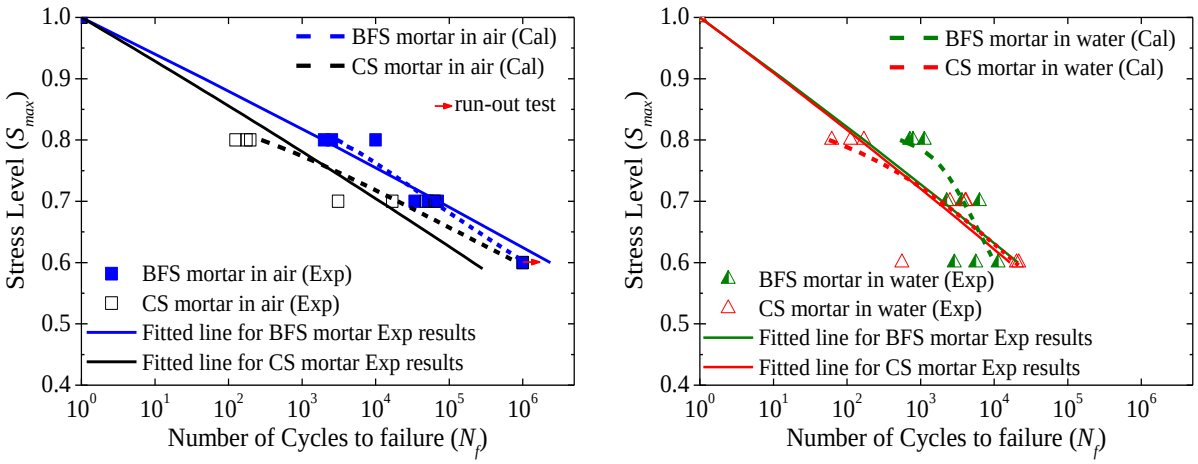

(a) In air (b) In water

Figure 2.13: Comparison between calculated and experimental *S*-*N* relationships for BFS mortar and CS mortar

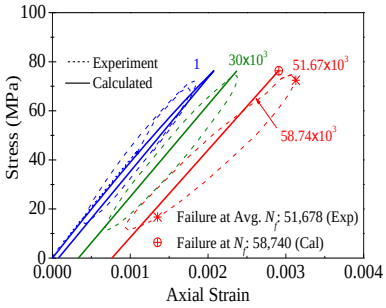

(a) BFS in air at 70% S_{max}

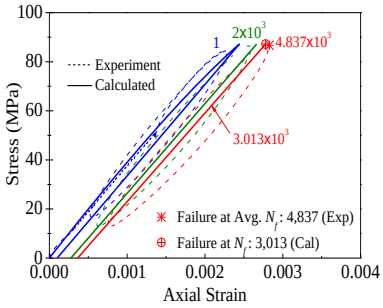

(b) BFS in air at 80% S_{max}

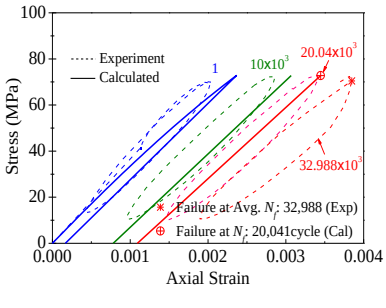

(c) CS in air at 70% S_{max}

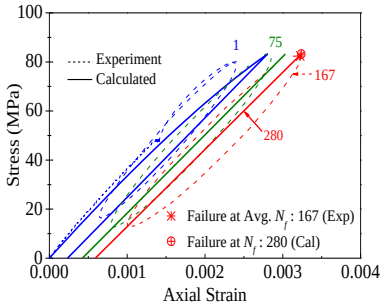

(d) CS in air at 80% S_{max}

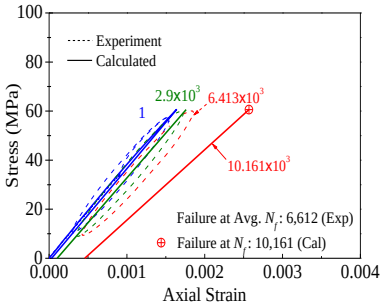

(e) BFS in water at 60% S_{max}

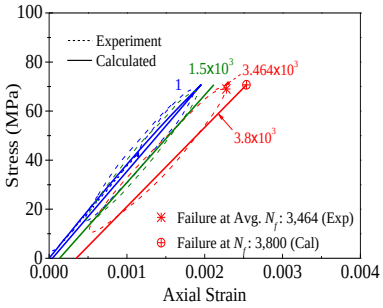

(f) BFS in water at 70% S_{max}

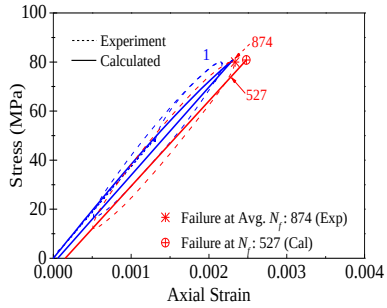

(g) BFS in water at 80% S_{max}

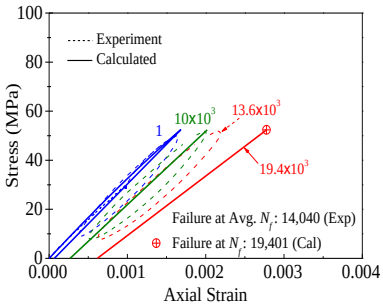

(h) CS in water at 60% S_{max}

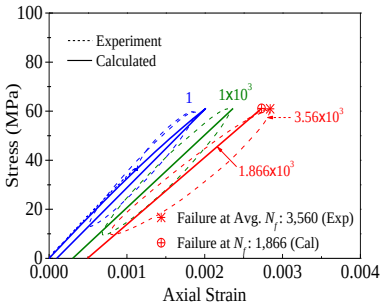

(i) CS in water at 70% S_{max}

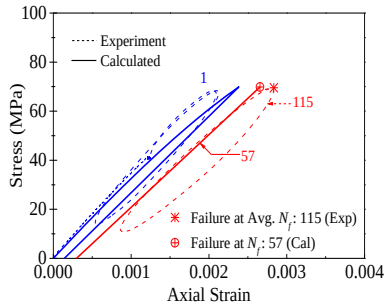

(j) CS in water at 80% S_{max}

Figure 2.14: Comparison between experimental stress strain loops and calculated fracture parameter for BFS mortar and CS mortar

The drawback of the proposed model for fatigue is that it is not applicable for low cycle fatigue and it is limited to high cycle fatigue.

2.5 CONCLUSIONS OF THIS CHAPTER

In this chapter, the fatigue behavior of mortar with BFS fine aggregates compared with mortar having crushed sand in air and water is studied and a simplified fatigue model is proposed. Following conclusions can be drawn:

1. With the incorporation of BFS sand as full amount of fine aggregates, the fatigue life of BFS mortar in air is enhanced compared to CS mortar because less plastic strain is developed when BFS sand is used due to improvement in compressive strength at longer age resulting in prolonged fatigue life. However, the overall fatigue performance of BFS mortar in water is almost similar to CS mortar, while the fatigue life of each mortar in water has reduced significantly compared to fatigue life in air.
2. At each stress level, the rate of plastic strain development in CS mortar is rapid compared to BFS mortar both in air and water, resulting in rapid degradation and shorter fatigue life of CS mortar.
3. The stress-strain model under static loading is extended to propose a simplified fatigue model, which can not only assess the plastic strain, maximum strain and change in fracture parameter at different number of loading cycles, but it can also predict the fatigue life of each mortar at different stress levels in air and water. The comparison between the results calculated by proposed simplified fatigue model and experimental results provides satisfactory agreement.

REFERENCES

[1] Beata L. P. (2010). "Influence of Anti-foaming admixture and polycarboxylic superplasticizer type on fresh and hardened properties of Self-compacting mortar." Journal of Architecture Civil Engineering Environment, Vol. 3, pp. 61-72.

[2] JIS A1108:2006 (2006), Standard Test Method for Compressive Strength of Concrete.

[3] Kesler C.E. (1953). "Effect of Speed of Testing on Flexural Fatigue Strength of Plain Concrete." Highway Research Board, Vol. 32, pp. 251-258.

[4] Mederios A., Zhang X., Ruiz G., Yu R.C. and Velasco M.S.L. (2015). "Effect of the Loading Frequency on the Compressive Fatigue Behavior of Plain and Fiber Reinforced Concrete." International Journal of Fatigue, Vol. 70, pp. 342-350.

[5] Sparks P.R., and Menzies J.B. (1973). "The Effect of Rate of Loading upon Static and Fatigue Strength of Concrete in Compression." Magazine of Concrete Research, Vol. 75, No. 83, pp. 73-80.

[6] Wittmann F. H., Sun Z. and Zhao T. (2010). "Surface energy and fracture energy." Fracture Mechanics of Concrete and Concrete Structures – Recent Advances in Fracture Mechanics of Concrete, Korea Concrete Institute, Seoul, ISBN 978-89-5708-180-8.

[7] Matsushita H. and Onoue K. (2006). "Influence of Surface Energy on Compressive

Strength of Concrete under Static and Dynamic Loading." Journal of Advanced Concrete Technology, Vol. 4, No. 3, pp. 409-421.

[8] Matsushita H. and Tokumitsu Y. (1979). "A study on compressive fatigue strength of concrete considered survival probability." Journal of Materials, Concrete Structures, Pavements, JSCE, Vol. 284, pp. 127-138.

[9] Cheng A., Chao S.J., and Lin W.T. (2013). "Effects of Leaching Behavior of Calcium Ions on Compression and Durability of Cement-Based Materials with Mineral Admixtures." Materials, Vol. 6, pp. 1851-1872, DOI:10.3390/ma6051851.

[10] Sugata N. and Ozaki S. (1998). "Fatigue Properties of High-Strength Concrete with Blast Furnace Slag." Concrete under Severe Conditions: Environment and Loading, Vol. 2, pp. 841-849.

[11] Guo L.P., Carpinteri A., Spagnoli A. and Sun W. (2010). "Experimental and Numerical Investigation on Fatigue damage propagation and Life Prediction of High-Performance Concrete containing Reactive Mineral Admixture." International Journal of Fatigue, Vol. 32, pp. 227-237.

[12] Zhang H. and Tian K. (2011). "Properties and Mechanics on Flexural Fatigue of Polypropylene Fiber Reinforced Concrete containing Slag." Journal of Wuhan University of Technology-Mater. Sci. Ed. Vol 26, No. 3, pp 533-540.

[13] Xiao J., Li H., Yang Z. (2013). "Fatigue behavior of recycled aggregate concrete under compression and bending cyclic loadings." Journal of Construction and Building Material, Vol. 38, pp. 681-688.

[14] Hümme J., Von der Haar C., Lohaus L., Steffen M. (2015). "Fatigue behaviour of a normal-strength concrete – number of cycles to failure and strain development." *fib* Journal of Structural Concrete, DOI: 10.1002/suco.201500139.

[15] Farooq M.A. (2016). "Static and fatigue behavior of mortar with blast furnace slag as fine aggregates in air and water." Masters' Dissertation, Hokkaido University, Japan.

[16] Maekawa K. and Okamura H. (1983). "The deformational behavior and constitutive equation of concrete using elasto-plastic and fracture model." Journal of the Faculty of Engineering, The University of Tokyo, Vol. XXXVII, No.2, pp. 253-328.

[17] El-Kashif K. F. and Maekawa K. (2004). "Time-Dependent Non-linearity of Compression Softening in Concrete." J. of Advanced Concrete Technology, Vol. 2, No. 2, pp. 233-247.

[18] Maekawa K., Toongoenthong K., Gebreyouhannes E. and Kishi T. (2006). "Direct Path-Integral Scheme for Fatigue Simulation of Reinforced Concrete in Shear." Journal of Advanced Concrete Technology, Vol. 4, No. 1, pp. 159-177.

[19] Sato M., Sato Y. and Kakuta Y. (2001). "Deformational Characteristic of Concrete under Cyclic Loading." Concrete Journal of JCI, 2001; Vol. 23, pp. 1063-1068.

[20] Whaley C.P., and Neville A.M. (1973). "Non-elastic deformation of concrete under cyclic compression." Magazine of Concrete Research, Vol. 25, No. 84, pp. 145-154.

Chapter 3

STATIC BEHAVIOR OF HIGH STRENGTH CONCRETE UNDER FREEZING AND THAWING – EXPERIMENTAL AND MODELING

3.1 GENERAL

In Chapter 2, it is found that high strength BFS mortar exhibit overall slightly improved fatigue behavior compared to ordinary high strength mortar in air. However, the mechanical properties of AE and non-AE high strength concrete with BFS fine aggregates for intact and frost-damaged specimens are not known, and the constitutive laws for such concrete are not available. Therefore, in this chapter, the experimental investigation is carried out to evaluate the change in mechanical properties of AE and non-AE high strength concrete with BFS fine aggregates with respect to increase in number of freezing and thawing cycles (FTC) and FTC induced plastic strain. The results are compared with those of AE concrete of normal strength and high strength. Moreover, considering the different rate of degradation of mechanical properties such as stiffness and plastic deformation of high strength concrete in comparison with normal concrete, the stress-strain relationships for intact and frost-damaged high strength concrete are formulated based on the elasto-plastic and fracture model. The calculated results using the proposed model are compared with those of obtained from the experiments.

3.2 EXPERIMENTAL DETAILS

3.2.1 Materials, Mix Proportions and Specimen Preparation

Four series of concrete specimens are used in this study, non-air entrained blast furnace slag concrete (NAEBFS), air entrained blast furnace slag concrete (AEBFS), air entrained high strength normal concrete (AEHSN) and air entrained normal strength normal concrete (AENSN). Ordinary Portland cement (OPC) is used as binder in NAEBFS and AENSN concrete while high early strength Portland cement (HESPC) is used in AEBFS and AEHSN concrete. The density of OPC and HESPC are 3.15 g/cm^3 and 3.13 g/cm^3, while the Blaine fineness are 3300 cm^2/g and 4490 cm^2/g respectively.

In the preparation of NAEBFS and AEBFS concrete specimens, BFS sand is used as full amount of fine aggregates which shows pozzolanic properties because of its amorphous structure containing a large amount of silica and alumina. For AEHSN and AENSN concrete specimens, crushed river sand is used as fine aggregates. The particle size of fine aggregates used in this study ranges from 0.15 to 5 mm. The physical properties of fine aggregates are given in Table 3.1. Table

Table 3.1: Physical properties of fine aggregates

Property	Crushed sand	Blast furnace slag sand
Saturated density (g/cm^3)	2.63	2.78
Fineness modulus	2.96	2.21

Table 3.2: Mix proportions of AEBFS, AEHSN, NAEBFS and AENSN concrete

Series	W/C (%)	AC (%)	s/a (%)	Unit content (kg/m^3)					WR	T	AE	AF
				W	C	BFS	CS	G	(C x %)			
NAEBFS	40	2.0	43	153	383	839	0	1065	1.1	0.04	-	0.03
AENSN	65	4.5	48	170	262	0	885	967	0.4	-	0.003	-
AEHSN	43	4.5±1	44	158	367	0	786	1012	0.4	-	0.50	-
AEBFS	43	4.5±1	45	158	367	831	0	1012	0.75	0.04	2.00	2.00

W: water, C: binder, AC: Air content, s/a: sand to aggregate ratio, BFS: Blast furnace slag sand, CS: crushed sand, G: Gravel, WR: High-performance air entraining water reducing admixture, T: Thickener, AE: Air-entraining agent, AF: Anti-foaming agent.

3.2 presents the mix proportion of AEBFS, AEHSN, NAEBFS and AENSN concrete. The polycarboxylate type of high-performance air entraining water reducing admixture is used in all types of concrete. In addition, the air content inside the NABFS and AEBFS concrete is controlled by using antifoaming agent.

The prismatic specimens of NAEBFS and AENSN concrete were casted with dimensions (H x W x L) of (100 x 100 x 400) mm, while cylindrical specimens measuring (100Φ x 200) mm were prepared for AEHSN and AEBFS series. After 36-h of casting, the specimens were demolded followed by curing of NAEBFS and AENSN concrete for 7 days by water moist jute sheets and the AEHSN and AEBFS concrete for 28 days in water at room temperature. Later, the specimens were stored in controlled temperature at 20^{o}C until the start of freeze-thaw test.

3.2.2 Test Method

3.2.2.1 Freeze-thaw Test

The cuboidal specimens of (100 x 100 x 200) mm were used for freeze-thaw test for NAEBFS and AENSN concrete and cylindrical specimens measuring (100Φ x 200) mm for AEHSN and AEBFS concrete. The end surfaces and 1-cm edges of the specimens were coated with epoxy to protect those locations against frost damage for mechanical tests. To measure the strain variation during freeze-thaw test, the foil strain gauges of 70 mm gauge length were attached to the surface of specimens both in axial and lateral directions. Firstly, the surface of specimens was polished using sand paper and a thin layer of epoxy adhesive was spread at the location of strain gauge and dried for 24-h. After that, the surface of epoxy adhesive was smoothened using the sand

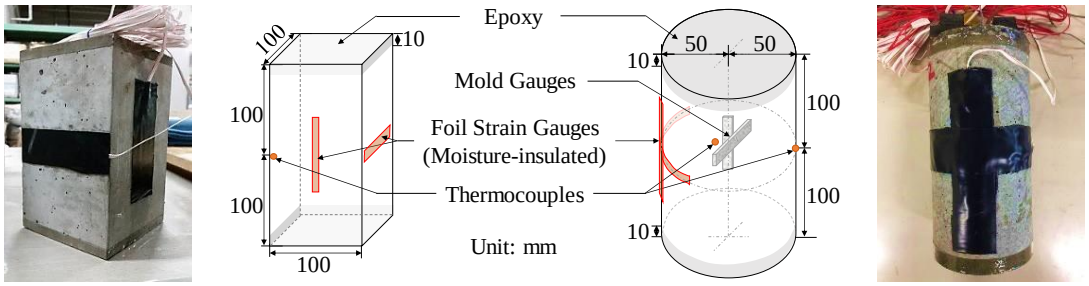

(a) NAEBFS and AENSN specimens (b) AEBFS and AEHSN specimens

Figure 3.1: Description of specimens for freeze-thaw test

paper and strain gauges were attached using the same adhesive and pressed for 24-h for proper attachment. Lastly, a coating layer of moisture proof epoxy was applied over the strain gauges to protect them during freeze-thaw test. The insulation tape was also pasted to further protect the strain gauges from moisture. In addition to the foil gauges, the mold gauges of 30 mm gauge length were placed at the center of the cylindrical molds of AEBFS and AEHSN specimens both in axial and lateral directions prior to casting. The temperature change during the freeze-thaw test was recorded using the thermocouples near the center and at the surface of specimen. The description of specimens is shown in Fig. 3.1.

The freeze-thaw test was performed in accordance with ASTM C-666 type-A **[1]** in 3% NaCl solution with the length of each freeze-thaw cycle (FTC) of 8-h ranging between +20°C and -25°C. The test was started at the age of 3¾ months for NAEBFS and AENSN concrete specimens, while at 5½ months for AEHSN and AENSN specimens. Prior to freeze-thaw test, the specimens were submerged in 3% NaCl solution for proper saturation inside the specimens. Then, the specimens were put inside the rubber tubes filled with 3% NaCl solution such that the top surface of specimen is located around 25 mm below the level of solution. The rubber tubes were then placed in the thermal exchange fluid of the freeze-thaw chamber. The wires of strain gauges and thermocouples were attached to the data logger for recording the data measurement during the freeze-thaw test. One thermocouple was also placed in the chamber to record the temperature variation of thermal exchange fluid. Figure 3.2 represents the set-up of freeze-thaw test.

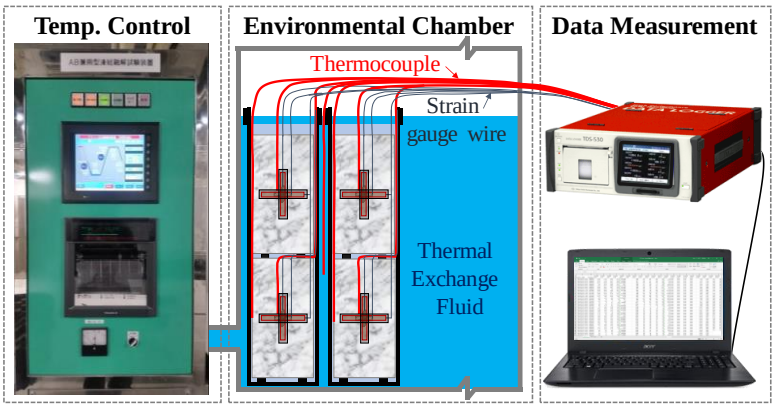

Figure 3.2: Freeze-thaw test setup

Figure 3.3: Ultrasonic pulse wave velocity setup

During the thawing phase at the end of specific number of FTC, the concrete specimens were taken out from FT chamber and the relative dynamic elastic modulus was measured through ultrasonic pulse wave velocity method by attaching the transmitter and receiver along the longitudinal axis of specimen as shown in Fig. 3.3. Moreover, the mass loss of the concrete specimens was also determined by measuring the weight of oven dried scaled mass collected from the rubber tubes. At certain number of FTC, some specimens of each concrete were taken out from the freeze-thaw chamber and stored until the commencement of static compression tests.

3.2.2.2 Static Compression Test

The uniaxial static compression tests were performed on three specimens of each concrete for different frost damage levels at the age of 13½ months for NAEBFS and AENSN concrete and 11 months for AEBFS and AEHSN concrete in accordance with ASTM C39/C39M–14 **[2].** The size of intact and frost damaged cuboidal specimens of NAEBFS and AENSN concrete was cut to (80 x 80 x 160) mm using concrete cutter just before static compression test as the stable compressive strength for prismatic specimens can be achieved with the aspect ratio of ≥2.0 **[3]**. The end surfaces of the concrete specimens were made smooth and parallel to the hinge surface placed between loading platen and specimen. The static compression tests were carried out using displacement-controlled method. The strain measurement was made using axial strain gauges of 60 mm gauge length and lateral strain gauges of 30 mm gauge length. Before attaching strain gauges, the surface of frost-damaged concrete specimens was made smooth by grinding and the strain gauges were attached using adhesive. A steel hinge was placed in between the loading platen of machine and top surface of specimen to avoid any eccentricity of loading. The loading arrangement for static tests is shown in Fig. 3.4.

After static compression tests, the static unloading and reloading (U&R) tests were performed on the specimens of each concrete for each damage level to examine the change in mechanical properties. The loading part of each cycle was applied up to various load levels using the same procedure as that of static tests, however, the unloading was done using manual control. After the application of some cycles during static (U&R) test, the specimens were loaded to failure.

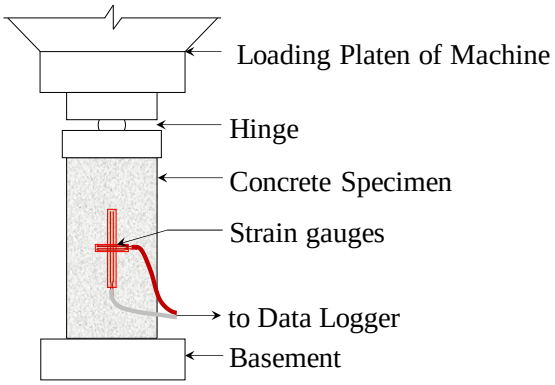

Figure 3.4: Loading arrangement for static test

3.3 RESULTS AND DISCUSSION

3.3.1 Freeze-thaw Properties

3.4.2.1 Temperature Variation

The histories of input temperature of FTC and recorded on the surface, at the center of specimens and inside thermal exchange fluid for 225-FTC are shown in Fig. 3.5. The temperature changes inside the thermal exchange fluid and on the surface of specimens well followed the input temperature. However, the temperature reached at the center of specimens of AEBFS and AEHSN concrete was bit behind the input temperature, and the maximum and minimum temperature reached to +15.5±0.5ºC and -24.5±0.5ºC at the end of each FTC. The similar tendency of temperature change was observed for the whole FT test.

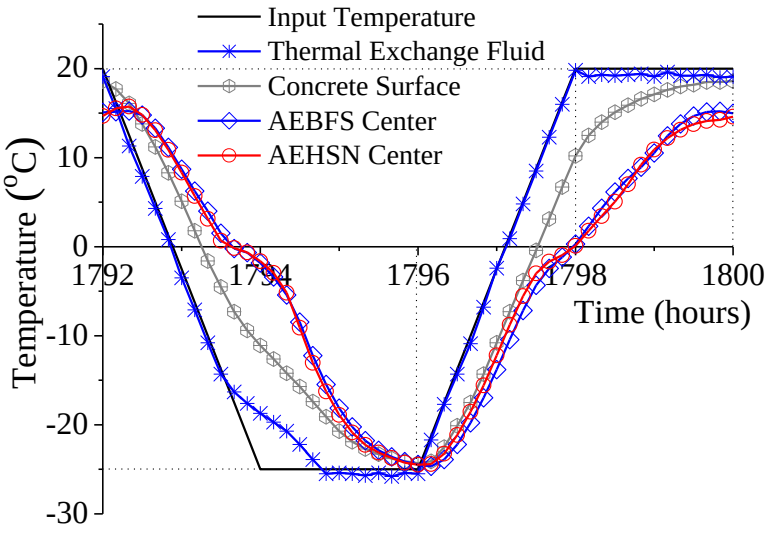

Figure 3.5: Temperature history observed (225th FTC)

3.4.2.2 Relative Dynamic Modulus of Elasticity and Mass Loss

The transit time of ultrasonic pulse wave (t_u) transmitting through the specimens was recorded during the thawing phase at the interval of each 10-FTC for NAEBFS and AENSN specimens and at each 15-FTC for AEBFS and AEHSN specimens and corresponding velocity of wave (V_u) was determined. The dynamic elastic modulus and relative dynamic modulus of elasticity (RDME) of BFS concrete and normal concrete specimens were calculated using Eq. (4.1) proposed by Ogata H. et al. (2002) **[4]** and Eq. (4.2) respectively.

$$E_d = 4.039V_u^2 - 14.438V_u + 20.708 \quad (4.1)$$

$$RDME\ (\%) = (E_{dn} / E_{d0}) \times 100 = (t_{un} / t_{u0}) \times 100 \quad (4.2)$$

Where,

E_d : dynamic modulus of elasticity, (GPa)

V_u : velocity of passing ultrasonic wave (km/sec)

E_{dn} : E_d at respective FTC (GPa)

E_{d0} : E_d at start of F-T test (GPa)

t_{un} : transit time of wave at respective FTC (μ-s)

t_{u0} : transit time of wave at start of F-T test (μ-s)

The RDME and mass change of specimens of each concrete corresponding to FTC number are shown in Fig. 3.6((a) & (b)). The RDME of NAEBFS specimens did not decrease before 150 cycles. After that, it started to reduce rapidly with the increase in number of FTC compared to other concrete specimens because of no AE agent inside NAEBFS concrete. No significant reduction in

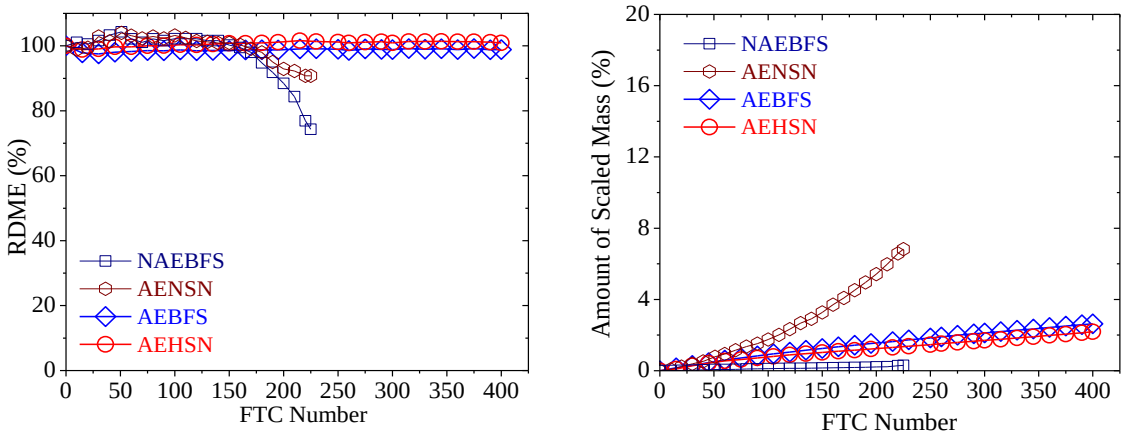

(a) RDME Change (b) Mass loss

Figure 3.6: Relative dynamic modulus of elasticity change and mass loss

RDME was found during the whole freeze-thaw test for AEBFS, AENSN and AEHSN concrete, which is because the AE voids in air entrained concrete specimens provided the space to compensate the freezing of the pore water preventing the micro-cracking inside the specimens. However, the amount of scaled mass for AENSN concrete is more than that of other concrete types, which might be because strength of AENSN is less compared to other series. Moreover, the amount of scaled mass for AEBFS concrete is almost same as that of AEHSN and more than that of non-AE BFS concrete. The relationship between RDME and mass loss is shown in Fig. **3.7**. It is found that the rate of reduction in RDME with the increase in mass loss is slow for AE concrete regardless of compressive strength. However, the RDME reduced rapidly with the mass loss for NAEBFS concrete, which is because of internal micro-cracking induced by FTC due to absence of AE voids. The surface of frost damaged AEBFS and AEHSN specimens at the end of 230-FTC in this study is shown in Fig. 3.8 along with 225-FTC damaged specimens of NAEBFS and AENSN concrete.

3.4.2.3 Plastic Strain Growth

The strain variations during each FTC with the change in temperature were recorded using the strain gauges attached to each concrete. The FTC induced residual strain in axial and lateral

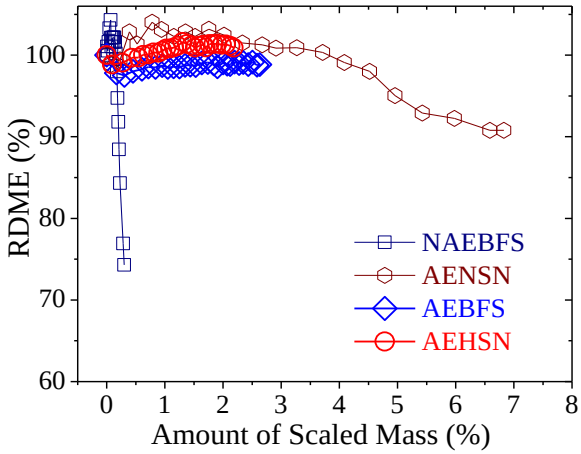

Figure 3.7: Change in RDME with mass loss

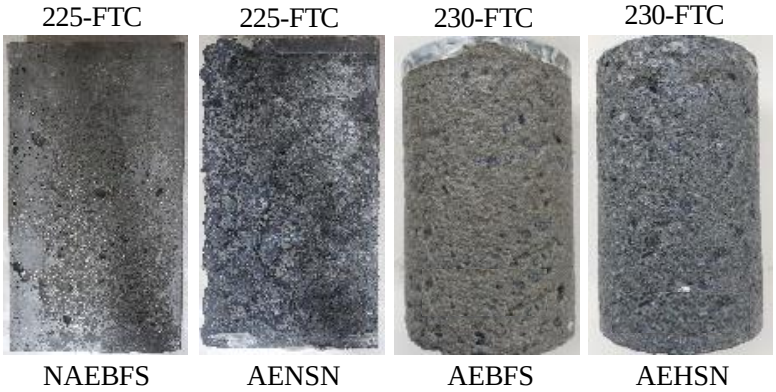

Figure 3.8: Surfaces of frost-damaged concrete

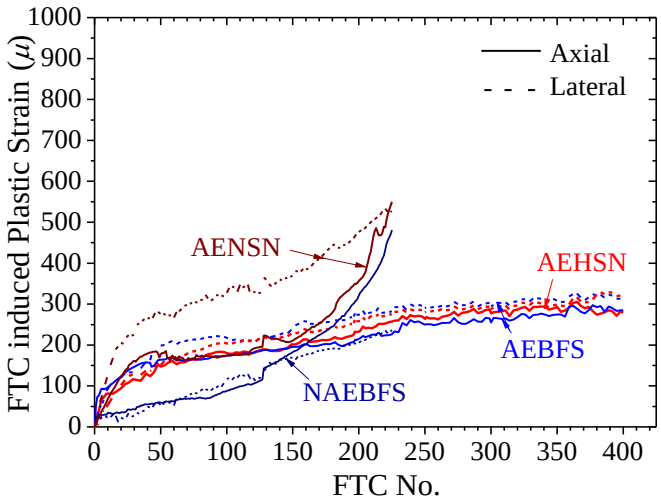

Figure 3.9: FTC induced plastic tensile strain

direction of each concrete at the end of different FTC was determined at maximum temperature during thawing as shown in Fig. 3.9. The plastic strain was increased with the increase in number of FTC, because the hydraulic pressure is generated owing to expansion caused by freezing of water inside the pores of saturated concrete during freezing and thawing resulting in irreversible strain. This irreversible strain is accumulated with the increase in FTC number.

The axial and lateral plastic strain of NAEBFS concrete was almost same up to 125-FTC, after that axial strain increased rapidly compared to lateral strain. While more lateral strain occurred in AENSN concrete compared to axial strain. Moreover, because of high strength and provision of AE voids in both AEBFS and AEHSN concrete, the cracking inside the concrete was prevented because of enough pores to accommodate the expansion of ice. Therefore, the rate of plastic strain development of AE high strength concrete is almost similar and very small, which might be because of slip at interfacial transition zone between aggregates and mortar. Moreover, the development of plastic strain in axial direction for both AEBFS and AEHSN concrete is found to be almost the same as that of lateral direction.

The equivalent plastic strain due to FTC (E_{pftc}) is calculated from FTC induced plastic strain in axial and lateral by using Eq. (3.3) developed by Maekawa and Okamura (1983) **[5]**.

$$E_{p,ftc}=\sqrt{\left(\frac{0.31\sqrt{2}}{\varepsilon'_{co}}(\varepsilon_l+\varepsilon_a)\right)^2+\left(\frac{0.49\sqrt{2}}{\varepsilon'_{co}}(\varepsilon_l-\varepsilon_a)\right)^2} \qquad (3.3)$$

Where,

ε'_{co} : peak strain at ultimate compressive strength

ε_l : FTC induced lateral strain

ε_a : FTC induced axial strain

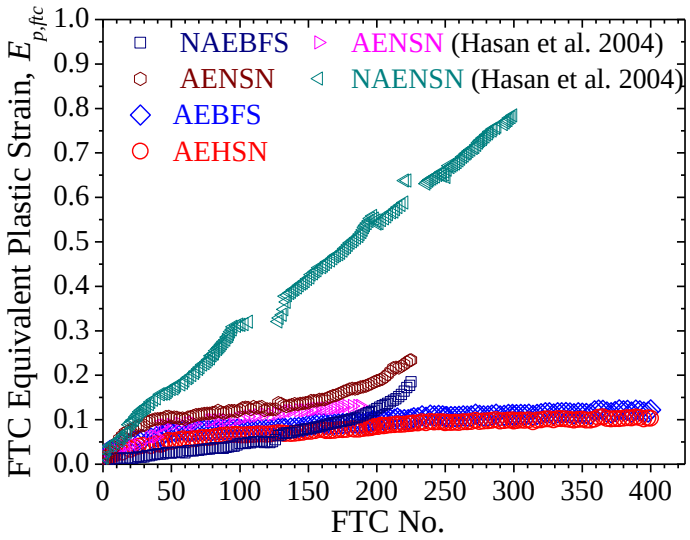

Figure 3.10: FTC induced equivalent plastic strain

The rate of increment of FTC equivalent plastic strain with the increase in FTC number is almost similar and very small for AE concrete, which is due to provision of AE voids in the concrete. The similar tendency of $E_{p,ftc}$ increment for AENSN concrete was observed by Hasan et. al. 2004 **[6]** as shown in Fig. 3.10. Moreover, it is found that the less plastic strain was developed in NAEBFS concrete compared to that of non-air entrained normal strength normal (NAENSN) concrete reported in previous study **[6]**, which might be because of high strength of NAEBFS concrete and presence of large volume of pores of same radii as that of AE voids **[7]**.

3.3.2 Monotonic Behavior of Concrete

3.3.2.1 Mechanical Properties of Concrete

The average compressive strength (f'_c), Young's modulus (E_0), Poisson's ratio (v) and strain at ultimate strength (ε'_{co}) of each concrete are summarized in Table **3.3**. The Young's modulus is calculated by determining the slope of stress-strain curve between longitudinal strain of 50 microns and point corresponding to one third of f'_c. The change in mechanical properties i.e. compressive strength and Young's modulus for NAEBFS, AENSN, AEBFS and AEHSN concrete with the increase in number of FTC are shown in Figs. 3.11 and 3.12 respectively, and with equivalent plastic strain due to FTC (E_{pftc}) in Figs. 3.13 and 3.14 respectively. The mechanical properties of AE concrete degraded at smaller rate compared to that of non-AE concrete regardless of type of fine aggregates and different compressive strengths, however, the rate of change for AE high strength concrete is minimal even after application of 400-FTC compared to that of AE normal strength concrete. The reason for minimal reduction in mechanical properties of AE high strength concrete might be because the amount and rate of equivalent plastic strain developed during FTC is very small owing to air-entrained voids and high strength of concrete. The other possible reason

Table 3.3: Mechanical properties of NAEBFS, AENSN, AEBFS, AEHSN concrete

Concrete Type	FTC No.	$E_{p,ftc}$	f'_c (MPa)	E_0 (GPa)	v	ε'_{co} (micron)
NAEBFS	0	0	75.4	44.9	0.23	2122
	50	0.0245	69.0	44.5	0.23	2069
	125	0.055	71.8	42.7	0.22	2210
	225	0.185	67.1	37.7	0.2	2233
AENSN	0	0	41.2	33.9	0.23	2306
	50	0.1	40.2	32.6	0.21	2236
	125	0.135	42.9	32.9	0.21	2102
	225	0.23	36.5	30.1	0.22	2173
AEBFS	0	0	61.3	34.8	0.23	2396
	250	0.106	64.8	38.1	0.24	2199
	400	0.122	61.0	37.4	0.24	2118
AEHSN	0	0	68.1	36.7	0.22	2562
	250	0.09	73.4	38.2	0.23	2641
	400	0.1	67.1	37.9	0.23	2485

$E_{p,ftc}$: FTC induced equivalent plastic strain, f'_c: Compressive strength, E_0: Young's modulus, v: Poisson's ratio, ε'_{co}: Strain at ultimate compressive strength

might be that the curing was resumed during FTC and it compensated the slight plastic damage caused by FTC. Moreover, the degradation rate of mechanical properties of NAEBFS concrete with the increase in FTC is less than that of NAENSN concrete from previous study **[6]**, nevertheless, it is almost similar for both non-AE concrete with respect to FTC equivalent plastic strain.

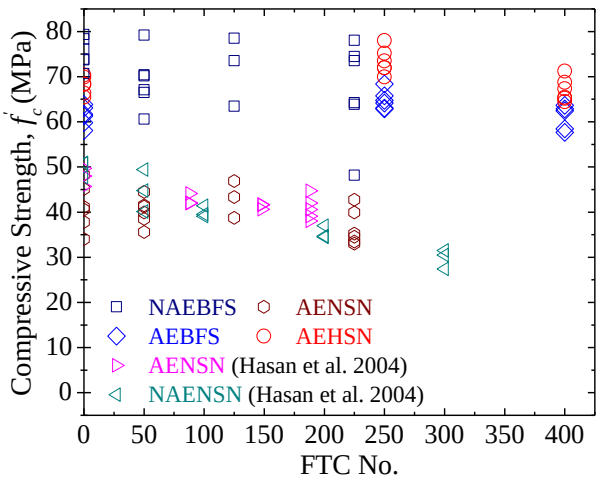

Figure 3.11: Change in compressive strength with FTC number

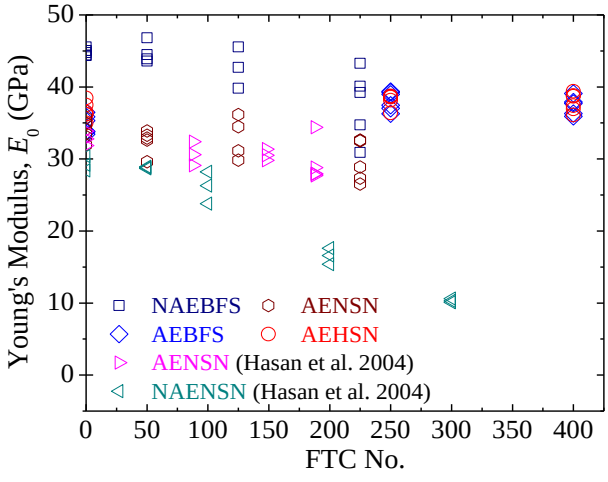

Figure 3.12: Change in Young's modulus with FTC number

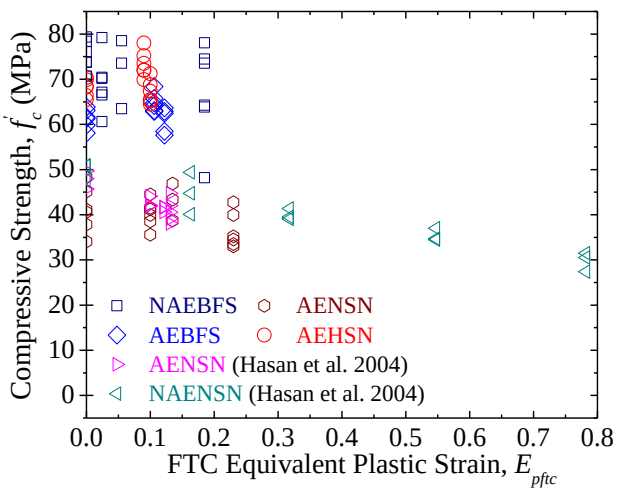

Figure 3.13: Change in compressive strength with FTC equivalent plastic strain

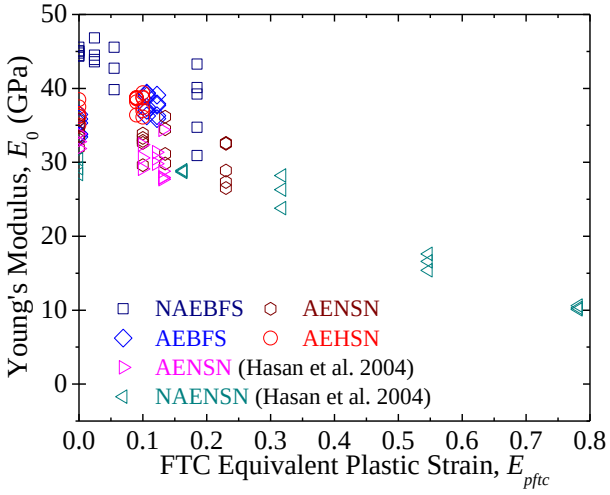

Figure 3.14: Change in Young's modulus with FTC equivalent plastic strain

3.3.2.2 Relationship between Compressive Strength and Young's Modulus

The relationships between compressive strength and Young's modulus of intact and frost-damaged specimens of each concrete are compared with those of obtained using the empirical Eqs. (3.4)-(3.12) given in Table 3.4 for different codes and from the literature **[8-15]** for normal strength concrete (NC) and high strength concrete (HSC) as shown in Fig. 3.15. EN1992-1-1 and MC2010 slightly overestimates the Young's modulus for normal concrete and AE high strength concrete, while ACI-363, CSA, Norwegian code and equation proposed by Noguchi et al. (2009) slightly underestimate the experimental results for high strength concrete. However, JSCE (2007) design equation agrees well with both normal and high strength concrete. Although there is scatter in the experimental results, the reduction in modulus of elasticity was observed with the decrease in

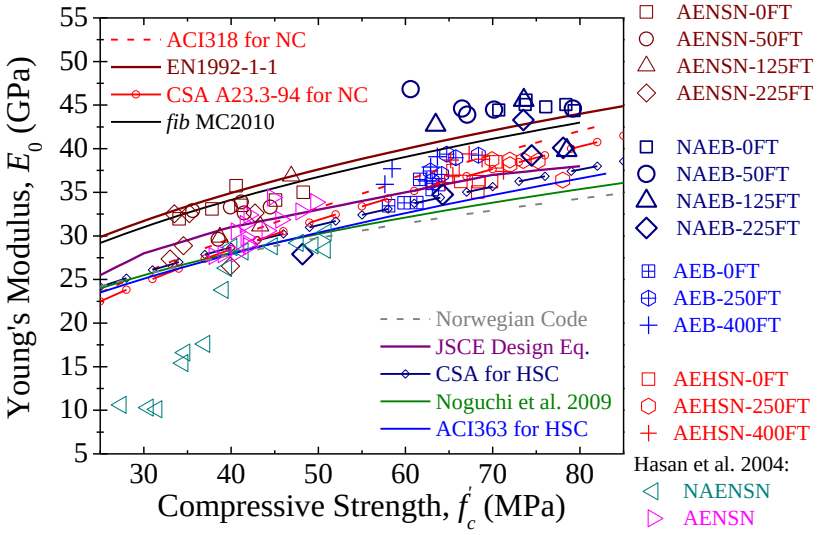

Figure 3.15: Relationship between compressive strength and modulus of elasticity

Table 3.4: Relationships between f'_c–E_0 from literature

Reference	Relationships	Eq.
ACI318-14 for NC **[8]**	$E_0 = 4.7\sqrt{f'_c}$	(3.4)
CSA A23.3-94 for NC **[9]**	$E_0 = 4.5\sqrt{f'_c}$	(3.5)
fib MC2010 **[10]**	$E_0 = E_{c0}.\alpha_E.\sqrt[3]{f'_c/10}$ where $E_{c0}.\alpha_E$ =21.5GPa for Quartzite aggregates	(3.6)
EN1992-1-1 **[11]**	$E_0 = 22\sqrt[3]{f'_c/10}$	(3.7)
ACI363R:2010 for HSC **[12]**	$E_0 = \left(3.32\sqrt{f'_c} + 6.9\right)\left(\frac{\gamma}{2346}\right)^{1.5}$	(3.8)
Noguchi et al. (2009) **[13]**	$E_0 = 33.5k_1k_2\left(\gamma/2400\right)^2\left(f'_c/60\right)^{\frac{1}{3}}$	(3.9)
JSCE 2007 Specifications for Design **[14]**	$E_0 = 10 \times \left(2.2 + \frac{f'_c - 18}{20}\right)\ for\ f'_c < 30MPa$ $E_0 = 10 \times \left(2.8 + \frac{f'_c - 30}{33}\right)\ for\ 30MPa \le f'_c < 40MPa$ $E_0 = 10 \times \left(3.1 + \frac{f'_c - 40}{50}\right)\ for\ 40MPa \le f'_c < 70MPa$ $E_0 = 10 \times \left(3.7 + \frac{f'_c - 70}{100}\right)\ for\ 70MPa \le f'_c < 80MPa$	(3.10)
Norwegian Code NS-3473(1992) **[15]**	$E_0 = \left(9.5{f'_c}^{0.3}\right)\left(\frac{\gamma}{2400}\right)^{1.5}$	(3.11)
CSA for HSC	$E_0 = \left(3.3\sqrt{f'_c} + 6.9\right)\left(\frac{\gamma}{2300}\right)^{1.5}$	(3.12)

E_0: Modulus of elasticity in GPa, f'_c, Compressive strength in MPa, γ: Density of concrete in kg/m^3, k_1 and k_2: correction factor

compressive strength of each concrete. Moreover, it is found that Young's modulus of frost-damaged concrete decreases sharply with respect to compressive strength with the increase in frost damage compared to that of proposed by different codes for intact concrete. It indicates that f'_c-E_0 relationships by different codes are not valid for frost-damaged concrete.

The relation of relative modulus of elasticity (E_{0d}/E_0) for frost-damaged concrete is proposed as shown in Eq. (3.13) and Fig. 3.16 by the regression of experimental data of this study and the data of frost-damaged concrete obtained from literature compiled in Table 3.5. The reduced modulus of elasticity (E_{0d}) of frost-damaged concrete for respective reduced compressive strength (f'_{cd}) can be determined using Eq. (3.14), where undamaged modulus of elasticity (E_0) is calculated by using f'_c-E_0 relationships by different codes.

Table 3.5: Data on compressive mechanical properties of frost-damaged concrete from literature

Concrete Grade[1]	W/C ratio	Air Entrain--ment (%)	f'_c (MPa)	Dimensions of Specimen in mm	FTC test Method	Temp. range (°C)	FTC test solut--ion	FTC No.	FTC & Compressive Mechanical Properties documented	Industrial Waste	Ref.
C30, C35, C50	0.46, 0.35	AE	38.63, 43.37, 59.85, 61.71	Φ100x 203 Φ100x 406	ASTM C666-84	-30↔+10 in chamber	Water	0,30,60,90	f'_c, E_0, ν	-	Shi 1997 [16]
C40	0.5	AE (5%)	46.18 (f'_{cu}:57.72)	100x100x100	ASTM C666-92	-17.8↔+4	Water	0,34,62,109,205,261,305	RDME, f'_c, E_0, ν, ε'_{co}	-	Hasan 2002 [17]
C50		Non-AE (2.25%)	55.6 (f'_{cu}:69.5)					0,10,17,28,41,76,205,305			
C40	0.6	AE (4.5%)	47.8	Φ100x 200	ASTM C666-92	-25↔+20	Water spray during thawin	0,88,148,188	E_{pftc}, f'_c, E_0, ε'_{co}	-	Hasan 2004 [6]
C40	0.5	Non-AE (1.5%)	49.8					0,50,100,200,300			
C20	0.5	Non-AE (1.7%)	27.4 (f'_{cu}:34.2)	100x100x100 100x100x400	GBJ82-85	-15↔+6 at centre	Water	0,25,50,75	RDME,	-	Shang 2006 [18]
C20	0.5	Non-AE (1.9%)	27.2, 24.6 (f'_{cu}:34.0, 30.71)	100x100x100 150x150x150	GBJ82-85	-17±1 ↔+8±1 at centre	Water	0,15,30,50	Mass loss, V_u, f'_c, E_0, ε'_{co}	Fly ash as 43% of binder	Ji 2007 [19]
C35	0.38	AE	42.98	100x100x400	ASTM C666	-18↔+4	Water	0,100,150,200,300	RDME, f'_c, E_0, ν, ε'_{co}	S.F. & F.A. as 4.6% and 9.2% of binder	Zou 2008 [20]
C20	0.47	Non-AE (1.5%)	28.19	Φ160x 320	RILEM TC-117	-20↔+10	Insulated w/o water	0,30,60,90,120,150,180,210,240	Permeability, f'_c, E_0	-	Wardeh 2010 [21]
C20, C30	0.6, 0.54, 0.48	Non-AE	28.73, 39.18, 41.54	100x100x300	GBJ82-85	-17↔+8 at centre	Water	0,50,75,100,125,150,175,200	f'_c, E_0, ε'_{co}	-	Duan 2011 [22]
C30	0.57	Non-AE	40.6	Φ100x 200	RILEM TC-176-	-20↔+20	Water	0, DL1, DL2	RDME, t_u, w, f'_c, E_0, ε'_{co}	-	Hanjari 2011 [23]
C40	0.39	Non-AE	50.45	100x100x300	GB/T 50082-	-15↔+6	Water	0,5,15,30,50,75,100,125	RDME, f'_c, E_0, ε'_{co}	Fly ash as 48.6% of binder	Liu 2012 [24]
C25	0.45	AE (5%)	33.54	100x100x300	GB/T 50082-	18±2↔+5±2	Water	0,100,200,300	f'_c, E_0, ε'_{co}	-	Liu 2018 [25]

t_u and V_u: time and velocity of UP wave, E_{pftc}: FTC equivalent plastic strain, w: crack width, f'_{cu}: Cube's f'_c

[1]Concrete grade listed are based on the classification of *fib* MC2010 [10].

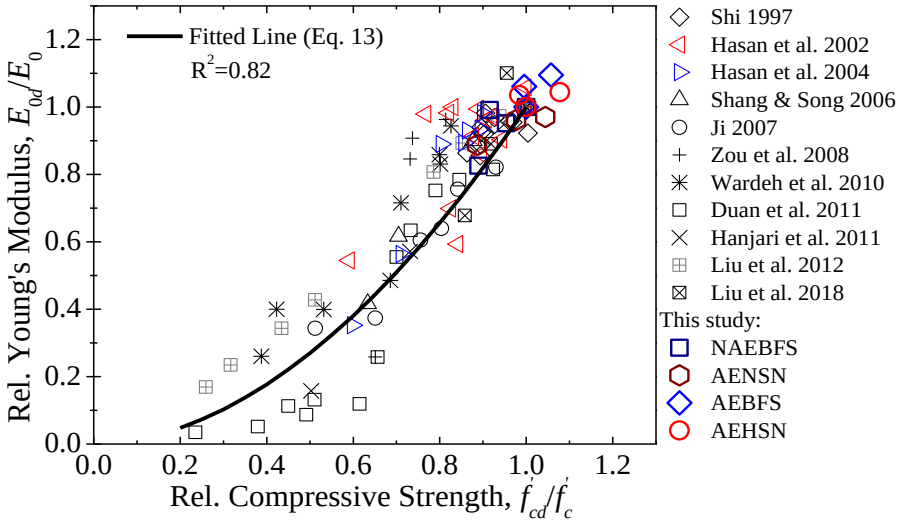

Figure 3.16: Change in Relative Modulus of Elasticity with Relative compressive strength

$$\frac{E_{0d}}{E_0} = \left(\frac{f'_{cd}}{f'_c}\right)^{1.89} \tag{3.13}$$

$$E_{0d} = \left(\frac{f'_{cd}}{f'_c}\right)^{1.89} . E_0 \quad \text{where} \quad E_0 = f(f'_c) \tag{3.14}$$

3.4 STATIC STRESS-STRAIN RELATIONSHIPS

3.4.1 Previous Models

In the previous study, Maekawa and Okamura (1983) presented the concept of elasto-plastic and fracture model (EPF) and developed the stress-strain relationship for intact normal concrete **[5].** In EPF model, concrete is assumed as an assembly of several constitutive micro-elements connected in parallel. Each microelement consists of an elastic spring to consider the internal stress mechanism and energy absorption and a slider for the plastic deformation. Under the application of mechanical loading, the collapse of voids and slip between mortar and coarse aggregates takes place inside the concrete resulting in the plastic deformation. The damage in the concrete is modeled by the fracture of elastic spring. Considering this assumption, the stress-strain relationship is given as shown in Fig. 3.17 and Eq. (3.13).

$$\sigma'_c = KE_0\left(\varepsilon'_{max} - \varepsilon'_p\right) \tag{3.13}$$

Where σ'_c is compressive stress, K is the fracture parameter and E_0 is the Young's modulus of concrete. ε'_{max} is maximum compressive strain which is the sum of elastic strain and plastic strain and ε'_p is plastic strain. Fracture parameter (K) and plastic strain (ε'_p) are the function of maximum

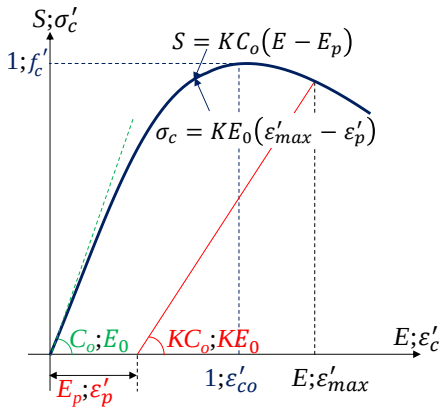

Figure 3.17: EPF model for undamaged concrete [5]

compressive strain (ε_{max}') and strain corresponding to ultimate strength (ε_{co}'). The relationships for fracture parameter (K) and plastic strain (ε_p') for concrete given in EPF model are shown in Eq. (3.14) and Eq. (3.15) respectively **[5]**.

$$K = exp\left\{-0.73\frac{\varepsilon_{max}'}{\varepsilon_{co}'}\left(1 - exp\left(-1.25\frac{\varepsilon_{max}'}{\varepsilon_{co}'}\right)\right)\right\} \tag{3.14}$$

$$\varepsilon_p' = \varepsilon_{max}' - \frac{20}{7}\varepsilon_{co}'\left(1 - exp\left(-0.35\frac{\varepsilon_{max}'}{\varepsilon_{co}'}\right)\right) \tag{3.15}$$

To consider the effect of combined action of freezing and thawing and mechanical loading, Hasan et al. (2004) extended the EPF model of intact normal concrete and proposed stress-strain relationships for frost damaged normal strength concrete as shown in Fig. 3.18 and Eq. (3.16) **[6]**.

$$S = \alpha\beta KC_o(E - E_p) \tag{3.16}$$

Where S is equivalent stress, E is equivalent strain, C_o is initial stiffness i.e. 2.0 for normal concrete, K and E_p are mechanical fracture parameter and mechanical equivalent plastic strain under static loading respectively. α is effective parameter and β is FTC fracture parameter. In frost-damaged concrete, FTC results in some of the constitutive elements to fracture and lose their load carrying capacity owing to microcracking caused by plastic tensile strain in constitutive elements. However, the unfractured elements with less plastic tensile strains cannot take the compression load effectively until the plastic tensile strain is canceled by compressive strain and after that these elements resume carrying the compression load effectively. This results in slight increase in stiffness of concrete with the increase in equivalent strain and is modeled by effective factor (α) as a function of mechanical equivalent strain (E_{max}) and FTC equivalent plastic strain (E_{pftc}) given in Eq. (3.17).

$$\begin{aligned} \alpha &= e^{-1.70E_{pf}}e^{1.70E_{pf}^{0.15}\times E_{max}^{0.85}} \text{ for } E_{\max} < E_{pftc} \\ \alpha &= 1.0 \text{ for } E_{\max} \geq E_{pftc} \end{aligned} \tag{3.17}$$

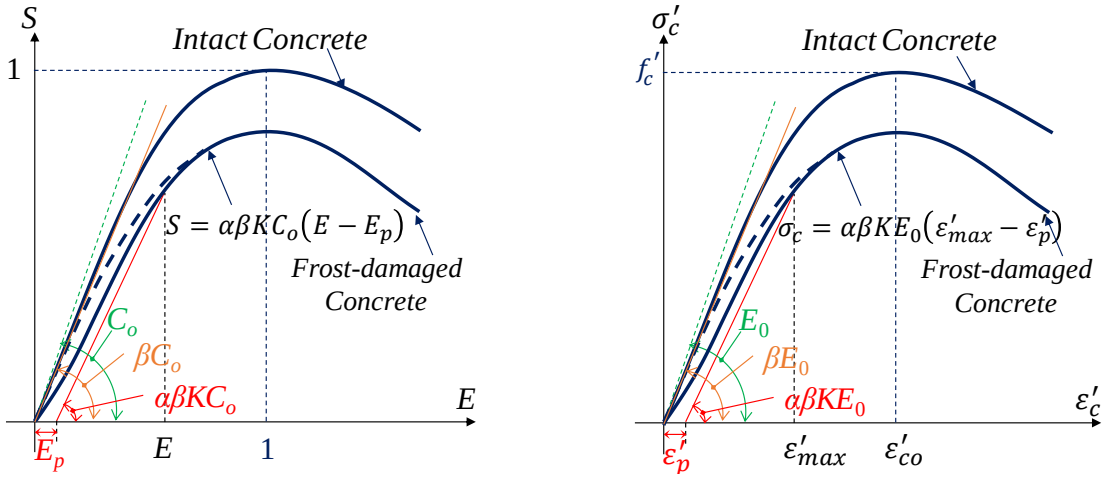

(a) Eq. Stress-eq. strain relationship [6] (b) Stress-strain relationship

Figure 3.18: EPF model for frost-damaged concrete

The damage in concrete increases with the increase in FTC induced plastic strain (E_{pftc}) due to reduction in initial stiffness resulting from fracture of some elements during FTC and is modeled by FTC fracture parameter (β) as given in Eq. (3.18).

$$\beta = e^{-0.45E_{pftc}\left(1-e^{-30E_{pftc}}\right)} \tag{3.18}$$

The equation of mechanical fracture parameter for frost-damaged concrete as a function of maximum equivalent strain remains same as given in Eq. (14) for intact concrete. However, it is reported that the mechanical equivalent plastic strain increases with the increase in damage of concrete caused by FTC, because the constitutive elements can take lesser compression load for higher FTC damage as these elements reach their plastic point more quickly resulting in more mechanical equivalent plastic strain as shown in Eq. (3.19).

$$E_p = E_{\max} - a(1 - e^{-bE_{\max}}) \tag{3.19}$$

$$a = \frac{20}{7} - 2.10E_{pftc} + 0.34E_{pftc}^2$$
$$b = 0.35 + 0.25E_{pftc} + 0.18E_{pftc}^2 \tag{3.20}$$

3.4.2 Formulation of Model for High Strength Concrete

The mechanical properties of high strength concrete such as stiffness and plastic deformation changes differently compared to that of normal concrete under the application of load. Therefore, the equations for fracture parameter (K) and plastic strain (ε_p') developed for intact and frost damaged normal concrete in EPF model **[5,6]** are not applicable for high strength concrete.

For this reason, the static unloading and reloading tests on intact and frost-damaged specimens of NAEBFS, AENSN, AEBFS, AEHSN concrete were performed to observe the stiffness change and plastic strain at unloading for respective maximum compressive strain. The concrete specimens were loaded to some value and then load was released to zero for some loading cycles followed by loading of specimen to the failure. The stiffness change and plastic strain of each loading cycle for each concrete are measured. The stress strain relationships for intact and frost-damaged high strength concrete are proposed on the similar concept of EPF model as shown in Fig. 3.18(b) and Eq. (3.21).

$$\sigma_c^{'} = \alpha\beta K E_0\left(\varepsilon_{max}^{'} - \varepsilon_p^{'}\right) \tag{3.21}$$

3.4.2.1 Relationship for Mechanical Fracture Parameter of High Strength Concrete

Mechanical fracture parameter (K) is the ratio of secant modulus of stress-strain loop for different loading cycle to Young's modulus (E_0) of concrete. It represents the degree of internal damage of concrete upon application of mechanical loads. The experimental data obtained from static unloading and reloading test is regressed to obtain the relations for mechanical fracture parameter (K) for AE and non-AE high strength concrete. The relationships for K for NAEBFS concrete and AEBFS and AEHSN concrete are formulated as given in Eq. (3.22).

$$K = exp\left\{-p\left(\frac{\varepsilon_{max}^{'}}{\varepsilon_{co}^{'}}\right)^{q}.\left(1 - exp\left(-r\frac{\varepsilon_{max}^{'}}{\varepsilon_{co}^{'}}\right)\right)\right\} \tag{3.22}$$

The input parameters for the equation of fracture parameter (K) are axial strain ($\varepsilon_{max}^{'}$), strain ($\varepsilon_{co}^{'}$) corresponding to ultimate compressive strength of respective concrete and the values of p, q and r for respective concrete can be obtained from Table 3.6. The experimental and calculated fracture parameter change of each concrete by for intact and frost-damaged specimens are shown in Fig. 3.19. The experimental results exhibit that the mechanical fracture parameter for high strength concrete decreases at a slower rate compared to that for normal concrete proposed in the EPF model due to weak interfacial transition zone between mortar and coarse aggregates in normal concrete. However, the mechanical fracture parameter change for AENSN concrete shows

Table 3.6: Values of parameter p, q and r for each concrete

Type	p	q	r
AENSN **[13,35]**	0.73	1	1.25
NAEBFS	0.37	$exp\left(1.40\frac{\varepsilon_{max}^{'}}{\varepsilon_{co}^{'}}\right)$	0.67
AEBFS	0.38	$exp\left(1.25\frac{\varepsilon_{max}^{'}}{\varepsilon_{co}^{'}}\right)$	0.68
AEHSN			

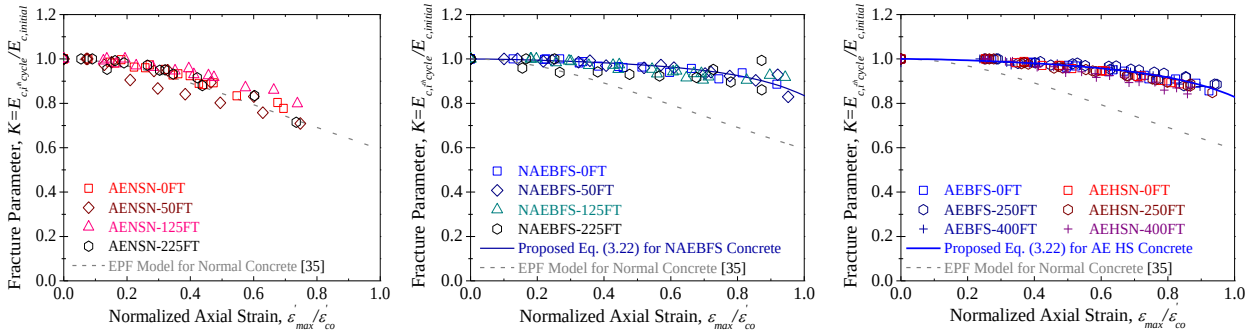

(a) AENSN concrete (b) NAEBFS concrete (c) AEBFS and AEHSN concrete

Figure 3.19: Fracture parameter change under static loading

good agreement with the Eq. (3.14) as proposed in EPF model. Moreover, the rate of change of fracture parameter of frost-damaged concrete is almost similar to that of intact concrete. The values of fracture parameter (K) calculated by proposed equations for each concrete are compared with those of measured experimentally. The average calculated values of fracture parameter (K) are close to the experimental values ($\bar{K}_{cal.}/\bar{K}_{exp.}$ =1.00) with a coefficient of variation of 3.6% showing the good agreement between the two as presented in Fig. 3.20. The line of equality is represented by solid line and line of $\bar{K}_{cal.}/\bar{K}_{exp.}$ is shown by dotted line.

3.4.2.2 Mechanical Plastic Strain Development

Plastic deformation is the irrecoverable damage even after the removal of load. The values of plastic strain development for AENSN concrete obtained from the experiments shows good agreement with the proposed Eq. (3.19) by Hasan et al. (2004) for normal concrete **[6]**. However, the rate of plastic strain development of high strength concrete is different compared to that of normal concrete therefore, the equations for the plastic strain of NAEBFS, AEBFS and AEHSN concrete are developed by regression of experimental data of static unloading and reloading tests

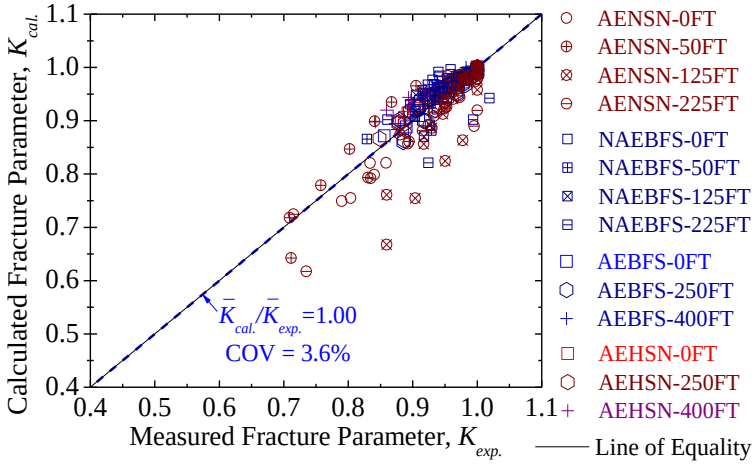

Figure 3.20: Comparison between the calculated and experimental mechanical fracture parameter

Table 3.7: Value of Parameter a and b for each concrete in Eq. (3.23)

Type	a	b
AENSN **[6]**	$\frac{20}{7} - 2.10E_{pftc} + 0.34E_{pftc}^2$	$0.35 + 0.25E_{pftc} + 0.18E_{pftc}^2$
NAEBFS	$\frac{20}{7} - 0.399E_{pftc} + 0.062E_{pftc}^2$	$0.35\{1 + (\varepsilon'_{\max}/\varepsilon'_{co}).(0.04 - 0.096E_{pftc} + 0.024E_{pftc}^2)\}$
AEBFS	$\frac{20}{7}$	$0.35 + 0.02(\varepsilon'_{\max}/\varepsilon'_{co})^2$
AEHSN		$0.35 + 0.0075(\varepsilon'_{\max}/\varepsilon'_{co})^2$

as shown in Eq. (3.23).

$$\varepsilon'_p = \varepsilon'_{max} - a\varepsilon'_{co}\left(1 - exp\left(-b\frac{\varepsilon'_{max}}{\varepsilon'_{co}}\right)\right) \tag{3.23}$$

The input for the plastic strain equation are the value of strain corresponding to the ultimate strength of respective concrete as given in Table 3.3 and maximum strain along with value of parameter a and b which can be obtained from Table 3.6 for different value of FTC induced equivalent plastic strain (E_{pftc}) of AENSN and NAEBFS concrete. However, the compressive strength and young's modulus of AEBFS and AEHSN concrete didn't show significant reduction even after 400-FTC, therefore, the equation proposed for 0-FTC is valid for 400-FTC due to low FTC induced equivalent plastic strain (E_{pftc}). The plastic strain for each concrete calculated by using the proposed Eq. (23), is normalized by (ε'_{co}) of each concrete and is shown in Fig. 3.21 along with the normalized plastic strain for intact normal concrete calculated by Eq. (3.15) as given in EPF model.

It can be seen from the figure that more plastic strain is developed in normal concrete compared to high strength concrete, because of more plasticity due to weak bond between matrix and aggregates in normal concrete. It is observed that less plastic strain is developed in BFS

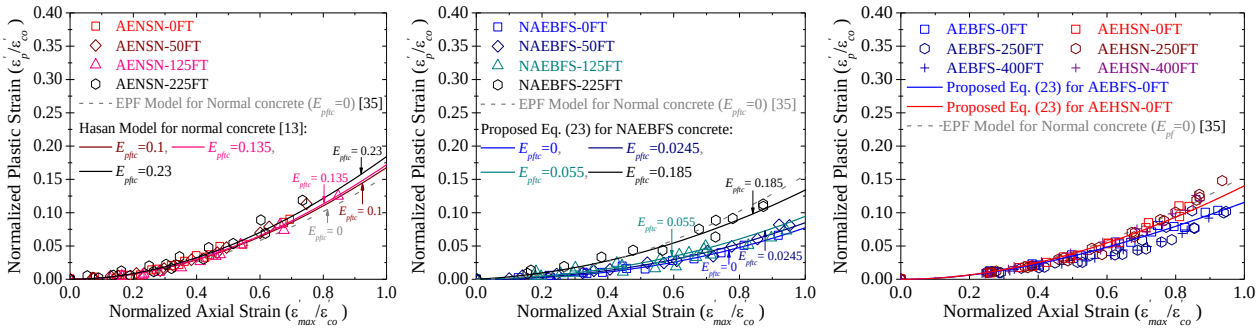

(a) AENSN concrete (b) NAEBFS concrete (c) AEBFS and AEHSN concrete

Figure 3.21: Plastic strain development under static loading

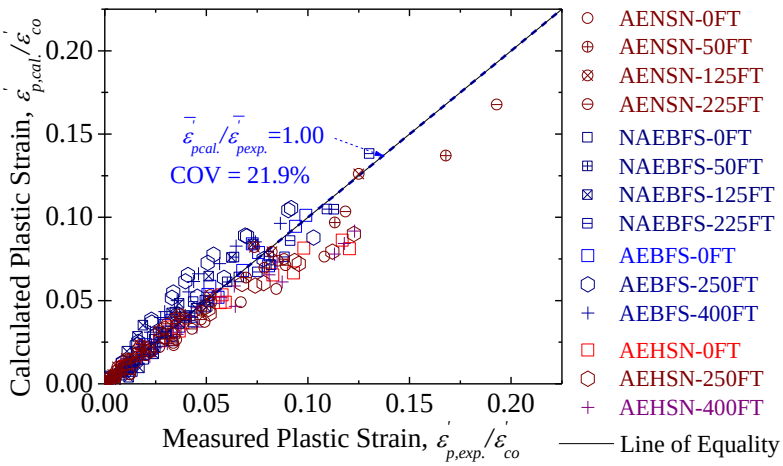

Figure 3.22: Comparison between the experimental and calculated plastic strain values

concrete under the application of monotonic loading compared to high strength normal concrete. The authors observed the similar tendency of less plastic strain development in high strength mortar with BFS fine aggregates compared to high strength mortar with river sand in the previous study **[26]**. Moreover, less plastic strain is produced in NAEBFS concrete compared to that AEBFS and AEHSN concrete. This might be because of the major part of the plasticity in AE concrete is caused by collapse of air voids. In addition, it is observed that as the frost damage inside the AENSN and NAEBFS concrete increases, the rate of plastic strain development becomes higher. This is because of the reason that the constitutive elements inside frost-damaged concrete fracture quickly upon the application of load compared to that of intact concrete resulting in higher plastic strain development.

The calculated plastic strain values of each concrete by Eq. (3.23) are compared with the experimental values as shown in Fig. 3.22. There is a satisfactory agreement between the experimental plastic strain values and calculated ones with ($\bar{\varepsilon}'_{p,cal}/\bar{\varepsilon}'_{p,exp}$ =1.00) and a coefficient of variation (COV) of 21.9%. The higher value of COV is due to scatter between the experimental plastic strain values.

3.4.2.3 Relationship for FTC fracture parameter and Effective Factor

The reduction in initial stiffness of concrete with the increase in frost damage is considered by FTC fracture parameter (β). The experimental results of frost damaged high strength NAEBFS concrete exhibit that the relationship of FTC fracture parameter for normal concrete (Eq. (3.18)) developed by Hasan et al. (2004) can also be used for high strength NAEBFS concrete. The relationships for FTC fracture parameter in terms of initial stiffness (C_o) and Young's modulus (E_0) with the increase in FTC equivalent plastic strain (E_{pftc}) are shown in Fig. 3.23(a, b). It is observed that for less value of FTC equivalent plastic strain, change in initial stiffness (C_o) is almost similar to that change in Young's modulus (E_0) of the concrete. However, the Young's modulus of frost-

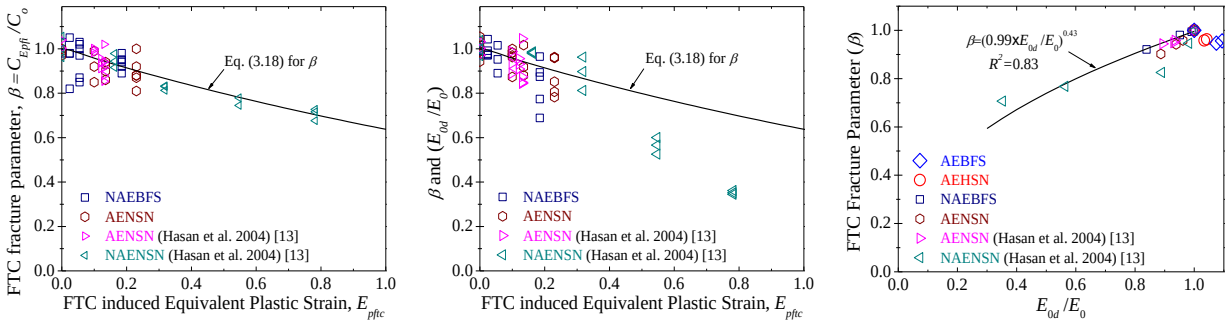

(a) initial stiffness (C_o) (b) Young's modulus (E_0) (c) Change in β with E_{d0}/E_0

Figure 3.23: FTC fracture parameter

damaged concrete reduces at rapid rate for higher value of FTC equivalent plastic strain compared to that of initial stiffness (C_o). It implies that Poisson's ratio has vital role in the compressive monotonic behaviour of frost damaged concrete for higher E_{pftc}. Therefore, the FTC fracture parameter should be based on the change of initial stiffness (C_o) of frost damaged concrete. The relationship between relative Young's modulus (E_{d0}/E_0) and FTC fracture parameter (β) is shown in Fig. 3.23(c).

The relationship of effective factor (α) for normal concrete proposed by Hasan et al. (2004) given in Eq. (3.17) is used for high strength concrete in this study, as FTC equivalent plastic strain developed in high strength is low. The values of maximum equivalent strain (E_{max}) for respective maximum axial strain (ε'_{max}) value is determined by using Eq. (3.24), which is the rearranged form of Eq. (3.3).

$$E_{\max} = \sqrt{\left(\frac{\varepsilon_{\max}}{\varepsilon'_{co}}\right)^2 . \{0.67(1 + v^2 + 0.86v)\}} \qquad (3.24)$$

where v is the Poisson's ratio for corresponding maximum axial strain (ε'_{max}), which can be calculated using the relationships of Poisson's ratio given in Sec. 3.4.2.4.

3.4.2.4 Change in Poisson's Ratio

Poisson's ratio (v) is the absolute value of the ratio of the lateral strain to the axial strain. To predict the lateral part of stress-strain curve, the equations for Poisson's ratio for each concrete are formulated as shown in Fig. 3.24. The Poisson's ratio of respective concrete can be calculated for certain maximum normalized axial strain by Eqs. (3.25)-(3.28) listed in Table 3.8.

Table 3.8: Equations for Poisson's ratio (v) for each concrete

Type	Poisson's ratio (v)		Eq.
	for $(\varepsilon'_{max}/\varepsilon'_{co}) \leq 0.7$	for $(\varepsilon'_{max}/\varepsilon'_{co}) > 0.7$	
AENSN	0.22	$0.22 + 3.10\left(\frac{\varepsilon'_{max}}{\varepsilon'_{co}} - 0.7\right)^2$	3.25
NAEBFS	0.22	$0.22 + 2.75\left(\frac{\varepsilon'_{max}}{\varepsilon'_{co}} - 0.7\right)^2$	3.26
AEBFS	0.23	$0.23 + 2.50\left(\frac{\varepsilon'_{max}}{\varepsilon'_{co}} - 0.7\right)^2$	3.27
AEHSN	0.22	$v = 0.22 + 2.0\left(\frac{\varepsilon'_{max}}{\varepsilon'_{co}} - 0.7\right)^2$	3.28

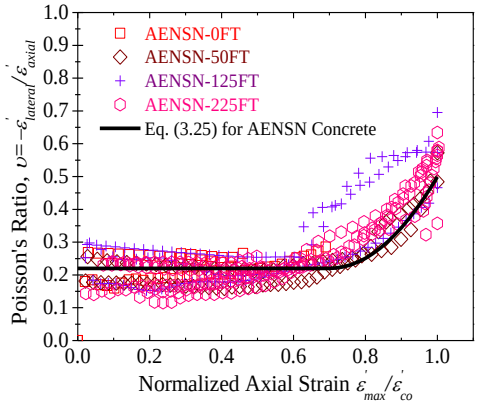

(a) AENSN concrete

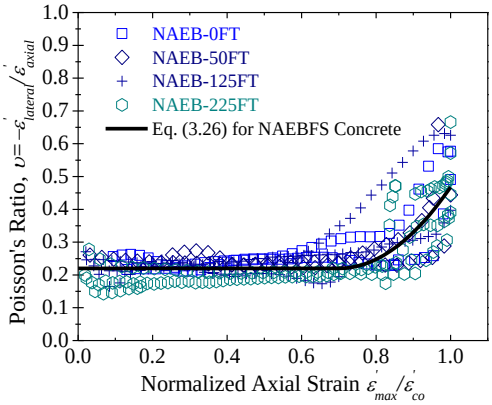

(b) NAEBFS concrete

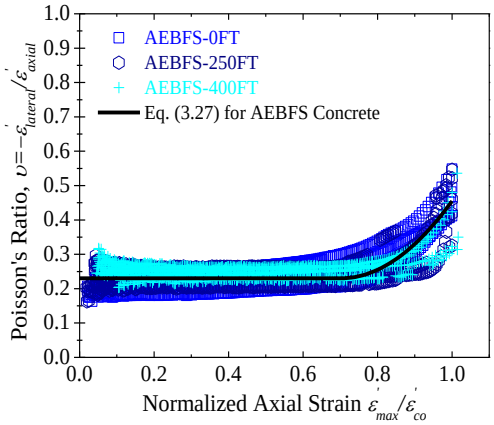

(c) AEBFS concrete

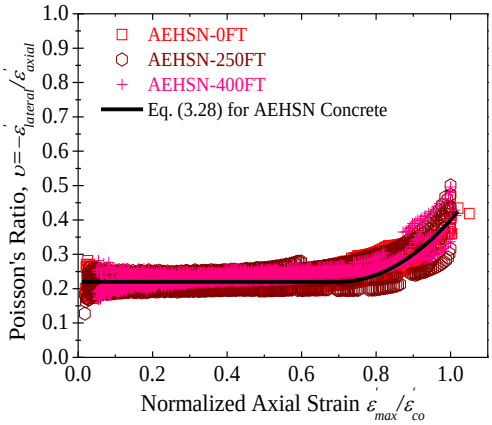

(d) AEHSN concrete

Figure 3.24: Change in Poisson's ratio

3.4.3 Correlation between Proposed Model and Experiment

The stress-strain relationships for AENSN concrete are calculated using Hasan's model **[6]** as given in Eq. (3.16). The input parameters are the FTC equivalent plastic strain (E_{pftc}), initial stiffness for normal concrete i.e. $C_o = 2.0$, average value of strain at ultimate compressive strength

(ε'_{co}) listed in Table 3.3 i.e. 2204 μ and reference value for compressive strength for AENSN as 41.2 MPa. The stress-strain relationships for NAEBFS concrete are determined using the proposed model as shown in Eq. (3.21) in this study. The input parameters for the model are the FTC equivalent plastic strain (E_{pftc}), maximum axial strain (ε'_{max}), reference value of Young's modulus (E_0) for 0-FTC i.e. 44.9 GPa and average value of strain at ultimate compressive strength (ε'_{co}) listed in Table 3.3 i.e. 2165 μ as no particular tendency of change of ε'_{co} was observed for different frost damage levels. The effective factor (α), FTC fracture parameter (β), mechanical fracture parameter (K) and plastic strain for AENSN and NAEBFS concrete are calculated by using Eqs. (3.17), (3.18), (3.22) and (3.23) respectively.

However, no significant reduction in mechanical properties of AEBFS and AEHSN concrete was observed even after 400-FTC due to very less value of FTC induced equivalent plastic strain (E_{pftc}). Therefore, the stress-strain relationships for AEBFS and AEHSN concrete are calculated using the actual values of Young's modulus for respective FTC number as listed in Table 3.3, without considering the effect of parameters α and β. The stress vs. lateral strain curves of each concrete are obtained by using the Poisson's ratio equations as given in Eqs. (3.25)-(3.28). The calculated stress-strain curves for each concrete are drawn in Fig. 3.25 along with the average experimental curves. The calculated curves are shown by solid lines, while the experimental curves with circular points. The calculated stress-strain curves are close to the experimental ones.

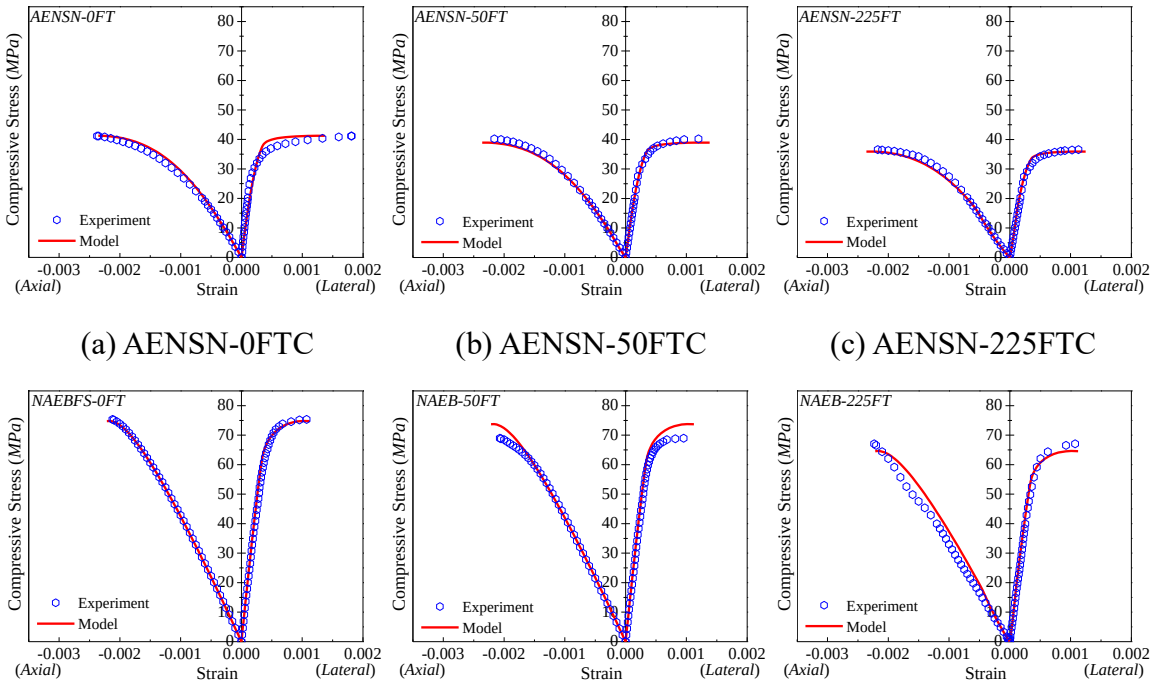

(a) AENSN-0FTC (b) AENSN-50FTC (c) AENSN-225FTC

(d) NAEBFS-0FTC (e) NAEBFS-50FTC (f) NAEBFS-225FTC

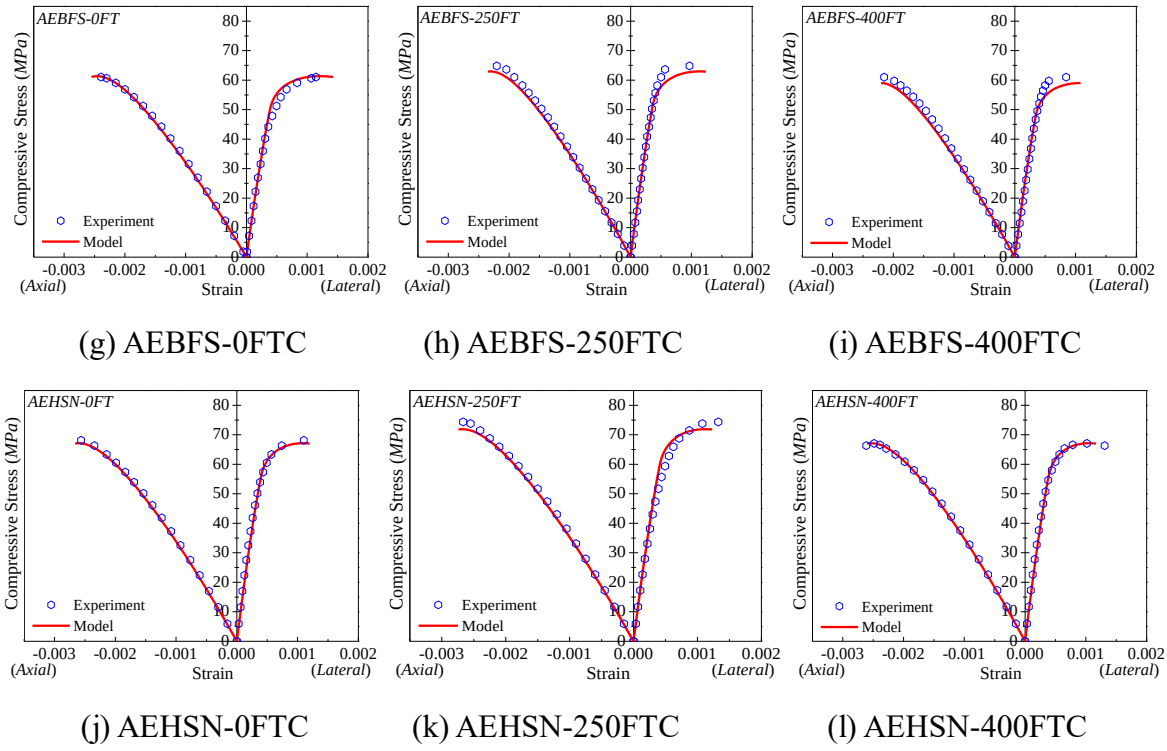

(g) AEBFS-0FTC (h) AEBFS-250FTC (i) AEBFS-400FTC

(j) AEHSN-0FTC (k) AEHSN-250FTC (l) AEHSN-400FTC

Figure 3.25: Comparison between experimental and calculated stress-strain curves

The ultimate compressive strength of each concrete determined by the proposed model are compared with those of measured during the experiment as shown in Fig. 3.26. The good correlation between the average of experimental compressive strength and calculated by the proposed model ($\bar{f}'_{c,exp}/\bar{f}'_{c,cal}$ =1.01) is obtained with COV of 8.1% confirming the applicability of the proposed model.

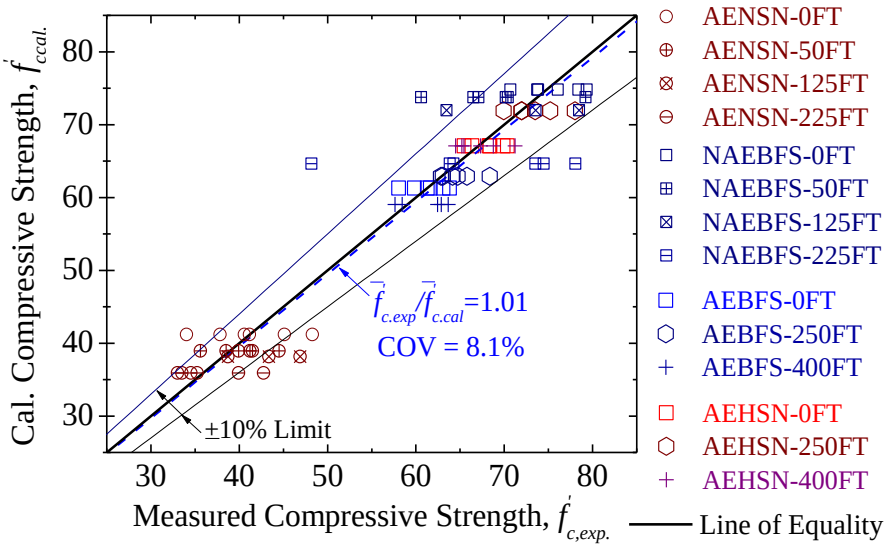

Figure 3.26: Comparison between calculated and experimental ultimate compressive strength

3.5 CONCLUSIONS OF THIS CHAPTER

This chapter explicates the monotonic behavior of AE and non-AE high strength concrete with BFS fine aggregates under freezing and thawing in comparison with AE normal and high strength concrete, and the formulation of the stress-strain relationships for AE and non-AE high strength frost damaged concrete. Following conclusions were drawn:

1. The overall rate of increase of FTC equivalent plastic strain in non-AE high strength concrete with BFS fine aggregates was slightly higher than that of AE high strength concrete with BFS and CS sand. However, it is slightly less than that of AE normal concrete. Compared with non-AE normal concrete from past study, the rate of plastic strain development in non-AE BFS concrete is much smaller. Moreover, the rate of plastic strain development in AE high strength concrete i.e. AEBFS and AEHSN is same regardless of type of fine aggregates.
2. The mechanical properties i.e. compressive strength and Young's modulus of AE concrete of both normal and high strength degrade at slower rate with the increase in number of FTC compared to non-AE concrete because of less FTC induced plastic strain in AE concrete. However, the mechanical properties of non-AE BFS concrete deteriorate at slower rate compared to non-AE normal concrete from previous study owing to high strength of non-AE BFS concrete. Nevertheless, the mechanical properties of each concrete change at almost same rate with the increase in FTC equivalent plastic strain. Moreover, it is observed that Young's modulus of frost-damaged concrete reduces sharply compared to decrease in compressive strength.
3. The stress-strain model for AE and non-AE concrete high strength with BFS fine aggregates subjected to freezing and thawing is proposed based on the concept of elasto-plastic and fracture theory. The rate of mechanical plastic strain development for non-AE high strength concrete with BFS fine aggregates is lower compared to that of normal concrete for all frost-damage levels, consequently the mechanical fracture parameter for high strength concrete decreases at slow rate. Therefore, the equations of plastic strain development and fracture parameter change of high strength concrete are formulated. Moreover, the rate of mechanical plastic strain development increases with the increase in frost damage level, however, the rate of mechanical fracture parameter change is almost similar for all frost damage levels. In addition, the Young's modulus of concrete for higher frost damage level reduces sharply compared to initial stiffness (C_o), therefore, the FTC fracture parameter should consider the change in C_o. The results obtained using the proposed model are in good agreement with those of experimental ones.

REFERENCES

[1] ASTM C666–97 (1997). "Standard Test Method for Resistance of Concrete to Rapid

Freezing and Thawing." Annual Book of ASTM Standards.

[2] ASTM C39/39-14 (2014), "Standard Test Method for Compressive Strength of Cylindrical Concrete Specimens," Annual Book of ASTM Standards.

[3] Guo, Z. H. (1997). "Experiments and Constitutive Relationship for Strength and Deformation of Concrete," Tsinghua University Press, Beijing, China, pp. 10-21.

[4] Ogata, H., Hattori K., Ryuichi T., Nonaka T. (2002). "Evaluation of Freezing and Thawing Characteristics of Concrete by Ultrasonic Method (Non-destructive Inspection and Diagnosis)," Proceedings of JCI, Vol. 24(1), pp. 1563-1568.

[5] Maekawa K. and Okamura H. (1983). "The deformational behavior and constitutive equation of concrete using elasto-plastic and fracture model." Journal of the Faculty of Engineering, The University of Tokyo, XXXVII (2), pp. 253-328.

[6] Hasan M., Okuyama H., Sato Y., and Ueda T. (2004). "Stress-Strain Model of Concrete Damaged by Freezing and Thawing Cycles." Journal of Advanced Concrete Technology Vol. 2, No. 1, pp. 89-99.

[7] Murata J., Kawasaki M., Sakai T., and Kawai T. (1983). "Resistance to Freezing and Thawing of Concrete Using Ground Blast-Furnace Slag." ACI Materials Journal, Vol. 79, pp. 999-1012.

[8] ACI 318-14 (2014). Building Code Requirements for Structural Concrete, American Concrete Institute, USA.

[9] CSA A23.04 (2004). Design of concrete structures. Canadian Standards Association, Canada.

[10] MC2010 (2013), *fib* Bulletin 65, Final draft, Vol. 1, International Federation for Structural Concrete.

[11] EN 1992-1-1, Eurocode 2 (2004). Design of Concrete Structures Part 1 - NA, 1. General Rules and Rules for Buildings; European Committee for Standardization: Brussels, Belgium.

[12] ACI 363R-10 (2010). "State of art Report on high strength concrete." Farmington Hills, MI, American Concrete Institute, USA.

[13] Noguchi T., Tomosawa F., Nemati K.M., Chiaia B.M. and Fantilli A.P. (2009). "A practical equation for Modulus of elasticity of concrete." ACI Structural Journal, Vol. 106, pp. 690–696.

[14] JSCE Standard specifications for concrete structures - Design. Japan Society of Civil Engineering, JSCE, 2007, Japan.

[15] NS-3473 (1992). Concrete structures-design rules, in Norges Standardi-serings Forbund. Norwegian Council for Standardization, Oslo, Norway.

[16] Shi, S., (1997). "Effect of Freezing-Thawing Cycles on Mechanical Properties of Concrete." China Civil Engineering Journal, Vol. 30, No. 4, pp. 36-42, DOI: 10.15951/j.tmgcxb.1997.04.005.

[17] Hasan M., Nagai K., Sato Y., and Ueda T. (2002). "Stress-strain behavior in Tension and

Compression of Concrete damaged by Freezing and Thawing Cycles." M. J. Setzer, R. Auberg and H. J. Keck, Eds. Proceedings of 2nd International RILEM Workshop on Frost Resistant of Concrete, Essen 8-19. Cachan Cedex: RILEM Publications S.A.R.L., 197-204.

[18] Shang H., and Song Y. (2006). "Experimental study of strength and deformation of plain concrete under biaxial compression after freezing and thawing cycles." Cement and Concrete Research, Vol. 36, pp. 1857–1864.

[19] JI X. (2007). "The Experimental Study and Theoretical Analysis on the Mechanical Performance of Concrete and Bond Behavior between Concrete and Steel Bar after Freezing and Thawing." Doctoral Dissertation, Dalian University of Technology, China.

[20] Zou C., Zhao J., Liang F. (2008). "Stress-strain relationship of concrete in freeze-thaw environment." Frontier Architecture Civil Engineering, China, Vol. 2, No. 2, pp. 184–188, DOI: 10.1007/s11709-008-0029-3.

[21] Wardeh G., Mohamed A., Ghorbel E. (2010). "Analysis of concrete internal deterioration due to frost action." Journal of Building Physics, Vol. 35, No. 1, pp. 54-82, DOI: 10.1177/1744259110370854.

[22] Duan A., Jin W., Qian J. (2011). "Effect of freeze–thaw cycles on the stress–strain curves of unconfined and confined concrete." Materials and Structures, Vol. 44, pp. 1309–1324.

[23] Hanjari K.Z., Utgenannt P., Lundgren K. (2011). "Experimental study of the material and bond properties of frost-damaged concrete." Cement and Concrete Research, Vol. 41, pp. 244–254.

[24] Liu M. and Wang Y. (2012). "Damage Constitutive Model of Fly Ash Concrete under Freeze-Thaw Cycles." ASCE Journal of Materials in Civil Engineering, Vol. 24, No. 9, pp. 1165-1174.

[25] Liu K., Yan J., Zou C., Wu H. (2018). "Cyclic Stress-Strain Model for Air-Entrained Recycled Aggregate Concrete after Freezing-and-Thawing Cycles." ACI Structural Journal, Vol. 115, No. 3, pp. 711-722, Title No. 115-S54.

[26] Farooq M. A., Sato Y., Ayano T., Niitani K. (2017). "Experimental and numerical investigation of static and fatigue behavior of mortar with blast furnace slag sand as fine aggregates in air and water." Journal of Construction and Building Materials, Vol. 143, pp. 429-443.

Chapter 4

FATIGUE OF AE HIGH STRENGTH CONCRETE UNDER FREEZING AND THAWING – EXPERIMETNAL AND MODELING

4.1 GENERAL

In the recent years, there has been much progress in the development of high strength and durable concrete through various approaches i.e. by using steel fibers, admixtures and industrial wastes like fly ash and blast furnace slag (BFS). In the previous chapters, the improved fatigue behavior of high strength mortar with BFS fine aggregates and better monotonic behavior of high strength concrete with BFS fine aggregates for different frost damage levels are found. However, no report related to S_{max}-N_f relationships and fatigue behavior of high strength concrete with BFS fine aggregates in compression at higher maximum stress levels is available. Ayano and Fujii (2017) reported the improved fatigue performance of frost-damaged concrete with BFS fine aggregates in water compared to ordinary concrete with crushed river sand **[1]**. Moreover, the fatigue behavior of high strength concrete has gained attention owing to its increasing use in bridge and off-shore structures **[2]** and because of slender sections obtained from high strength concrete **[3]**. However, understanding the fatigue behavior of high strength concrete is still a main concern due to its brittle nature compared to normal concrete and owing to conflicting information on fatigue performance of high strength presented in the literature **[2-7]**. Therefore, in this chapter, the fatigue behavior of AE high strength concrete with BFS fine aggregates is elucidated compared to AE normal concrete of high strength. The S_{max}-N_f relationship of AE high strength concretes with BFS sand and crushed river sand are proposed in addition to the S_{max}-N_f developed for non-AE high strength concrete using the extracted data from literature compared with the S_{max}-N_f relationships for normal concrete proposed by different codes.

4.2 LITERATURE REVIEW

4.2.1 Fatigue of Concrete

Fatigue is a process of progressive and internal permanent damage caused by the application of repetitive cyclic loading, leading to failure at much lower load level than the capacity of structure. In fatigue testing, the load is applied in the form of loading wave with a particular frequency and constant maximum and minimum stress levels (S_{max}, S_{min}). The maximum and minimum stress levels are taken as percentage of compressive strength (f'_c) of concrete with S_{max}

ranging from 50% to 95% of f'_c and S_{min} is usually maintained as near to zero. With the increase in loading cycles, the strain development follows three phases in the form of inverted S-shaped curve due to occurrence of cracks. The number of cycles up to failure (N_f) are usually represented in the form of S_{max}-N_f curve, also known as Wohler curve, which is graph between maximum stress level (S_{max}) and number of cycles up to failure (N_f). There are various factors affecting the fatigue strength of concrete i.e. S_{max}, S_{min}, frequency, stress range and concrete material properties. It is well agreed that with constant S_{max}, fatigue life of concrete increases as the S_{min} increases due to decrease in stress range.

Different empirical formulas are available for the prediction of fatigue life of concrete. Most commonly used are the S_{max}-N_f equations derived through the regression of experimental data between S_{max} and N_f. However, various other models have been proposed in the literature considering other factors like probabilistic concept due to scatter of fatigue test results, strain rate and stiffness degradation rate in 2nd phase of cycle-strain cure under fatigue loading **[2]** and few fatigue models are also capable of assessing the strain development, stiffness and of prediction of fatigue life of cementitious materials **[8]**.

4.2.2 Fatigue of High Strength Concrete

Over the years, the definition of high strength concrete has been changing, depending upon the design requirements and depending on the country. In the 1950s, the concrete having the specified compressive strength of 34 MPa was termed as high strength **[9]**. However, at present, ACI363R-10:2010 defines the high strength concrete as concrete with specified compressive strength of ≥55 MPa **[10]**. Higher strength of concrete can be achieved by incorporating steel fibers, additives or admixtures. This study focuses on the compressive fatigue behavior of high strength plain concrete. To evaluate and propose the design equation for compressive fatigue of high strength plain concrete using BFS fine aggregates, it is essential to have better understanding of past research work related to high strength plain concrete under fatigue loading in compression.

Numerous research work has been carried out to evaluate the fatigue performance of ordinary concrete of normal strength, but limited data is available related to fatigue behavior of high strength plain concrete in compression. Nevertheless, there is still disagreement in the literature that whether the compressive fatigue strength of concrete increases or decreases with the increase in compressive strength.

Petkovic G. et al. (1990) investigated the fatigue properties of three types of high strength concretes i.e. two normal density concretes ND65, ND95 and one lightweight aggregate concrete LWA75. The effect of moisture condition (i.e. air, water and sealed) of concrete was studied using three different sizes of concrete cylinders. However, the main investigation dealt with the influence of variation in stress levels on fatigue behavior of concrete. The maximum stress level (S_{max}) was

varied from 55% to 95% of f'_c with different minimum stress levels (S_{min}) for different tests. It was reported that fatigue life was increased when the stress range was reduced by increasing the S_{min} keeping S_{max} as constant. Moreover, no clear difference between the fatigue properties of concrete qualities (ND65, ND95, LWA75) was found, if the load levels were defined relative to static strength **[3]**.

A fatigue study was performed by Do M-T. et al. (1993) on two commercial concretes of compressive strength (f'_c) of 70 MPa and 95 MPa. Fatigue tests were performed on cylindrical specimens with constant amplitude of sinusoidal wave. Longitudinal strain evolution and stiffness degradation with the number of cycles in high-strength concrete were found to be similar to those of normal concrete. Although, no clear statement about the fatigue life of high strength concrete compared with normal concrete is given, however, it can be said that there is no obvious difference between the fatigue life of high strength concrete and normal concrete based on similar strain evolution and stiffness degradation of both concretes **[2]**.

In the past research, increased sensitivity to fatigue loading for brittle materials is reported. Hordijk D.A. et al. (1995) found that limestone concrete behaves more brittle in fracture mechanics than gravel concrete. Therefore, the fatigue behavior of high strength concrete with limestone coarse aggregates was studied in comparison with high strength concrete with river gravel aggregates. Although for almost similar compressive strength of both concrete, there were differences in Young's modulus, fracture energy and brittleness under static loading. However, no significant differences in fatigue behavior of both concrete were found. The S-N relationships for normal strength concrete developed in the previous study were found to be well applicable to investigated more brittle high strength concrete types **[4]**.

Kim J-K and Kim Y-Y (1996) investigated the fatigue behavior of concrete of four different compressive strengths ranging from 26 MPa to 103 MPa. The decrease in fatigue life with the increase in concrete's compressive strength was reported owing to higher rate of fatigue strain increment of high strength concrete resulting in brittle nature under fatigue loading compared to low strength concrete. It was found 2nd phase of cycle strain curve in high strength concrete was longer and fatigue strain at failure was smaller for higher strength concrete due to great localization of internal damage for high strength concrete at fatigue failure **[5]**.

Tue N.V. and Mucha S. (2006) studied the fatigue behavior of high strength concrete with f'_c of 65MPa under compression using 170 specimens and found that the fatigue strength of high strength concrete is smaller than that of normal concrete for maximum stress levels higher than elasticity limit. However, in the other regions, the fatigue strength of both concrete was almost similar. The difference in fatigue behavior at higher S_{max} was found due to brittle nature i.e. smaller stress redistribution within the compression zone of high strength concrete leading to severe crack propagation and more damager per cycle compared to normal concrete with different stress amplitudes **[6]**.

Oneschkow N. (2016) investigated the fatigue behavior of high strength concrete focusing on the influence of the maximum stress level, loading frequency and waveform (sinusoidal and triangular) on the fatigue life and stiffness and strain development. The compressive fatigue tests were carried out on the cylindrical specimens (Φ60x180) mm with $f'_{cm,cube150}$ of 116MPa, within the low cycle fatigue range. The S_{max} was varied from 60% to 95% with S_{min} as 5%, and the frequency was varied between 0.1 and 10 Hz. In comparison with results of normal concrete form literature, it was reported that the influence of S_{max}, frequency and wave form on the fatigue life of high strength is almost similar. Longer fatigue life was observed for higher frequency tested for S_{max} >0.8. Moreover, it was found that the fatigue resistance of high strength concrete is not necessarily worse than the fatigue resistance of normal strength concrete **[7]**.

The summary of review data collected from literature and the comparison between the results on the effect of increased f'_c of high strength concrete on fatigue life is given in Table 4.1, whether the enhanced f'_c have any effect on fatigue life of concrete or not.

4.2.3 Fatigue of Air-entrained and Frost-damaged Concrete

The use of air-entrained concrete in RC structural elements becomes inevitable in cold regions where these structures are subjected to compressive mechanical actions combined with freezing and thawing. It is well understood that with the increase in porosity and air entrainment of the concrete, the mechanical properties e.g. compressive strength etc. of concrete become inferior **[12-16]**. Zhang et al. (2018) reported that no obvious reduction in f'_c of ordinary concrete with an appropriate air content (4-5%) **[14]**. Limited research work has been conducted related to fatigue of air-entrained concrete of normal and high strength. Antrim J. (1958) investigated the compressive fatigue properties of AE normal concrete with f'_c of 4430 psi (30.5 MPa) and air content of 8.3% along with non-AE normal concrete of f'_c of 4090 psi (28.2 MPa) and air content of 0.9% **[17,18]**. The tests were conducted on cylindrical specimens of (Φ75x150) mm at S_{max} of 50%, 60%, 70%, 80 and 90% of f'_c and frequency of 16.7 Hz. It was reported that within the limits of investigation, overall fatigue behavior of AE and non-AE concrete is not significantly different. However, at lower S_{max} (< 77% of f'_c), the fatigue life of AE concrete was comparatively longer than non-AE concrete and shorter fatigue life at higher S_{max} as shown in Fig. 4.1. However, Vicente M.A. (2018) investigated the influence of pore morphology i.e. nominal maximum pore size, pore volume, pore density and percentage of pores of specific fraction of high strength concrete on the fatigue life **[19]**. The 40 mm edge cubic specimens of concrete with different amount of AE agent were tested against fatigue at only one stress level i.e. S_{max} of 80% with S_{min} of 5% and frequency of 2 Hz. The empirical relationships between porosity morphological parameters and the fatigue life were proposed and it was found that a greater porosity and larger pores lead to a lower fatigue life, however, the concrete with higher percentage of small pores with pore volume between 0 and 0.01 mm^3 reveal longer fatigue life.

Table 4.1: Comparison between results on effects of f_c' on N_f of non-AE high strength plain concrete from literature

Concrete Grade[1]	W/C ratio	Size of Specimen in mm	f_c' (MPa)	S_{max}	S_{min}	f (Hz)	Load Wave type	Effect of higher f_c' on N_f	Ref.
C45, C60, LC70	-	Φ50x100, Φ100x300, Φ450x1350	55, 75, 80	55%, 60%, 65%, 70%, 75%, 80%, 85%, 90% 95%	5%, 20%, 30%, 40%, 60%	1 for Φ50& Φ100. 0.5 for Φ450	Sine	No effect	Petkovic 1990 **[3]**
C60, C80	0.28, 0.23	Φ100x200	70, 95	70% 75%, 85%, 95%	5%	1	Sine	No effect	Do 1993 **[2]**
C60, C70	0.4	100x100 x250	73.1, 78.2	65%, 70% 80%	5%	6	Sine	No effect	Hordijk 1995 **[4]**
C16, C40, C70, C90	0.68, 0.35, 0.3, 0.19	Φ100x200	26, 52, 84, 103	75%, 80%, 85%, 95%	25%	1	Sine	N_f decreases	Kim 1996 **[5]**
C55	0.33	Φ100x300	f_{cRef}:65	60%, 65%, 70%, 75%, 80%, 85%	5%, 10%, 20%, 30%, 40%,	8.4	Sine	N_f decreases at higher S_{max}	Tue 2006 **[6]**
C80/95	-	Φ60x180	f_{ccube}: 116	60%,70% 80%, 90%, 95%	5%	0.1, 1, 5, 10	Sine, tr.	Overall No effect	Oneschkow 2016 **[7]**

[1]Concrete grade listed are based on the classification of *fib* MC2010 **[11]**.

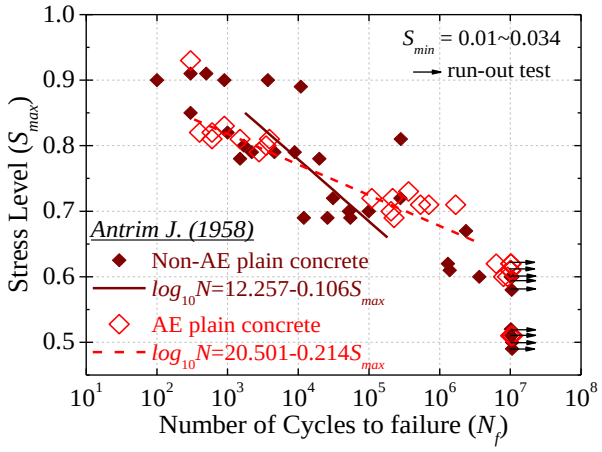

Figure 4.1: *S-N* diagram for AE and non-AE concrete (Source: Antrim J. (1958) **[17]**)

Limited studies have focused on the investigation of fatigue behavior of frost-damaged normal concrete. Hasan et al. (2008) investigated the compressive fatigue behavior of non-AE normal concrete for different degrees of frost damage and proposed the stress-strain model of frost damaged concrete under cyclic loading. The reduction in fatigue life was found with the increase in frost damage **[20]**. Lu J. et al. (2017) studied the influence of different sequences of damage caused by freeze-thaw and fatigue on dynamic compressive strength of concrete **[21]**. Li W. et al. (2011, 2015) investigated the simultaneous combined effect of freeze-thaw and flexural fatigue and reported higher damage due to combined effect than only fatigue loading **[22,23]**. However, detailed studies related to high strength concrete under combined action of freeze-thaw and fatigue are nearly non-existent. Ayano and Fujii (2017) evaluated the fatigue life of high strength concrete with BFS fine aggregates at lower maximum stress levels in water for different frost damage levels and reported the improved fatigue performance of frost-damaged concrete with BFS fine aggregates compared to concrete with crushed river sand **[1,24]**.

4.3 EXPERIMENTAL DETAILS

4.3.1 Materials, Mix Proportions and Specimen Preparation

Two series of concrete specimens are used in this study, air entrained blast furnace slag concrete (AEBFS) and air entrained high strength normal concrete (AEHSN). High early strength Portland cement with density and Blaine fineness of 3.13 g/cm^3 and 4490 cm^2/g respectively, is used as binder. Blast furnace slag (BFS) sand is incorporated as full amount of fine aggregates in AEBFS concrete specimens, whereas crushed river sand is used in AEHSN concrete. The particle size of fine aggregates used in this study ranges from 0.15 to 5 mm. The physical properties of fine aggregates are given in Table 3.1, and the mix proportions of AEBFS and AEHSN concrete are presented in Table 3.2. The polycarboxylate type of high-performance air entraining water reducing admixture is used in both types of concrete along with the antifoaming agent to control the air

content in AEBFS concrete.

The cylindrical specimens measuring (100Φ x 200) mm were prepared from three batches of both AEHSN and AEBFS series. After 36-h of casting, the specimens were demolded followed by curing for 28 days in water at room temperature. Later, the specimens were stored in controlled temperature at 20°C until the start of freeze-thaw test. The outline and results of freeze-thaw test are given in *Sec. 3.2.2.1* and *Sec. 3.3.1* respectively.

4.3.2 Compressive Fatigue Test Method

Prior to the compressive fatigue tests, the uniaxial static compression tests were performed on the cylindrical specimens of both types of concrete for frost damage levels of 0, 250 and 400 freeze-thaw cycles. The details and results of static compressive strength tests are given in *Sec. 3.2.2.2* and *Sec. 3.3.2* respectively.

The servo hydraulic machine was used to carry out the fatigue tests in compression for intact and frost-damaged specimens of AEBFS and AEHSN concrete. The maximum stress levels of 70% and 80% of uniaxial compressive strength were adopted and the minimums stress level of 5% of uniaxial compressive strength was maintained. The load was applied using the sinusoidal wave with a constant amplitude as shown in Fig. 4.2. Previous studies have reported minimal effect of loading frequency on the fatigue strength of concrete within the range of 1-15 Hz for S_{max} of 75% of compressive strength **[25]**. However, the fatigue life of plain concrete decreases with the decrease in frequency at higher stress levels due to creep effects **[26,27]**. In this study, the loading frequency of 3.5 Hz was opted considering the safety of fatigue machine and the likelihood of instability of loading arrangement. Two strain gauges of 60 mm gauge length were mounted on the specimens using adhesive. For recording strains, high speed measuring system "ADREC" is used having sampling frequency of 100 Hz. Loading cycles were applied until the failure of specimens or 2 million cycles (i.e. 6⅔ days) whichever reached earlier. The schematic diagram of loading arrangement is shown in Figure 4.3. A steel hinge was placed between the top surface of specimen

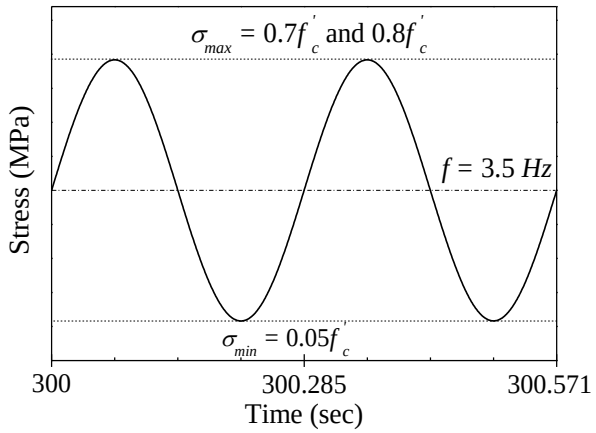

Figure 4.2: Illustration of sinusoidal loading wave form

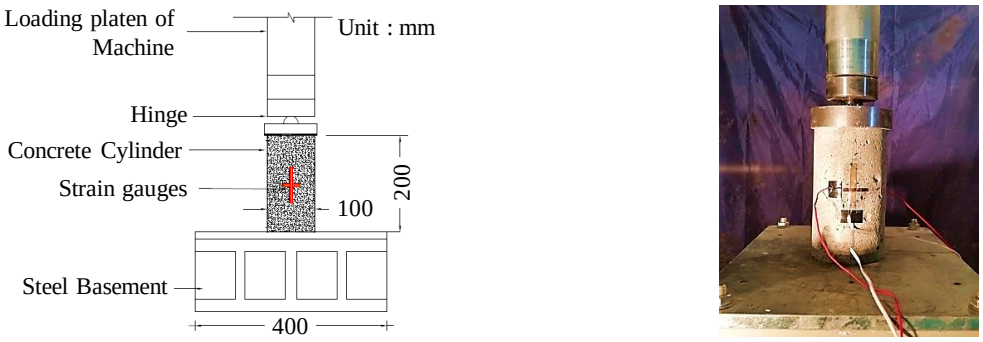

Figure 4.3: Loading arrangement for fatigue test

and loading platen of the machine to avoid the eccentricity of loading. The schematic diagram of experimental setup is shown in Figure 4.4. The PC-1 system was used to input the test parameters like maximum and minimum load, frequency, and monitoring the applied load wave at required number of loading cycles. The PC-2 was used for recording the strain measurement along with the load values for each loading cycle.

4.4 RESULTS AND DISCUSSION

4.4.1 Stress-Strain Loops

The normalized stress- normalized strain loops of AEBFS and AEHSN concrete for 0-FTC under cyclic loading at S_{max} of 80% are shown in Fig. 4.5 along with the static stress-strain curves. The number in the figure represent the number of loading cycle for which stress-strain loops are drawn. The stress and strain values are normalized with ultimate compressive strength and strain at peak stress for static tests. It can be seen that with the increase in number of loading cycles, the stress-strain loops shifted towards right due to increase in plastic strain under fatigue loading. The strain at failure under cyclic loading for both types of concrete is in good agreement with that of peak strain of static test. Moreover, the minor axis of stress-strain loops is wide, which is due to the influence of loading frequency. For higher frequency i.e. 5 Hz, the larger minor axis of fatigue

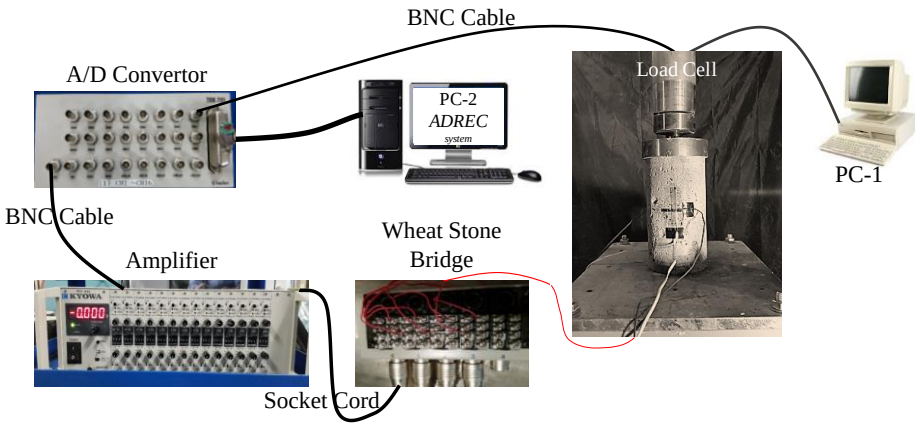

Figure 4.4: Experimental setup

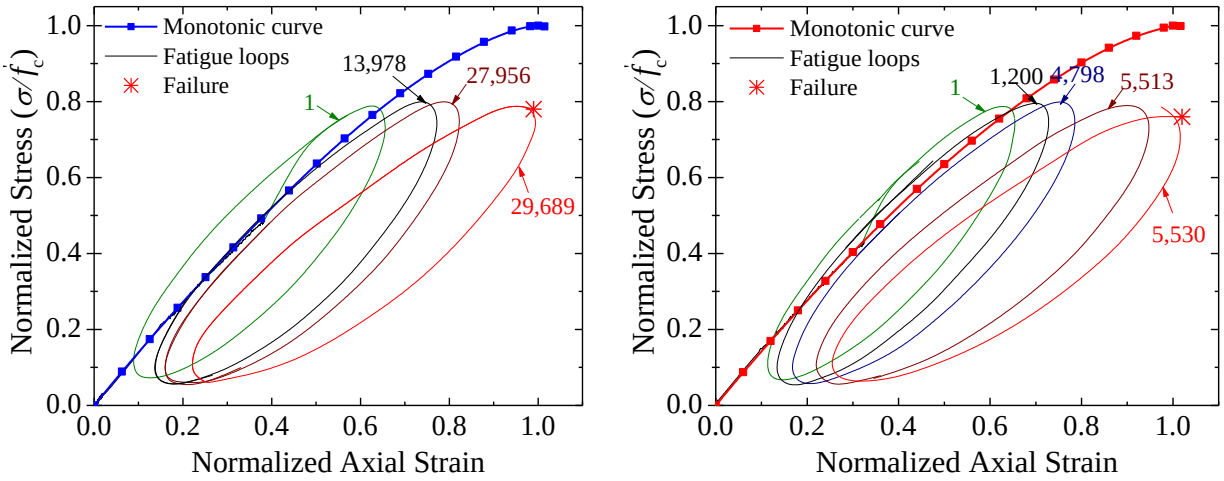

Figure 4.5: Stress-strain loops of AEBFS and AEHSN concrete at 80% stress level

loops were observed compared to those for lower frequency i.e. 1 Hz **[28]**.

4.4.2 Wöhler Curves

The Wöhler curve is the negative linear relationship between applied maximum stress level (S_{max}) and log scale of number of cycles up to failure (N_f). The maximum stress level is generally normalized by ultimate compressive stress of concrete. The S_{max}-N_f relationships for AEBFS and AEHSN concrete for 0, 250 and 400FTC are shown in Fig. 4.6 representing the fatigue lives at respective stress levels. No significant difference in fatigue life of each concrete for different frost damage levels is found. Therefore, the experimental data for 0-FTC is used for regression. The dashed lines represent the regressed line using the experimental data of 0-FTC, for which the equations are given by Eq. (4.1) and Eq. (4.2) for AEBFS and AEHSN concrete respectively.

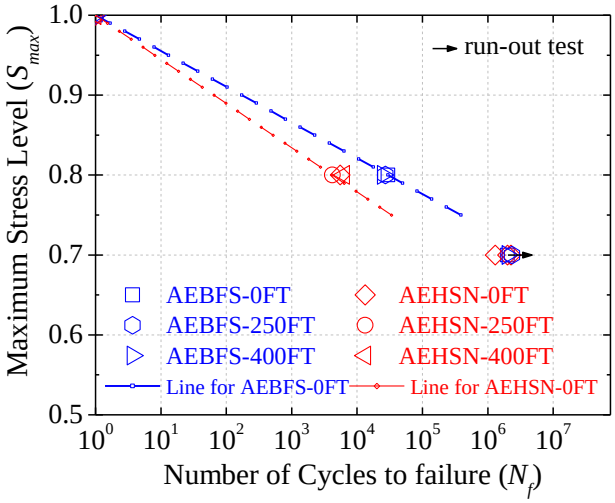

Figure 4.6: Wohler curves for AEBFS and AEHSN concrete

$$\log N = 21.24\frac{1-S_{max}}{1-S_{min}} \quad \text{for AEBFS-0FT} \tag{4.1}$$

$$\log N = 17.2\frac{1-S_{max}}{1-S_{min}} \quad \text{for AEHSN-0FT} \tag{4.2}$$

For all frost-damage levels, the fatigue life of AEBFS concrete is longer than that of AEHSN concrete. The similar phenomenon of longer fatigue life for BFS mortar compared to ordinary mortar is observed in the Chapter-2. This difference in fatigue life can be due to weaker interfacial transition zone (ITZ) of AE high strength normal concrete between matrix and aggregates compared to AEBFS concrete. In the past studies, it has been reported that with ground granulated BFS (GGBFS), the ITZ is improved due to additional C-S-H gel in matrix and matrix-aggregate interfacial transition zone (ITZ) because of pozzolanic reaction of GGBS grains. This results in better crack resistance and fatigue performance of concrete with slag **[29,30]**. Moreover, Onoue K. (2019) reported that energy consumed to form new microcracks in concrete with granulated BFS sand under cyclic loading is less compared to normal concrete indicating less damage and higher fatigue durability in concrete with BFS sand **[31]**.

At 70% S_{max}, two specimens of AEHSN concrete didn't fail until 2 million cycles and the tested specimens of AEBFS concrete also sustained 2 million cycles at 70% S_{max} without fracture. It reveals that the endurance limit of AE high strength concrete is at around 70% S_{max} compared to 60% S_{max} for non-AE normal and high strength concrete. The static compression test was performed on the "run-out" fatigue test specimens and the increase in compressive strength within the range of 0 to 5% was observed compared to static compressive strength of specimens without fatigue loading. This might be because of extrusion of the specimens and further stiffening of the specimens owing to increase in temperature from cyclic loading. The phenomenon of temperature increment is supported by the evidence that the surface of runout specimens was comparatively hot at the time of run-out compared to other specimens. The similar phenomenon of increase in f'_c has been observed in the previous studies **[32,33]**.

4.4.3 Comparison of S_{max}-N_f Relationships

The comparison between data points of N_f at different $S_{max.}$ for non-AE high strength plain concrete and normal concrete extracted from literature is shown in Fig. 4.7 along with those of AEBFS and AEHSN concrete tested in this study. The S_{max}-N_f relationship for non-AE high strength is obtained using the regression of data points for S_{min} of 5% and various frequencies and compressive strengths by different authors listed in Table 4.1. The S_{max}-N_f relationships for normal concrete calculated by equations (Eqs. (4.3-4.6)) for *CEB/FIP* Model Code 1990, Eurocode 2, *fib* Model Code 2010, JSCE specification 2007 **[11,34-36]** are also drawn along with proposed by Hsu T.T.C. (1981) **[37]** and data points for normal concrete extracted from literature **[38,39]**. Model code 1990 underestimates the fatigue life of non-AE high strength **[7]**. However, the regression of data points for non-AE high strength concrete having compressive strength class (≥C45: *fib*

MC2010) show that overall fatigue performance of non-AE high strength is almost similar to normal concrete as determined by *fib* MC 2010. The S_{max}-N_f curve for normal concrete developed by Hsu T.T.C. (1981) show slight longer fatigue life than non-AE high strength, but with the same slope. At higher stress levels (>0.8), the S_{max}-N_f curves show conservative results at these are bound at the coordinates (1,1). The proposed S_{max}-N_f relationship for non-AE high strength concrete is

CEB/FIP MC1990:
$$\log N = \{12 + 16S_{min} + 8S_{min}^2\}.(1 - S_{max}) \quad (4.3)$$

Eurocode 2:
$$\log N = 14\frac{1 - S_{max}}{\sqrt{1 - S_{min}/S_{max}}} \quad (4.4)$$

fib MC2010:
$$\log N = \frac{8(S_{max} - 1)}{\left\{(0.45 + 1.8S_{min})/(1 + 1.8S_{min} - 0.3S_{min}^2)\right\} - 1} \quad (4.5)$$

JSCE (2007):
$$\log N = 17\frac{1 - S_{max}}{1 - S_{min}} \quad (4.6)$$

Proposed for non-AE high strength plain concrete:
$$\log N = 14.8\frac{1 - S_{max}}{1 - S_{min}} \quad (4.7)$$

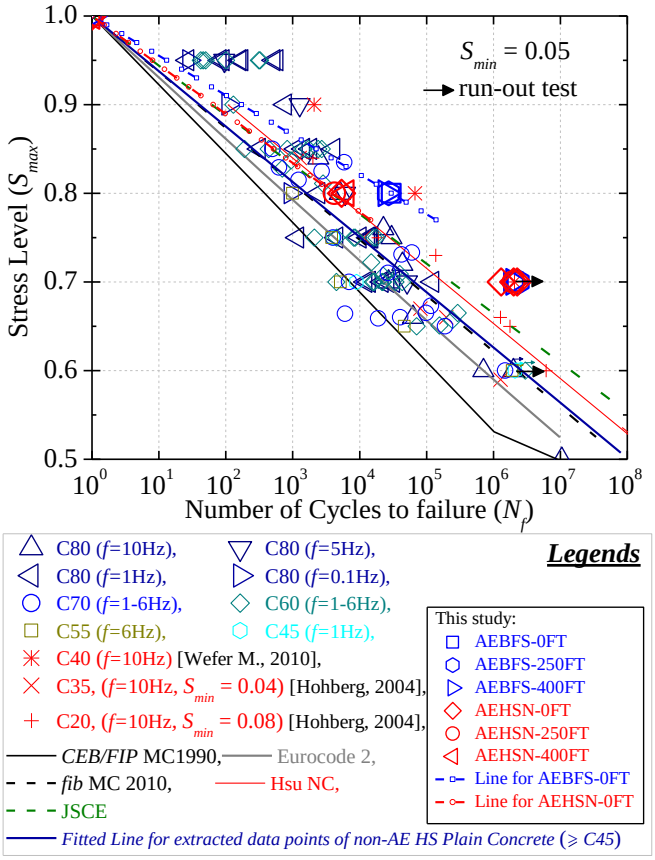

Figure 4.7: Comparison of *S-N* relationships of AEBFS and AEHSN concrete with data of non-AE high strength plain concrete from literature

shown in Eq. (4.7).

Moreover, the fatigue life of AEHSN concrete is almost same as that of non-AE high strength plain concrete at 80% stress level, but it is longer for AEBFS concrete. However, as the S_{max} reduces, the fatigue life of AE high strength concrete increases at high rate compared to non-AE high strength normal concrete. This increase is more pronounced for AEBFS concrete as the tested specimen from one batch for each frost damage level didn't fail after 2 million cycles at 75% S_{max}. This increase in fatigue life at lower S_{max} for AEHSN and AEBFS concrete can be because with appropriate air entrainment i.e. air content of 4-5%, the small, stable, and closed spherical air bubbles can be uniformly introduced into the concrete, effectively interrupting the pore connectivity **[14]**. The large number of small pores inside the AE concrete prolongs the fatigue life of concrete **[19]**, which might because of less energy dissipation under cyclic loading at lower S_{max}. The longer fatigue life of normal strength concrete with AE voids at lower stress levels is reported compared to that of without AE voids in the past study **[17,18]**.

4.4.4 Fracture Parameter Change and Plastic Strain Development

The stress-strain loops recorded throughout the fatigue tests were analyzed to get the stiffness reduction and cycle strain curves. The data of run-out specimens is not used for analysis. The illustration for the analysis along with different parameters of stress-strain loops is shown in Fig. 4.8. The cycle-strain curve represents the relationship of plastic strain and total axial strain development with the increase in loading cycles. The cycle ratio is the ratio between loading cycle (N_i) and number of cycles up to failure (N_f). The total or maximum strain is the value of strain of stress-strain loop at S_{max} for respective loading cycle, and the plastic strain is determined by extending the line joining the highest point of strain at S_{max} and lowest point of strain at S_{min} towards the horizontal axis, and the slope of this line gives the stiffness at that particular loading cycle. The change of stiffness with the increase in loading cycles is shown by the stiffness reduction curve.

The stiffness reduction and cycle-strain curves with respect to number of cycle ratio and

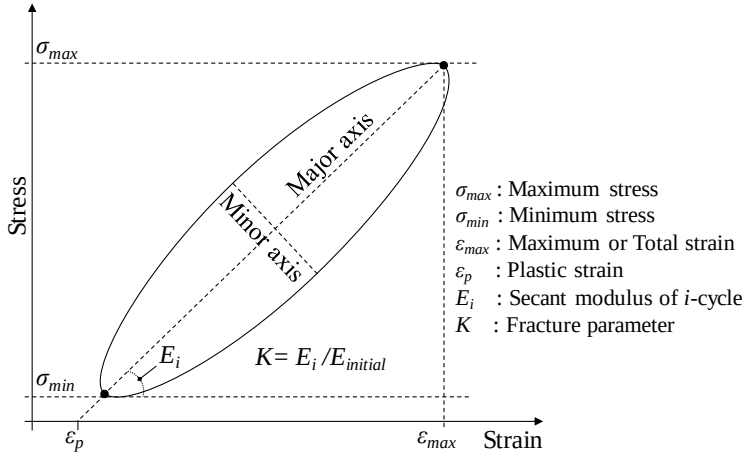

Figure 4.8: Illustration of different parameters of fatigue loop

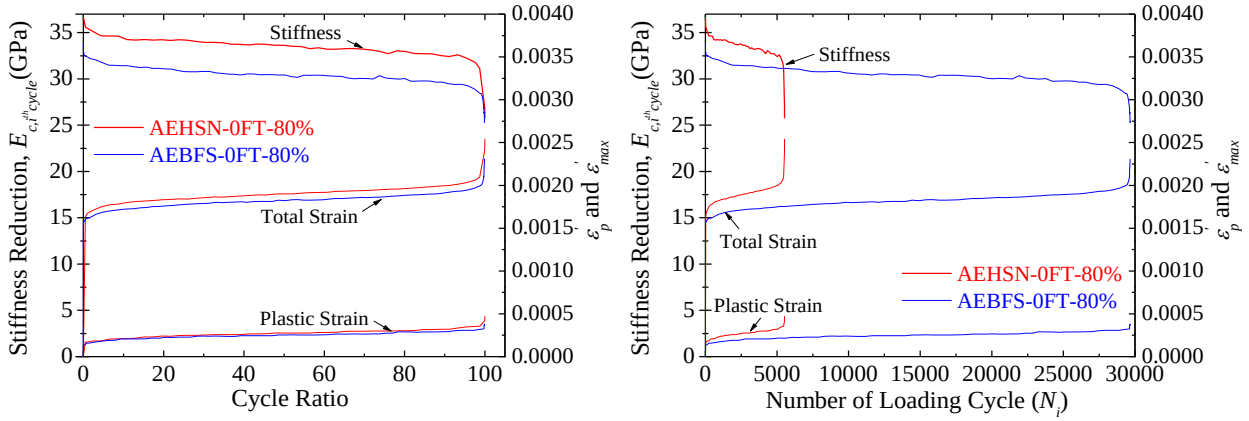

(a) with respect to cycle ratio (b) with respect to number of loading cycle

Figure 4.9: Stiffness reduction and Cycle-strain curves for AEBFS and AEHSN concrete for 0-FTC at 80% stress level

number of loading cycles are shown in Fig. 4.9 for AEBFS and AEHSN concrete for 0-FTC. The cycle strain curve is an inverted S-shape curve consisting of three phases. The phase-I is the rapid increase due to due to initiation of microcracks up to 8-10% of fatigue life, followed by uniform increase in strain due to progress of formation of microcracks until 90-93% of fatigue life, while in phase-III microcracks join each other to form macro-cracks resulting in rapid increment in strain until failure. The stage-II for AE high strength concrete is almost similar to that of non-AE high strength plain concrete from past studies **[3,7]** and longer compared to normal strength concrete. The rate of change of stiffness reduction and strain development for both AEBFS and AEHSN concrete at 80% S_{max} is almost similar with respect to cycle ratio as shown in Fig. 4.9(a). However, the rate of plastic strain development with the increase in number of loading cycle is higher for AEHSN concrete, consequently the stiffness reduces rapidly depicting higher damage per cycle compared to AEBFS concrete as shown in Fig. 4.9(b). Therefore, the fatigue life of AEHSN concrete is shorter compared to AEBFS concrete.

The change in fracture parameter and plastic strain development with the increase in normalized axial strain under cyclic loading are shown in Figs. 4.10((a)&(b)) respectively, along with the fracture parameter change and plastic strain development of high strength concrete under monotonic loading and for normal concrete in EPF model **[40]**. It can be seen that the fracture parameter and plastic strain change at almost similar rate for both AEBFS and AEHSN concrete. However, the plastic strain development of each concrete under cyclic loading is more than that under monotonic loading. This is due to the fact that two types of strains are involved in fatigue testing i.e. time independent plastic strain same as under static loading and time dependent strain due to creep and cyclic effect **[41,42]**. Moreover, the fracture parameter of each concrete under cyclic loading reduces at higher rate compared to static loading, which might be due to collapse of AE voids and damage at ITZ under cyclic loading at 80% S_{max}.

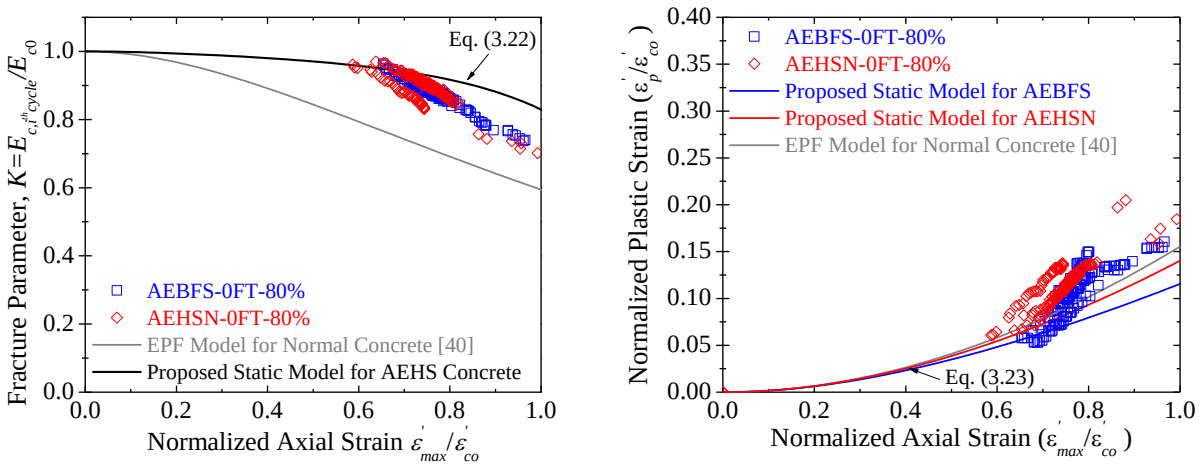

(a) Fracture Parameter change (b) Plastic Strain development

Figure 4.10: Fracture parameter and plastic strain development for AEBFS and AEHSN concrete at 80% stress level

4.5 CONCLUSIONS OF THIS CHAPTER

In this chapter, the fatigue behavior of AE high strength concrete with BFS fine aggregates is investigated in comparison with AE high strength normal concrete. The *S-N* relationships are formulated, and the results are compared with the non-AE normal and high strength concrete based on available data in the past research work. Following conclusions can be drawn:

1. The fatigue life of AEBFS concrete with BFS fine aggregates is longer compared to AEHSN concrete with crushed river sand. Moreover, at higher stress levels, the fatigue life of AEHSN concrete is almost same as that of non-AE high strength concrete from literature. However, with the reduction in maximum stress level, the fatigue life of AE high strength increases at higher rate compared to non-AEHS concrete from literature. This difference is more pronounced for AEBFS concrete. The experimental results reveal that the endurance limit of AE high strength concrete is at S_{max} higher than 60% compared to 60% S_{max} for non-AE high strength and normal concrete in literature.

2. The rate of plastic strain development and stiffness reduction of AEHSN concrete is higher compared to AEBFS concrete leading to shorter fatigue life than AEBFS concrete. This might be because of weak ITZ of AEHSN concrete. Moreover, the rate of change of stiffness and plastic strain with respect to cycle ratio and normalized axial strain is almost same for both concrete. However, the fracture parameter reduces at more rate under fatigue compared to static loading.

3. In literature, there is conflicting information regarding fatigue behavior of non-AE high strength concrete. However, the S_{max}-N_f relationship for non-AEHS concrete obtained through regression of data from literature shows that overall fatigue performance is same as that of normal concrete.

REFERENCES

[1] Ayano T. and Fujii T. (2017). "Fatigue life in water condition of concrete with blast furnace slag sand subjected to freeze-thaw attach." Journal of the Society of Material Science, Japan, Vol. 66, No. 8, pp. 588-593. (*in Japanese*)

[2] Do M-T, Chaallal O., Aitin P.-C., (1993). "Fatigue behavior of High-Performance Concrete." ASCE Journal of Materials in Civil Engineering, Vol. 5(1), pp. 96-111.

[3] Petkovic G., Lenschow R., Stemland H., Rosseland S. (1990). "Fatigue of High-Strength Concrete" ACI SP-121: High-strength Concrete, pp. 505-525.

[4] Hordijk D.A., Wolsink G.M., Vries J. de (1995). "Fracture and fatigue behavior of a high strength limestone concrete as compared to gravel concrete." HERON, Vol. 40, No. 2, pp. 125-146.

[5] Kim J-K., Kim Y-Y. (1996). "Experimental Study of Fatigue Behavior of High Strength Concrete." Journal of Cement and Concrete Research, Vol. 26, No. 10, pp. 1513-1523.

[6] Tue, N. V. and Mucha, S. (2006) "Ermüdungsfestigkeit von hochfestem Beton unter Druckbeanspruchung." *Bautechnik*, V. 83, No. 7, pp. 497-504.

[7] Oneschkow N. (2016). "Fatigue behavior of high-strength concrete with respect to strain and stiffness." International Journal of fatigue, Vol. 87, pp. 38-49.

[8] Farooq M. A., Sato Y., Ayano T., Niitani T. (2017). "Experimental and numerical investigation of static and fatigue behavior of mortar with blast furnace slag sand as fine aggregates in air and water." Journal of Construction and Building Materials, Vol.143, pp. 429-443.

[9] ACI Committee 363 (2005), "High-strength concrete (ACI 363R)" by ACI Committee 363 – High-Strength Concrete, Special publication SP-228-5, Washington, D.C., USA.

[10] ACI 363R-10 (2010). "State of art Report on high strength concrete." Farmington Hills, MI, American Concrete Institute, USA.

[11] MC2010 (2013), *fib* Bulletin 65, Final draft, Vol. 1, International Federation for Structural Concrete.

[12] Cheng X, Wu S, and Zhou J. (2013). "Influence of porosity on compressive and tensile strength of cement mortar." Journal of Construction and Building Materials, Vol. 40, pp. 869-74.

[13] Cheng Y, Wang K, Wang X, Zhou W. (2013). "Strength, fracture and fatigue of pervious concrete. Journal of Construction and Building Materials, Vol. 42, pp. 97-104.

[14] Zhang P., Li D., Qiao Y., Zhang S., Sun C. and Zhao T. (2018). "Effect of air entrainment on the mechanical properties, chloride migration, and microstructure of ordinary concrete and fly ash concrete." ASCE Journal of Materials in Civil Engineering, Vol. 30(10).

[15] Drzymala T., Jackiewicz-Rek W., Galaji J., and Sukys R. (2018). "Assessment of mechanical properties of high strength Concrete (HSC) after exposure to high temperature." Journal of Civil Engineering and Management, Vol. 24(2), pp. 138-144.

[16] Yavuz D. (2016). “The effect of air entraining agents on compressive strength.” International Journal of Civil and Environmental Engineering, Vol. 10(12), pp. 1662-1664.

[17] Antrim J. (1958). “A study of the fatigue properties of air-entrained concrete.” Joint Highway Research Project No. C36-58-B, Purdue University, USA.

[18] Antrim J. and McLaughlin J. (1958). “Fatigue study of air-entrained concrete.” American Concrete Institute Journal Proceedings, Vol. 55(5), pp.1173-1182.

[19] Vicente M.A, Gonzáleza D.C, Míngueza J., Tarifac M.A., Ruizd G., and Hindi R. (2018). “Influence of the pore morphology of high strength concrete on its fatigue life.” International Journal of Fatigue, Vol. 112, pp. 106-116.

[20] Hasan M., Ueda T., and Sato Y. (2008). “Stress-strain relationship of frost-damaged concrete subjected to fatigue loading.” ASCE Journal of Materials in Civil Engineering, Vol. 20(1), pp. 37-45. DOI: 10.1061/(ASCE)0899-1561(2008)20:1(37).

[21] Lu J., Zhu K., Tian L., and Guo L. (2017). “Dynamic compressive strength of concrete damaged by fatigue loading and freeze-thaw cycling.” Journal of Construction and Building Materials, Vol. 152, pp. 847-855.

[22] Li W., Sun W., and Jiang J. (2011). “Damage of concrete experiencing flexural fatigue load and closed freeze/thaw cycles simultaneously.” Journal of Construction and Building Materials, Vol. 25(5), pp. 2601-2610.

[23] Li W., Jiang Z., Yang Z., Jiang J., Sun W., and Deng Z. (2015). “Interactive effect of mechanical fatigue load and the fatigue effect of freeze-thaw on combined damage of concrete.” ASCE Journal of Materials in Civil Engineering, Vol.27(8).

[24] Ayano T., Fujii T., Niitani K., Takahashi K. and Hosotani K. (2017). “Improvement of durability of precast concrete member by granulated blast furnace slag sand.” Journal of Disaster Research, Vol. 12(3), pp. 459-469.

[25] Kesler C.E. (1953). “Effect of Speed of Testing on Flexural Fatigue Strength of Plain Concrete.” Highway Research Board, Vol. 32, pp. 251-258.

[26] Mederios A., Zhang X., Ruiz G., Yu R.C. and Velasco M.S.L. (2015). “Effect of the Loading Frequency on the Compressive Fatigue Behavior of Plain and Fiber Reinforced Concrete.” International Journal of Fatigue, Vol. 70, pp. 342-350.

[27] Sparks P.R., and Menzies J.B. (1973). “The Effect of Rate of Loading upon Static and Fatigue Strength of Concrete in Compression.” Magazine of Concrete Research, Vol. 75, No. 83, pp. 73-80.

[28] Isojeh B., El-Zeghayar M., and Vecchio F.J. (2017). “Simplified Constitutive Model for Fatigue Behavior of Concrete in Compression.” ASCE Journal of Materials in Civil Engineering, Vol. 29(7), DOI: 10.1061/(ASCE)MT.1943-5533.0001863.

[29] Guo L.P., Carpinteri A., Spagnoli A. and Sun W. (2010). “Experimental and Numerical Investigation on Fatigue damage propagation and Life Prediction of High-Performance Concrete containing Reactive Mineral Admixture.” International Journal of Fatigue, Vol. 32, pp. 227-237.

[30] Zhang H. and Tian K. (2011). “Properties and Mechanics on Flexural Fatigue of Polypropylene Fiber Reinforced Concrete containing Slag.” Journal of Wuhan University of Technology-Mater. Sci. Ed. Vol 26, No. 3, pp 533-540.

[31] Onoue K. (2019). “Energy consumption characteristics of concrete using granulated blast-furnace slag sand related to nucleation and propagation of microcracks.” Journal of Construction and Building Materials, Vol. 218, pp. 404-412.

[32] Bennett E.W. and Muir S.E. (1967). “Some fatigue tests of high-strength concrete in axial compression.” Magazine of Concrete Research, Volume 19(59), pp. 113-117.

[33] Lohaus, L. and Anders, S. (2006). "High-cycle Fatigue of Ultra-high Performance Concrete – Fatigue Strength and Damage Development." Proceedings of the 2nd *fib* International Congress, Naples, Italy.

[34] CEB/FIP Model Code 90 (1993). *fib* - federation Internationale du beton. International Federation for Structural Concrete. Lausanne.

[35] EN 1992-1-1, Eurocode 2 (2004). Design of Concrete Structures Part 1 - NA, 1. General Rules and Rules for Buildings; European Committee for Standardization: Brussels, Belgium.

[36] JSCE Standard specifications for concrete structures - Design. Japan Society of Civil Engineering, JSCE, 2007, Japan.

[37] Hsu T.T.C. (1981). “Fatigue of Plain Concrete.” Journal of American Concrete Institute, Vol. 78(4), pp. 292-305.

[38] Wefer M. (2010). “Materialverhalten und Bemessungswerte von ultrahochfestem Beton unter einaxialer Ermudungsbeanspruchung. Fatigue behaviour and design values of ultra-high-strength concrete subjected to uniaxial fatigue loading.” PhD Thesis, Leibniz Universitat, Hannover [in German].

[39] Hohberg R. (2004). “Ermudungsverhalten von Beton. Fatigue behaviour of concrete.” Doctoral dissertation, TU Berlin, Berlin.

[40] Maekawa K. and Okamura H. (1983). “The deformational behavior and constitutive equation of concrete using elasto-plastic and fracture model.” Journal of the Faculty of Engineering, The University of Tokyo, XXXVII (2), pp. 253-328.

[41] Sato M., Sato Y. and Kakuta Y. (2001). “Deformational Characteristic of Concrete under Cyclic Loading.” Concrete Journal of JCI, Vol. 23, pp. 1063-1068 (in Japanese).

[42] Whaley C.P., Neville A.M. (1973). “Non-elastic deformation of concrete under cyclic compression.” Magazine of Concrete Research, Vol. 25, No. 84, pp. 145-154.

Chapter 5

CONCLUSIONS AND RECOMMENDATIONS

5.1 CONCLUSIONS

Owing to improved environmental related durability properties of mortar and concrete with blast furnace slag fine aggregates, the mechanical behavior of high strength mortar and concrete subjected to freezing and thawing is investigated, and the compressive mechanical models are formulated. Based on the studies of previous chapter, the following conclusions can be drawn:

1. The fatigue life of BFS mortar in air is enhanced compared to CS mortar because of less plastic strain development in BFS mortar due to improvement in compressive strength at longer age resulting in prolonged fatigue life. However, the overall fatigue performance in water is almost for both BFS and CS mortar, while the fatigue life of each mortar in water has reduced significantly compared to fatigue life in air. Moreover, the rate of plastic strain development in CS mortar is rapid compared to BFS mortar at each stress level both in air and water, resulting in rapid degradation and shorter fatigue life of CS mortar.

2. The static stress-strain model of high strength mortar under static loading is extended to propose a simplified fatigue model, which can not only assess the plastic strain, maximum strain and change in fracture parameter at different number of loading cycles, but it can also predict the fatigue life of each mortar at different stress levels in air and water. The comparison between the results calculated by proposed simplified fatigue model and experimental results provides satisfactory agreement.

3. The mechanical properties i.e. compressive strength and Young's modulus of AE concrete of both normal and high strength degrade at slower rate with the increase in number of FTC compared to non-AE concrete because of less FTC induced plastic strain in AE concrete. However, the mechanical properties of non-AE BFS concrete deteriorate at slower rate compared to non-AE normal concrete from previous study owing to high strength of non-AE BFS concrete. Nevertheless, the mechanical properties of each concrete change at almost same rate with the increase in FTC equivalent plastic strain. Moreover, it is observed that Young's modulus of frost-damaged concrete reduces sharply compared to decrease in compressive strength.

4. The stress-strain model for AE and non-AE concrete high strength with BFS fine aggregates subjected to freezing and thawing is proposed based on the concept of elasto-plastic and

fracture theory. The rate of mechanical plastic strain development for non-AE high strength concrete with BFS fine aggregates is lower compared to that of normal concrete for all frost-damage levels, consequently the mechanical fracture parameter for high strength concrete decreases at slow rate. Moreover, the rate of mechanical plastic strain development increases with the increase in frost damage level, however, the rate of mechanical fracture parameter change is almost similar for all frost damage levels. In addition, the Young's modulus of concrete for higher frost damage level reduces sharply compared to initial stiffness (C_o), therefore, the FTC fracture parameter should consider the change in C_o. The results obtained using the proposed model are in good agreement with those of experimental ones.

5. The fatigue life of AEBFS concrete with BFS fine aggregates is enhanced compared to AEHSN concrete with crushed river sand. Moreover, at higher stress levels, the fatigue life of AEHSN concrete is almost same as that of non-AE high strength concrete from literature. However, more increase in fatigue life of AEHSN concrete is observed with the reduction in maximum stress level compared to non-AEHS concrete from literature. This difference is more pronounced for AEBFS concrete. The experimental results reveal that the endurance limit of AE high strength concrete is at S_{max} higher than 60% compared to 60% S_{max} for non-AE high strength and normal concrete from literature.

6. The rate of plastic strain development in AEHSN concrete is higher and consequently the stiffness reduces sharply compared to AEBFS concrete resulting in more damage per cycle for AEHSN concrete leading to shorter fatigue life than AEBFS concrete. Moreover, the rate of change of stiffness and plastic strain with respect to cycle ratio and normalized axial strain is almost same for both concrete. However, the fracture parameter reduces at higher rate under cyclic loading compared to static loading.

5.2 RECOMMENDATIONS FOR FUTURE STUDIES

In this study, the experimentation was carried out to investigate the compressive mechanical behavior of high strength mortar with BFS fine aggregates under fatigue loading in air and water and the mechanical behavior of high strength concrete with BFS fine aggregates against combined action of mechanical loading and frost action compared to ordinary ones. Moreover, the compressive mechanical models for high strength mortar and concrete are proposed. Based on the discussion in the previous chapter, following developments are suggested for future studies:

1. The proposed simplified fatigue model for high strength mortar is limited to high cycle fatigue only and is not applicable for low cycle fatigue. Therefore, it is suggested to study the fatigue behavior of high strength mortar under low cycle fatigue and extend the proposed model for low cycle fatigue.

2. The rate of FTC induced plastic strain in non-AE high strength concrete with BFS fine aggregates was found lower than that of non-AE normal concrete from previous study. The stress-strain model for frost-damaged high strength concrete could only be proposed using the experimental data for frost damage level up to $E_{pftc} = 0.185$. Therefore, the freeze-thaw test on non-AE high strength concrete should be carried out for higher number of FTC to cause higher frost damage and the proposed stress-strain model should be validated for high degree of frost damage level.
3. The fatigue performance of AE high strength concrete with BFS fine aggregates under frost action is evaluated in comparison with AE high strength normal concrete. However, the fatigue performance of non-AE high strength concrete with BFS fine aggregates is not investigated yet. Therefore, the fatigue performance of non-AE high strength concrete with BFS sand subjected to freezing and thawing should be evaluated for different degrees of frost damage in comparison with non-AE high strength normal concrete.
4. At present, to investigate the combined effect of frost action and fatigue, once freeze-thaw test is performed on concrete specimens, the fatigue tests are carried out on the same frost-damaged specimens until failure for simplification. However, the real RC bridge structures are subjected to series of different sequences of fatigue and frost damages during the service life. Therefore, it is vital to consider the sequence of damage caused by freeze-thaw and fatigue loading while evaluating the behavior of concrete so that the concrete can be used in construction more effectively.
5. The fatigue life of AE high strength concrete was found longer at lower S_{max} than that of non-AE high strength concrete from literature. Further experimentation should be carried out to study the fatigue performance of AE high strength concrete with different AE contents to determine the optimum AE content for high strength concrete subjected to combined action of freeze-thaw and cyclic loading.